1-1-1996

Surface-chemical approaches to asymmetric gas separation membranes.

Juha-Matti Leväsalmi
University of Massachusetts Amherst

SURFACE-CHEMICAL APPROACHES TO ASYMMETRIC GAS SEPARATION MEMBRANES

A Dissertation Presented

by

JUHA-MATTI LEVÄSALMI

Submitted to the Graduate School of the
University of Massachusetts Amherst in partial fulfillment
of the requirements for the degree of

DOCTOR OF PHILOSOPHY

September 1996

Polymer Science and Engineering

SURFACE-CHEMICAL APPROACHES TO ASYMMETRIC GAS SEPARATION MEMBRANES

A Dissertation Presented

by

JUHA-MATTI LEVÄSALMI

Approved as to style and content by:

Thomas J. McCarthy, Chair

Alan J. Lesser, Member

Paul M. Lahti, Member

Richard J. Farris, Department Head
Polymer Science and Engineering

To my parents Helli and Matti Leväsalmi

ACKNOWLEDGMENTS

Several people made my stay in graduate school an enjoyable learning experience - sometimes scientifically, sometimes nonscientifically. In both cases I will fondly remember the experiences in the years to come.

I am grateful to my advisor Dr. Thomas J. McCarthy for being an exceptional scientist and teacher. Not only has he taught me a lot of science, but he also gave me the freedom to learn things my own way.

The friendships that evolved from the McCarthy labs made the work there a very smoothened and positive experience. We helped and challenged each other in the lab and in various acceptable activities outside the lab. I want to thank you all, in particular Bob, Tak, Brian, Raul, Vip, Wei, Jim, Gene and Jack!

Most of all I want to thank my wife Lisa whom I met while performing the numerous polymer surface wettability experiments up on the Deerfield. Lisa's quiet support, patience and love helped me in ways that only she can.

ABSTRACT

SURFACE-CHEMICAL APPROACHES TO
ASYMMETRIC GAS SEPARATION MEMBRANES

SEPTEMBER 1996

JUHA-MATTI LEVÄSALMI, M.S., UNIVERSITY OF OULU, FINLAND

Ph.D., UNIVERSITY OF MASSACHUSETTS AMHERST

Directed by: Professor Thomas J. McCarthy

Poly(4-methyl-1-pentene) (PMP) films were surface-selectively chlorinated, controlling the extent and the depth of modification with chlorine vapor pressure, photointensity and reaction time. Chlorinated PMP samples were analyzed with surface and bulk sensitive techniques to choose reaction conditions for selected modification types. Gas permeability studies with the selected membranes showed that a thick layer of densely chlorinated PMP was needed to change the gas barrier properties of a PMP membrane. The decrease in flux through the highly and deeply chlorinated PMP membrane was more pronounced in cases of large gas molecules resulting in improvements in selectivity of the membrane.

PMP membranes were also surface-selectively oxidized to yield a carboxylated PMP surface (PMP-COOH). Alternating ultrathin layers of poly(allyl amine hydrochloride) (PAH) and poly(sodium styrene sulfonate) (PSS), and polyaniline (PAn) and PSS, were self-assembled onto the PMP-COOH surface. The stratification and the thickness of the layers were determined with surface-sensitive analytical techniques. The polyelectrolyte molecules were shown to be packed into the PAH/PSS multilayers in a dense and rigid manner giving improved gas barrier properties. The PAn/PSS multilayers were shown to be stratified in a similar fashion to PAH/PSS, but the molecules were bound in a loose network resulting in no changes in the gas permeability properties of the composite membranes.

TABLE OF CONTENTS

LIST OF TABLES

LIST OF FIGURES

CHAPTER 1

INTRODUCTION

This thesis is divided into four parts: An introduction to gas permeation through polymers is presented in Chapter 1. Included in Chapter 1 is a section on structure and properties of poly(4-methyl-1-pentene) (PMP), which is the substrate material in the work presented here. Project-specific introductions and references to related work published by others, are presented in Chapters 2 and 3.

Chapter 2 contains experimental data and its interpretation for using surface-selective chlorination to control gas permeation through PMP. In Chapter 3, the experimental data are interpreted for surface oxidation of PMP film, formation of polymeric multilayers supported on the oxidized layer, and the effect of the multilayers on gas permeability properties of the resulting composite membranes.

The text in Chapters 2 and 3 contains the figures that are used to interpret the data. Tables that complete the data packages are located at the end of the chapters, abbreviations and detailed descriptions of experimental and analytical methods are presented in the appendix section after Chapter 3.

This format was chosen in an attempt to make the thesis compact and easily readable without leaving out details that may be helpful to another person working in the field in the future.

Overview

Gas permeation through polymers is affected by the chemical nature and physical state of the material in question. In some applications such as protective coatings or packaging films, permeation of gases through the polymer is undesirable as it leads to degradation of the material that is being protected by the polymer. In gas separation processes that are based on polymeric membranes, on the other hand, it is preferable to have one component in a mixture of gases permeate through the membrane faster than the rest of the components, leading to gas separation due to a selective barrier property of the membrane.

Increasing demand for on-site-production of inert gas, oxygen-enriched air, and hydrogen recovery from refinery and petrochemical processes has led to both academic and industrial interest in understanding and controlling gas permeability through polymer films. In the future various bioprocess applications such as landfill gas upgrading may also receive increased attention. Asymmetric membranes were developed to optimize productivity and selectivity of a membrane. Asymmetry can be created by chemical or physical modifications of the skin of the film, or by preparing a bilayered or multilayered composite.

Two novel approaches to controlling gas permeability through polymer films are presented in this thesis. Chemical surface modification of poly(4-methyl-1-pentene) film is used in Chapter 2 to create a barrier layer of controlled modification density and depth within the substrate. In Chapter 3, a barrier layer is formed on poly(4-methyl-1-pentene) film by consecutive adsorptions of ultrathin polyelectrolyte monolayers to create a multilayered composite structure.

Gas Separation Membranes

In gas separation processes, membranes are cost-effective filters that can separate components of mixtures differing in sizes on the Ångström level. The first commercial membranes were introduced at the end of 1979 and during the 1980s the original polysulfone and cellulose acetate based membranes were joined by polyimide, polyamide, polycarbonate, polyetherimide and sulfonated polysulfone membranes. [1]

Gas separation using membranes is a rate-controlled process and complete separation of components is thus not achieved. In designing a gas separation membrane, one often has to compromise between productivity and selectivity, selectivity having the greater importance based on economical reasons; productivity can be increased by using larger membrane areas. [2] Use of a membrane of high productivity but low selectivity leads to multistep separation processes which are not economically attractive. For commercial gas separation membranes, other parameters to be considered are mechanical strength and resistance to various pH and temperature conditions.

Asymmetric membranes with a thin selective layer (0.1 to 0.5 μm) supported on a highly permeable substrate (50 to 300 μm) were developed to meet the goals of a balanced performance. [3] Traditionally asymmetric membranes are prepared by phase-inversion, and by constructing composite structures. The phase-inversion technique uses a tertiary system consisting of polymer, solvent and non-solvent; the precipitant is added to a partially evaporated polymer/solvent system causing the system to separate into polymer-rich and polymer-poor phases. Thus the asymmetry in the membrane after evaporation is morphological. In composite membranes the asymmetry is in the chemical structure of different layers. At the end of the 1980s surface modification of polymeric films was introduced as a new means of creating the asymmetry.

Membranes come traditionally in tubular, plate, hollow-fiber and spiral wound modules. In gas separations, hollow fibers and spiral wounds are most commonly used whereas plate modules - widely used in pervaporation - are unattractive due to low area per unit volume ratio. Gas separation membranes have to be defect-free because of high diffusion coefficients of gases. Possible defects on the membrane can be sealed with a highly permeable coating such as silicone rubber in "caulking" process. [1]

Gas Permeation

Gas transport through nonporous polymer membranes takes place by a sorption-diffusion-desorption process where the driving force for permeation is the difference in partial pressures of a gas on the upstream and downstream sides of the membrane. Transient gaps of the size of the penetrating molecule are generated within the polymer matrix by thermal motion of chain segments to accommodate the gas transport. In semicrystalline polymers the permeation takes place almost exclusively in the amorphous phase. "Metal" membranes made of palladium-silver alloys give exceptionally high selectivities for hydrogen gas as the molecule is catalytically dissociated within the membrane and recombined at the downstream face. The function of these membranes is an exception within gas separation membranes and are thus not discussed any further here.

Permeability P of a gas molecule through a homogeneous membrane is the product of diffusion and solubility coefficients as shown in equation 1;

$$P = D \cdot S \qquad [1]$$

In a composite membrane one has to take into account the fact that the membrane has two (or more) layers that differ in their thicknesses and permeability characteristics. The series resistance model, which is based on analogy between gas permeation through multiple layers and flow of electricity through resistances

connected in series, illustrates the relationship between total membrane thickness and the thickness of the active layer. The pressure normalized permeation flux P/l for gas i through a composite membrane consisting of layers A and B with thicknesses l_A and l_B, and permeabilities P_A and P_B, respectively, is given by

$$\left(\frac{P}{l}\right)_i = \left[\left(\frac{l_A}{P_A}\right)_i + \left(\frac{l_B}{P_B}\right)_i\right]^{-1} \qquad [2]$$

Defining the pressure normalized permeation flux for an asymmetric membrane that is prepared by surface modification is more complicated (equation 3) since the modification does not create two distinct layers, but a gradient of modified structural units in a heterogeneous selective layer;

$$\left(\frac{P}{l}\right)_i = \left[\left(\frac{l_P}{P_P}\right)_i + \left(\int_{l_P}^{l} \frac{dx}{P(x)_i}\right)_i\right]^{-1} \qquad [3]$$

In this membrane there is a region of unmodified polymer, l_P, with the permeability P_P. Throughout the modified thickness, $(l - l_P)$, the gas permeability is a function of position, x. [4-6]

In gas permeability determinations (see equation 4 on page 6) one typically measures the time t (in seconds) that it takes for a certain volume V of gas (in cubic centimeters at standard temperature and pressure) to permeate through a membrane of thickness l (in centimeters) and area A, when a pressure gradient ΔP (in cmHg) is applied as the driving force for the gas permeation.

$$P = \frac{V \cdot l}{A \cdot t \cdot \Delta P} \qquad [4]$$

$$[P] = \frac{cm^3(STP) \cdot cm}{cm^2 \cdot t \cdot cmHg} \qquad [4']$$

When the partial pressures on the downstream side of the membrane are negligible for both component of a gas mixture of A and B, the separation factor is simply

$$\alpha_{AB} = \frac{[D_A]}{[D_B]} \cdot \frac{[S_A]}{[S_B]} \qquad [5]$$

The above equations can be used to form permeability versus selectivity graphs such as that in Figure 1, where the solid line illustrates the experimentally observed trade-off between CO_2/CH_4 selectivity and membrane productivity. In this particular example, pure membrane material A has a four times better selectivity for the gas pair than pure B, whereas B has 300 times higher CO_2 flux than A. The dashed line is a calculated selectivity/productivity curve for a composite membrane constructed of a layer of A on substrate B, where the percentages indicate the fraction that the thickness of A contributes to the total thickness of the composite membrane. Such graphs clearly demonstrate the fundamental reason why the asymmetric membrane type is so attractive a choice in gas separations as large increases in selectivity can be achieved without extensive loss of productivity.

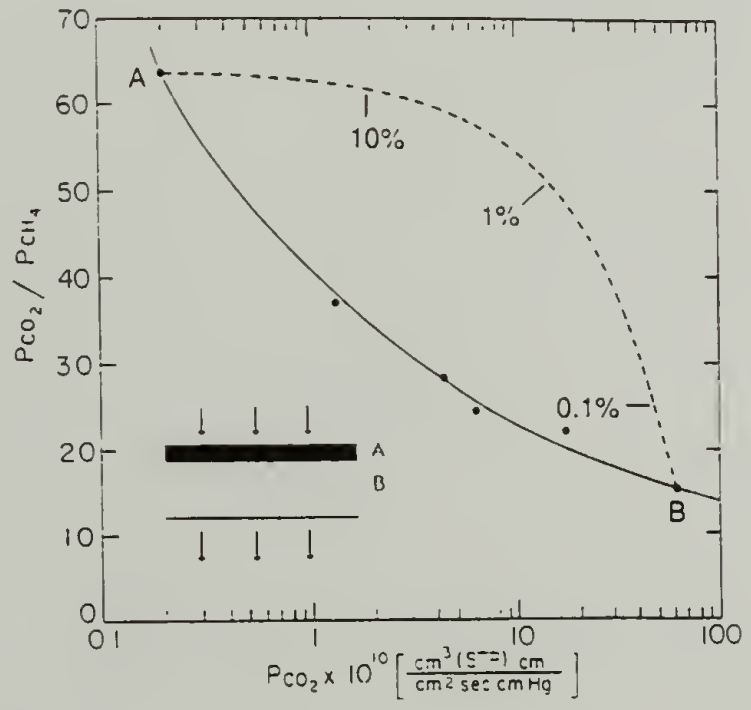

Figure 1. Selectivity as a function of permeability for symmetric (solid line) and asymmetric (dashed line) membranes. [6]

Unless there is a specific interaction between the membrane and one of the gas molecules, the solubility component of the separating factor is mainly determined by the condensability of the gases which is related to the critical temperature. Thus oxygen with a critical temperature of -118.95 °C is typically more soluble in polymers than nitrogen (critical temperature -147.1 °C). As a comparison carbon dioxide has a critical temperature of 31.3 °C and it is known to plasticize a number of polymers due to its high solubility. In most cases, however, the solubility selectivities are very low and diffusion selectivity plays the determining role in the separation process.

Diffusion coefficient D in a given membrane matrix is a function of the size the penetrant. This can be seen in equations 6 and 7 as the activation energy for diffusion E_d that is a function of the diameter of the gas molecule (σ), jump length (λ) and cohesive energy density of the polymer (CED);

$$D = D_o \exp\left(-E_d/RT\right) \qquad [6]$$

$$E_d = \frac{\lambda \pi \sigma^2 CED}{4} \qquad [7]$$

Molecular sieving diameters for some industrially important gases are presented in Table 1:

Table 1. Kinetic sieving dimensions.

molecule	H_2	CO_2	O_2	N_2	CH_4
sieving diameter/Å	2.89	3.3	3.46	3.64	3.8

The small size of the hydrogen molecule that leads to the high coefficient of diffusion explains its high permeation rates through polymers, even though the low critical temperature (-239.9 °C) suggests low solubility of the gas in the substrate.

As was shown above, within a given polymer matrix a difference in the size of the penetrants leads to separation of gases due to inherently different diffusion coefficients. On the other hand, for a given gas molecule, membrane design can tune the permeation rates by adjusting the cohesive energy density. This can be done by selecting a suitable polymer for the selective layer, or by changing the cohesive energy density of the substate in a chemical or physical modification process.

Poly(4-methyl-1-pentene)

Commercially poly(4-methyl-1-pentene) (PMP) is manufactured solely by Mitsui Petrochemical Industries, LTD. of Japan by dimerization of propylene to 4-methyl-1-pentene followed by Ziegler-Natta polymerization. The resulting PMP is highly temperature and chemical resistant with a softening point of 160-170 °C, melting point of 230-240 °C and density of 0.813 to 0.828 g/cm^3 for the crystalline regions and 0.838 to 0.839 g/cm^3 for the amorphous phase. The glass transition region has been reported as 22-30 °C, and the heat of fusion as 62-65 J/g. [7-10]

The density characteristics of PMP at room temperature are unusual: For all other polymers the crystals are more dense, typically by 10-15 %, than the amorphous phase. At temperatures higher than 50-60 °C, the density profile normalizes and PMP expands upon melting. [10] Thus comparisons of melting behavior of PMP and ice are not justified.

The low density of PMP crystals may be explained by inefficient packing of chains in the various crystalline forms shown in Table 2 on page 9.

Table 2. The crystalline modifications of PMP and their lattice parameters. [11,12]

Modification	Crystal form	Lattice constants / Å a = b	c
I	tetragonal	18.66	13.65
II	tetragonal	19.16	7.12
III	tetragonal	19.38	6.98
IV	hexagonal	22.17	6.69
V	tetragonal	-	-

Modification I has a 7/2 helix structure [13] and 4/1 helices have been assigned to modifications II and III. [14] Gaps of 4 Å exist between chains in crystalline regions that facilitate solubility of gas molecules smaller in size than the gap dimension. For gas molecules smaller than 4 Å in diameter, the solubility in PMP crystals is about 25-30 % of that in the amorphous phase. On the other hand, for gas molecules larger than 4 Å in size, the crystals behave as barriers to diffusion due to restrictions in thermal motions of chain segments needed to accommodate the large gas molecules.

Mohr and Paul have studied the effect of casting solvent on the permeability and found that casting solvent affects which crystalline modification is formed and how the crystallites are spatially arranged in the membrane. Films cast from decalin, xylene and chloroform have up to six times lower permeabilities relative to a melt processed film, whereas casting solvents such as cyclopentane, cyclohexane and carbon tetrachloride give films with permeation rates similar to a melt processed film. [15]

Poly(4-methyl-1-pentene) was introduced to the gas separation membrane market in 1985 by Dow because of its fairly attractive oxygen/nitrogen separating factor of 4. Selectivities of PMP membranes have also been tried to be improved by surface-fluorination. For some gas pairs the selectivity increased considerably (H_2/CH_4 selectivity from initial value of 7 to 85) whereas for some selectivities the improvement was only moderate (from 4 to 6 for O_2/N_2) upon fluorination. [16,17]

Objectives

The objective of this work is to control gas permeation through polymer films by creating a skin layer that acts as a selective barrier to gases. Two different approaches are used: first: a chemical modification of the surface to create the selective layer within the film; and second: consecutive depositions of highly oriented polymers into monolayers to build-up selective multilayers on top of the polymer film.

References

(1) Spillman, R. W.; Sherwin, M. B. *CHEMTECH* **1990**, *June*, 378.

(2) Rautenbach, R.; Janisch, I. *Ad. Polym. Technol.* **1987**, *7*, 221.

(3) Koros, W. J.; Fleming, G. K. *J. Membr. Sci.* **1993**, *83*, 1.

(4) Petropoulos, J. H. *J. Membr. Sci.* **1990**, *53*, 229.

(5) Ashworth, A. J. *J. Membr. Sci.* **1992**, *71*, 169.

(6) Mohr, J. M.; Paul, D. R.; Mlsna, T. E.; Lagow, R. J. *J. Membr. Sci.* **1991**, *55*, 131.

(7) Mitsui Plastics, *commercial literature.*

(8) Puleo, A. C.; Paul, D. R. *Polymer* **1989**, *30*, 1357.

(9) Charlet, G.; Delmas, G. *J. Polym. Sci., Polym. Phys. Ed.* **1988**, *26*, 1111.

(10) Zoller, P.; Starkweather, H. W.; Jones, G. A. *J. Polym. Sci., Polym. Phys. Ed.* **1986**, *24*, 1451.

(11) Charlet, G.; Delmas, G. *Polymer* **1984**, *25*, 1619.

(12) He, T.; Porter, S. *Polymer* **1987**, *28*, 1321.

(13) Kusanagi, H.; Takase, M.; Chatani, Y.; Tadokoro, H. J. *J. Polym. Sci., Polym. Phys. Ed.* **1978**, *1*, 131.

(14) Takayanagi, M.; Kawasaki, M. J. *J. Macromol. Sci., Phys.* **1967**, *1*, 741.

(15) Mohr, J. M.; Paul, D. R. *Polymer* **1992**, *33*, 57.

(16) Chiao, C. C. *U.S. Patent 4,828,585, 1989.*

(17) Mohr, J. M.; Paul, D. R.; Pinnau, I.; Koros, W. J. *J. Membr. Sci.* **1991**, *56*, 77.

CHAPTER 2

GAS PERMEABILITY OF SURFACE-SELECTIVELY CHLORINATED POLY(4-METHYL-1-PENTENE)

Introduction

Surface halogenations have been reported for polymers, such as chlorination, [1,2] bromination[2] and iodination[2] of polyethylene films and bromination of polystyrene-*block* -polybutadiene. [3] Under certain conditions the photochlorination of polyethylene was found to be surface-selective. The surface selectivity was attributed to the formation of a barrier layer (chlorinated polyethylene) that inhibits permeation of chlorine to greater depths. [1]

The only previously reported reaction used to modify poly(4-methyl-1-pentene) (PMP) surfaces is gas phase fluorination. Fluorination is a very exothermic reaction and reaction conditions have to be well controlled. Reported gas phase fluorinations have been performed using a dilute (2 vol. %) F_2/He mixture in a dynamic manner slowly increasing the fluorine concentration in the reaction flask by replacing helium with the F_2/He mixture. [4-6] Low fluorine concentration at the initial stages of reaction minimizes the probability of reaction taking place at adjacent carbons which would lead to localization of released energy and breaking of carbon-carbon bonds. Further reaction proceeds deeper into the bulk of the polymer film. Nevertheless gas phase fluorination is difficult to control and tends to degrade the skin of a polymer film by breaking carbon-carbon bonds. Changes as great as 0.91 to 0.41 in the fluorine:carbon ratio from XPS measurements over the period of a year have been reported with subsequent changes in permeabilities of the film. [7]

Nevertheless, controllable surface-selective modifications of this type (that exhibit autoinhibition and create a less permeable skin) may be useful for the preparation of asymmetric nonporous membranes that have tunable selectivity and productivity properties.

Surface Selective Chlorination of Poly(4-methyl-1-pentene)

A study of the heterogeneous (gas-solid) chlorination of PMP is reported here. PMP was an attractive choice for several reasons: It has the lowest density of all commercially available thermoplastics and a higher permeability to gases than the other hydrocarbon polymers. It is reasonably temperature and chemical resistant with a softening point of 160-170 °C, and an all-aliphatic structure. As a saturated hydrocarbon it should react with chlorine via an unexceptional photoinitiated chain reaction as shown for one of six possible reaction sites in Figure 2 on page 13.

Fluorination of PMP membranes has been shown to improve selectivity for certain gas pairs. [4,5] Chlorination is a less exothermic reaction than fluorination which can cleave C-C bonds resulting in polymer degradation. Thus it should be easier to prepare modified PMP layer of controlled modification density and depth by chlorination than by fluorination.

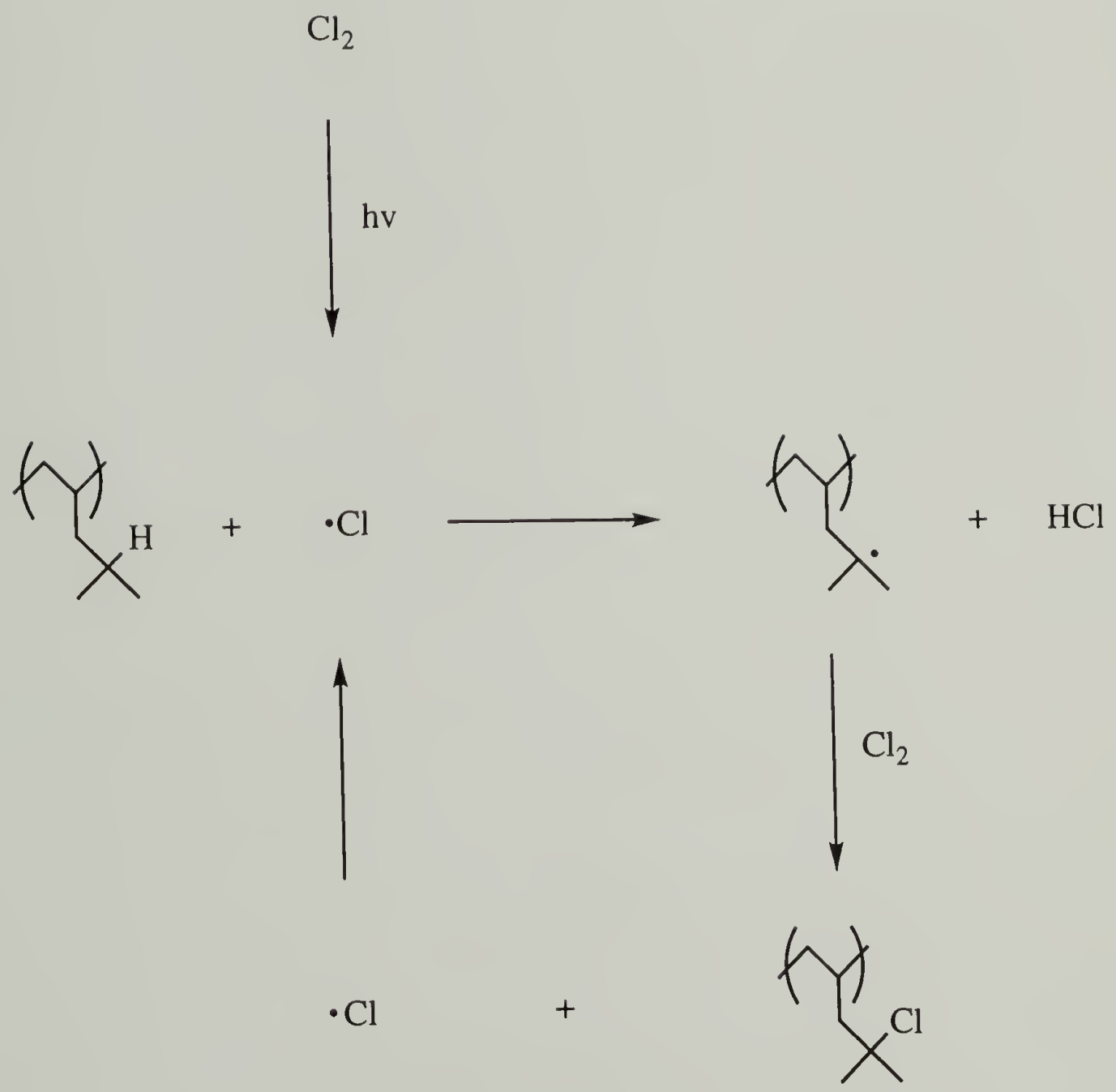

Figure 2. Chlorination mechanism at one possible reaction site on the PMP chain.

Experimental Section

General Procedures

PMP film (50 μm Mitsui TPX) was extracted in refluxing dichloromethane for 1 h and dried at reduced pressure and room temperature to constant mass. Chlorine gas (Aldrich: 99.5+%) was used as received. XPS spectra were obtained with a Perkin-Elmer Physical Electronics 5100 spectrometer using Mg Kα excitation (400 W, 15.0 kV). Spectra were routinely recorded at a takeoff angles of 15° and 75° (measured between the film surface plane and the entrance lens of the detector optics). Atomic composition data were determined using sensitivity factors obtained from samples of known composition: C_{1s}, 0.225; Cl_{2p}, 0.655; O_{1s}, 0.628. Attenuated total reflectance infrared (ATR IR) spectra were recorded using an IBM 38 FTIR at 4 cm^{-1} resolution with a 10 x 5 x 1 mm internal reflection element (45° KRS-5; 30°, 45° and 60° Ge). Gravimetric measurements were made with a Sartorius 1612MP-1 analytical balance. Dynamic advancing (θ_A) and receding (θ_R) contact angles were measured with a Ramé-Hart telescopic goniometer and a Gilmont syringe with a flat-tipped 24-gauge needle as probe fluid was added (θ_A) or withdrawn (θ_R) from the drop. Phase interference microscopy was performed using a Zygo Maxim 3D Model 5700. Differential scanning calorimetry was performed using a TA Instruments Model 2910 Modulated DSC. Surface chlorinations were run on both sides of the film controlling reaction time (15 s to 17 h), chlorine pressure (5 mm to 1 atm - regulating the vapor pressure with cold baths), and light intensity (darkness, ambient hood light, a medium-intensity UV light source (UVP Inc., Model UVG-11) of 330μW/cm^2 at 254 nm, and a high-intensity UV light source (UVP Inc., Blak-Ray B-100A) of 6000 μW/cm^2 at 365 nm.

Chlorination

A secondary vacuum manifold (Figure 3) that could be evacuated and filled with nitrogen or chlorine was used for the heterogeneous chlorinations of PMP film. For reactions that were run in the dark, the manifold was wrapped with a thick, black cloth. Reactions were also run in ambient hood light or using a UV light source placed at the base of an aluminum foil funnel below the sample container.

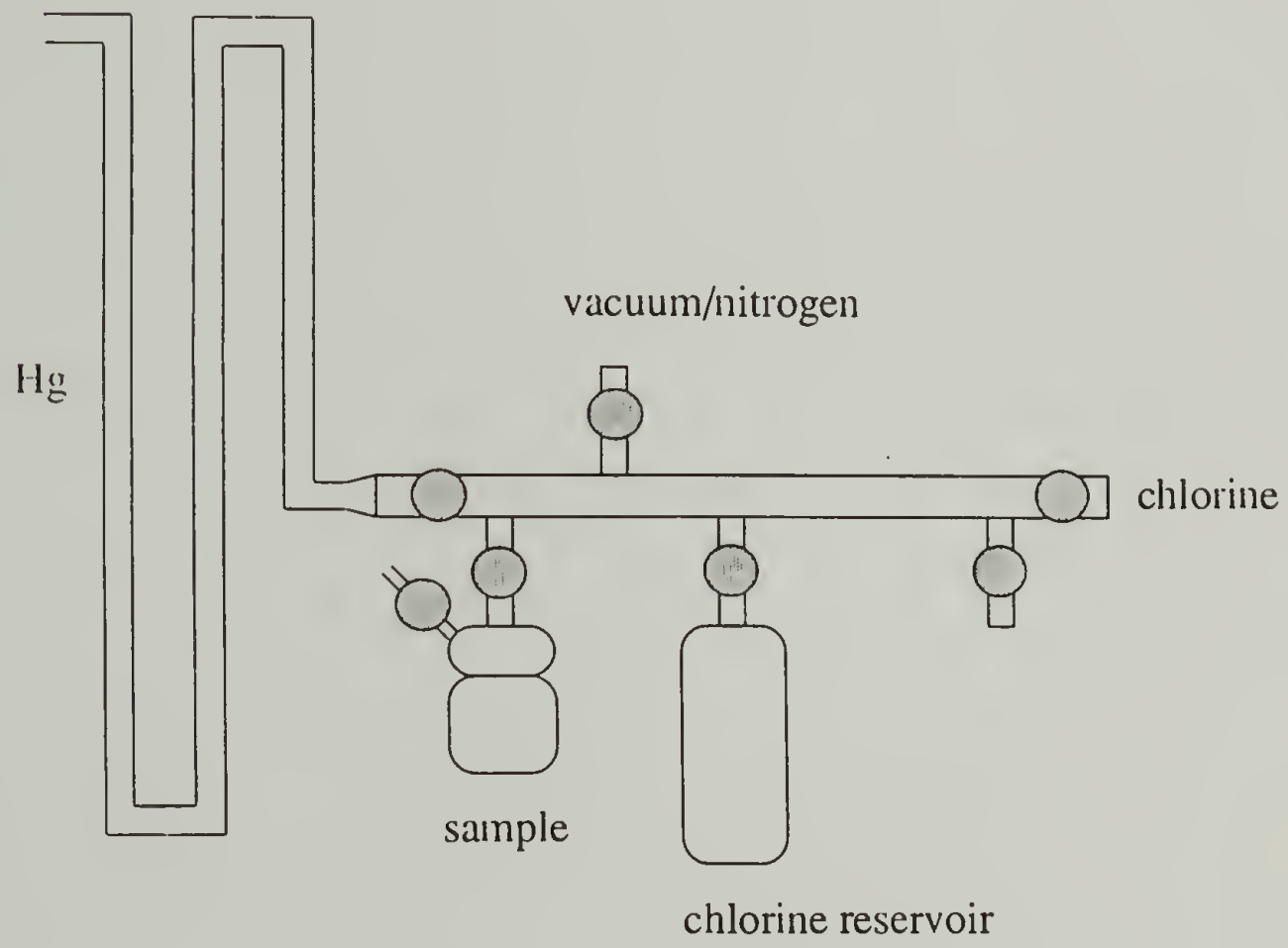

Figure 3. Gas/vacuum manifold used for heterogeneous chlorination reactions.

The sample vessel (containing the tarred sample), chlorine reservoir, and secondary manifold were evacuated, subsequently filled with nitrogen several times, and then evacuated. The sample container was isolated form the rest of the manifold, and chlorine gas (5 psig) was introduced. Chlorine boils at -34.8 °C and below this temperature its vapor pressure is a function of temperature as shown in Figure 4.

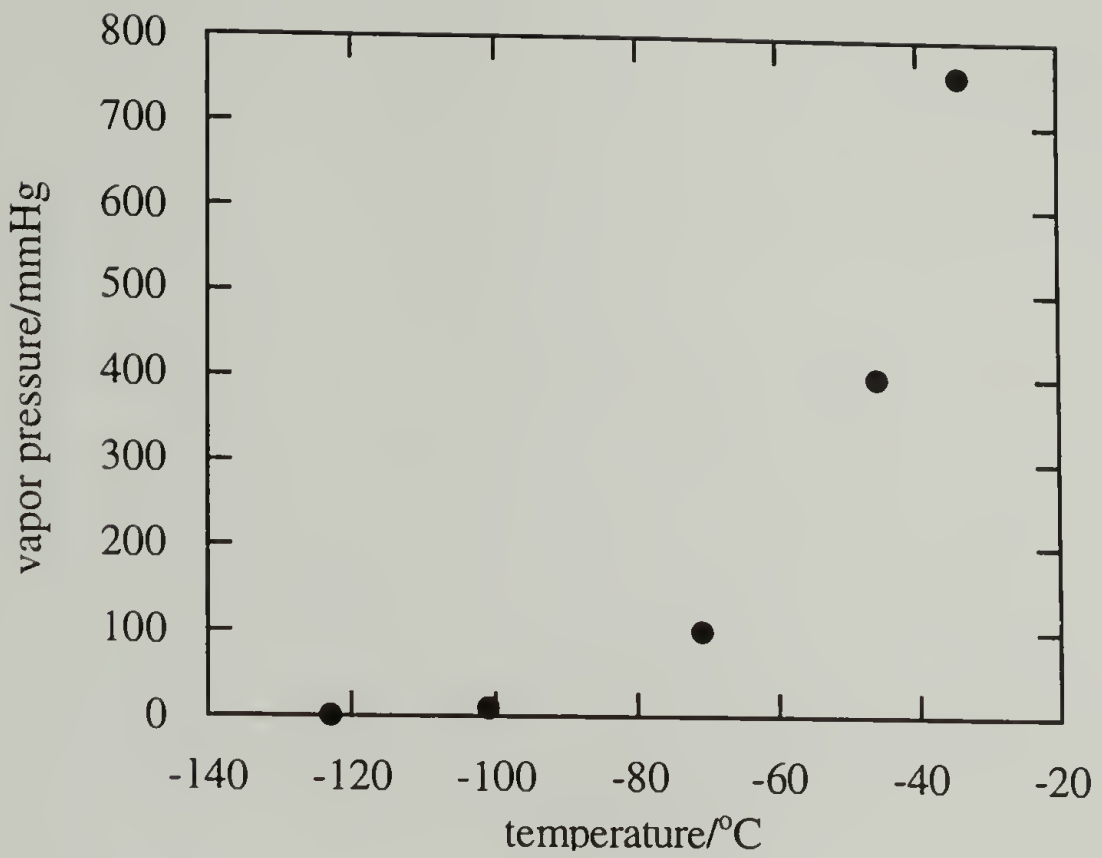

Figure 4. Chlorine vapor pressure as a function of temperature.

Cold baths were used to adjust the chlorine vapor pressure by placing the bath around the chlorine reservoir. The vapor pressure in the closed system was allowed to equilibrate, and the reaction was started by opening the sample container valve after closing the chlorine reservoir valve. The reaction manifold/sample container was calibrated to have reaction pressures of 176, 47, 16 and 5 mm using cold baths of -44 ˚C (acetonitrile/N_2), -63 ˚C (chloroform/N_2), -83 ˚C (ethyl acetate/N_2) and -97 ˚C (methanol/N_2), respectively. Taking into consideration the volume of the manifold system with the sample valve closed and that with the valve open (73 ml and 216 ml, respectively), the actual chlorine vapor pressure that the reaction was run at (table 3) can be calculated.

For reactions run at 1 atm chlorine pressure, the manifold was depressurized (from slight overpressure) through a bubbler to let pressure equilibrate with the outside pressure. The reaction was stopped by evacuating the system and replacing the unreacted chlorine and byproduct HCl with nitrogen. Film samples were dried/degassed to constant mass and stored under nitrogen prior to additional analyses.

Gas Permeation Rate Measurements

Gas permeation studies were run one gas at a time with hydrogen, carbon dioxide, oxygen, and nitrogen at 40 °C with an upstream pressure of 6 atm (3.5 atm for H_2) and a downstream pressure of 0 atm. After reaching a steady-state flux of gas, a pressure increase of 0.50 mm in a known volume on the downstream side was timed. A home-built pressure/vacuum manifold shown in Figure 5 was built around a Millipore 25 mm membrane cartridge (25 mm diameter) and a Celesco DP 31 differential pressure transducer (see Appendix 1 for detailed description of the instrumentation and the permeability measurement).

Results and Discussion

Cleaning procedure for poly(4-methyl-1-pentene)

The solubility of poly(4-methyl-1-pentene) (PMP) in tetrahydrofuran (THF), methanol (MeOH) and dichloromethane (CH_2Cl_2) was studied by gravimetric analysis. Stirring PMP samples for 60 min at room temperature led to weight losses of 0.9 % (THF), 0.04 % (MeOH), and 0.07 % (CH_2Cl_2). Since dichloromethane has been widely used to extract additives from polyolefin samples and it was shown not to lead to

extensive PMP weight losses that would be likely to lead to corroded surface topography due to preferential dissolution of amorphous regions, it was chosen as the solvent for cleaning PMP film samples.

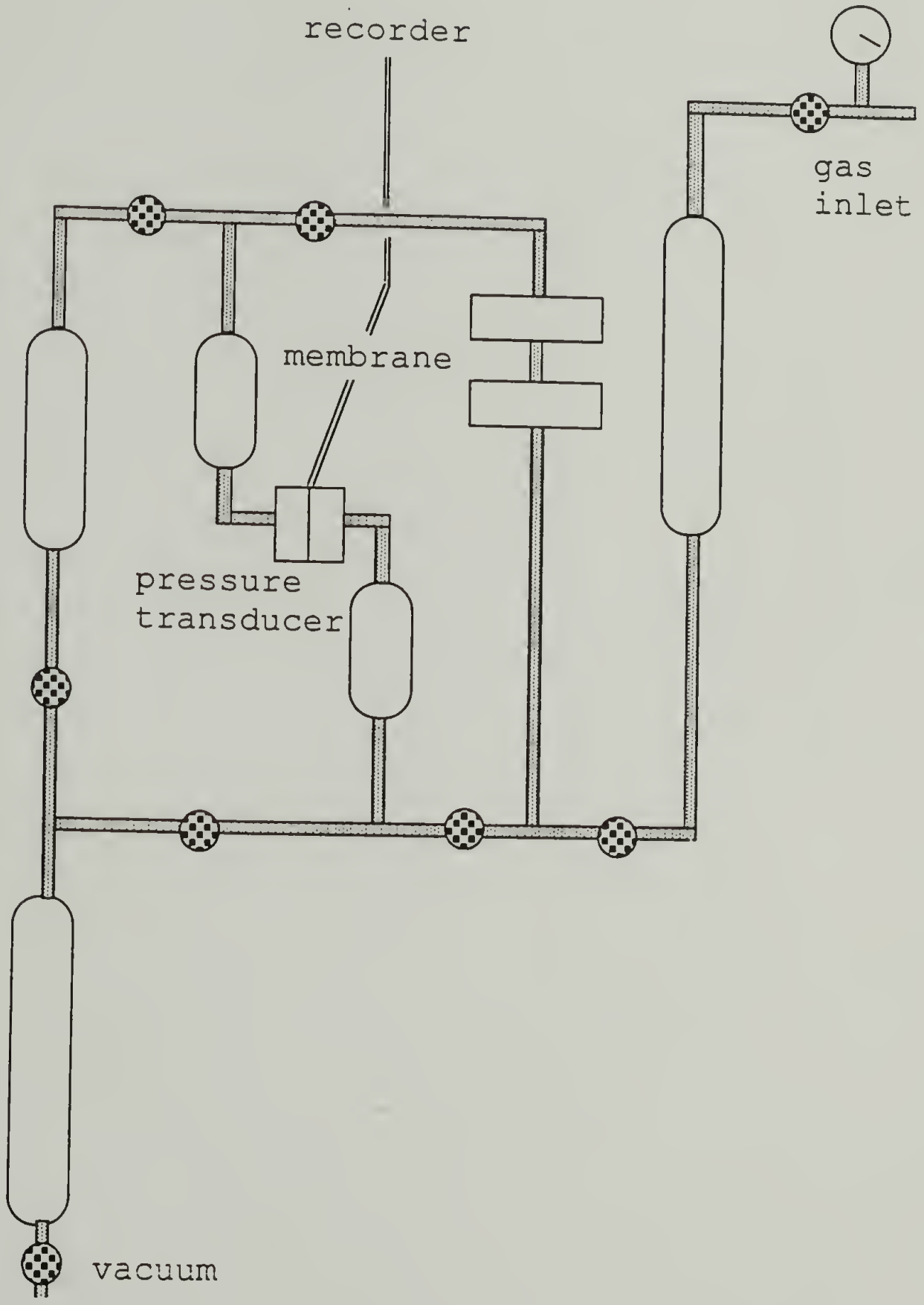

Figure 5. Gas Permeation instrument.

X-ray photoelectron spectroscopy (XPS) study of PMP samples refluxed in dichloromethane for 60 min under nitrogen gave elemental compositions of 99.6 % carbon and 0.4 % oxygen in the outermost 10 Å (15° takeoff angle experiment), and 99.9 % carbon and 0.1 % oxygen in the outermost 40 Å (75° takeoff angle experiment). As a comparison, PMP has an elemental composition of 95.6 % carbon, 3.5 % oxygen and 0.9 % sulfur in the top 10 Å region before the cleaning procedure. 60 minutes was shown to be sufficiently long time for cleaning PMP film samples as longer reflux times gave no further reductions in the oxygen content based on XPS analysis. The degree of crystallinity for PMP used in this study was shown to be 45 % based on 28 J/g heat of fusion from differential scanning calorimetry analysis shown in Figure 6.

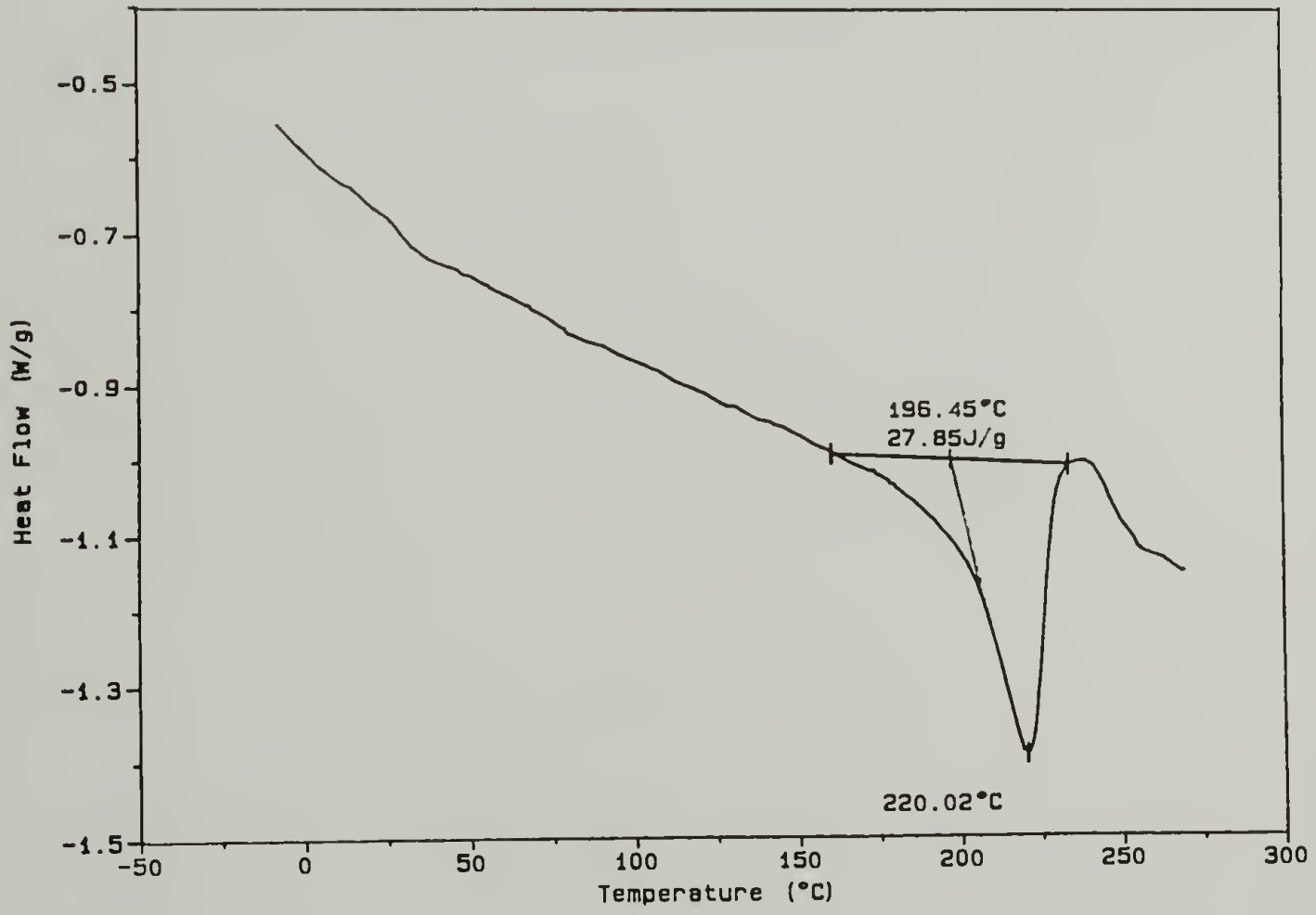

Figure 6. Differential scanning calorimetry profile of PMP used in chlorinations.

Phase Measurement Interference Microscopy indicates that the average surface roughness of clean PMP is on the nanometer scale (Figure 7).

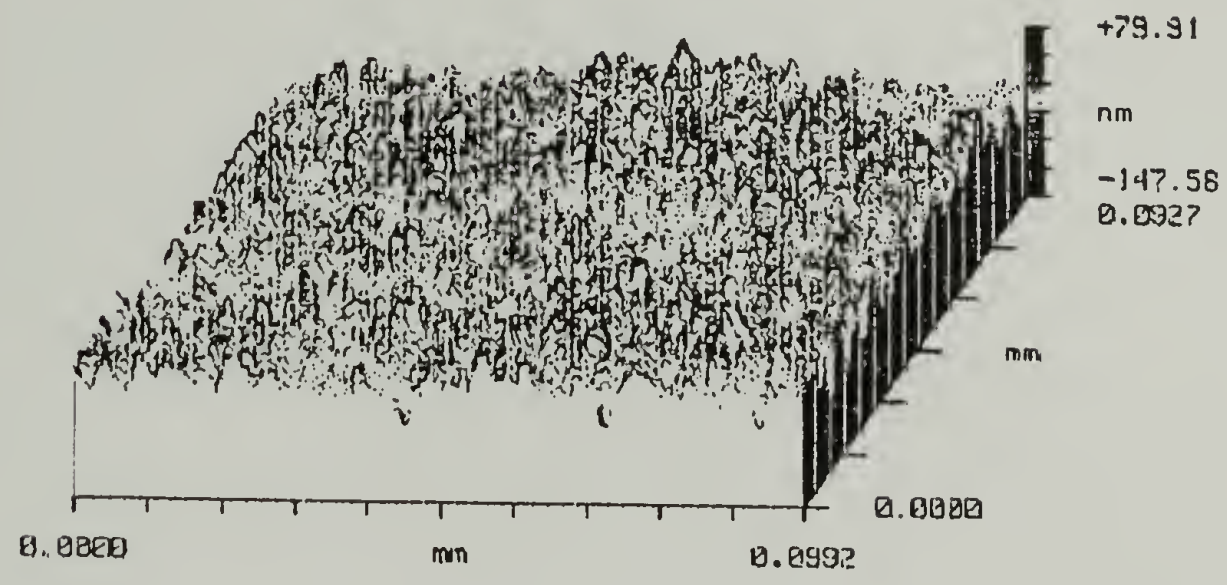

Figure 7. Surface roughness profile of clean PMP film from Phase Measurement Interference Microscopy.

Chlorination

Exposure of PMP film samples to Cl_2 gas at room temperature and ambient light conditions induces a rapid and extensive radical chain chlorination as evidenced by X-ray photoelectron spectroscopy (XPS) and gravimetric analysis. Figure 8 shows XPS survey and C_{1s} region spectra for a virgin PMP film sample and a sample that had been exposed to 1 atm of Cl_2 for 1 min.

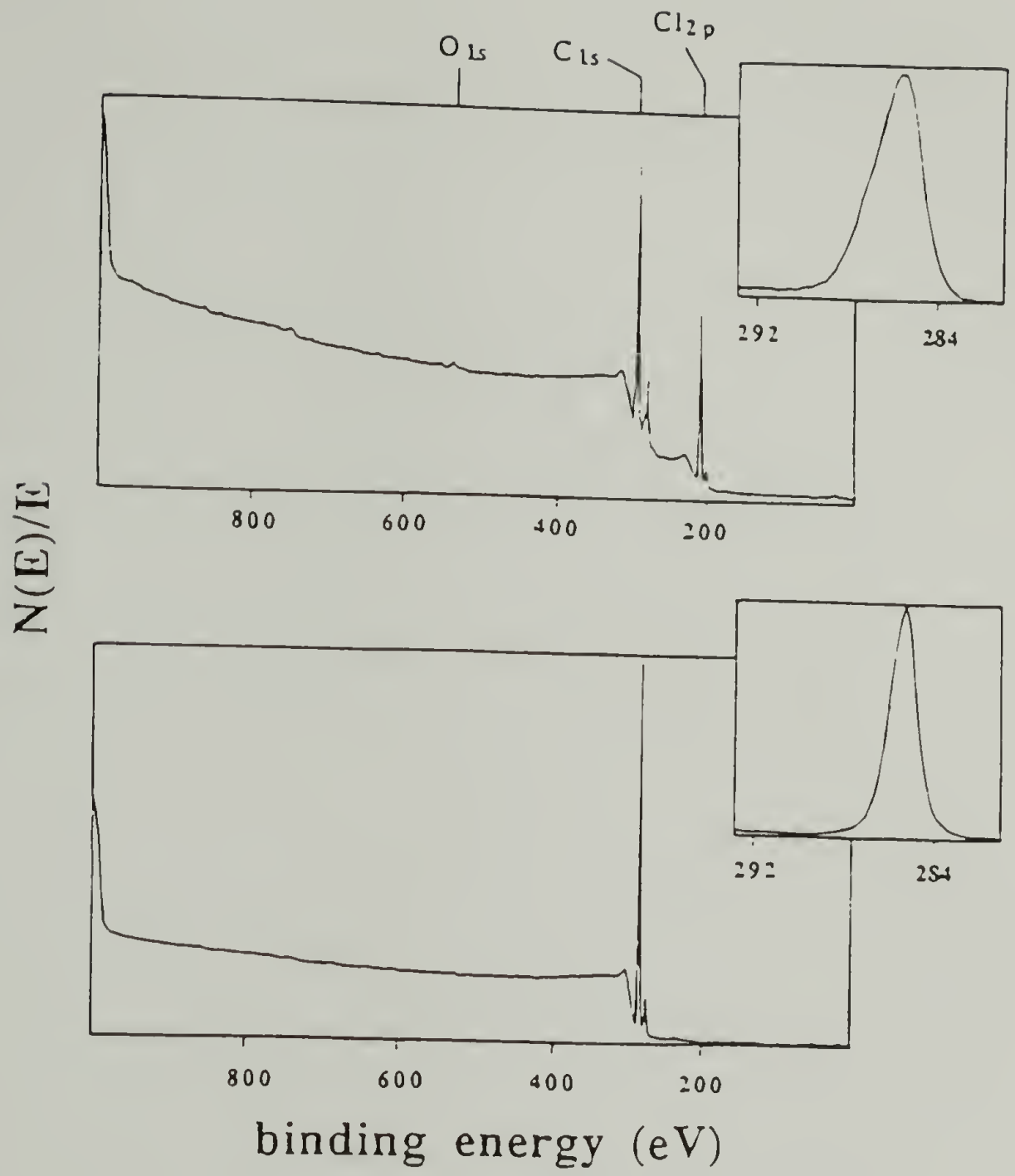

Figure 8. XPS survey spectra for unmodified PMP (lower) and PMP exposed to 1 atm of Cl_2 for 1 min (upper).

This sample increased in mass by 2.4 %. The XPS spectra were recorded at a 75° takeoff angle, which assesses the composition of the outer ~40 Å of the film. The composition of this region is C_{100} Cl_{23} (~1.4 Cl per PMP repeat unit) which corresponds to 37 wt % chlorine. The broadened C_{1s} spectrum indicates that C-Cl (carbon bound to one chlorine) is present in this sample. C-Cl and CCl_2 (carbon bound to two chlorines) are important structural features of chlorinated PMP (see below). Variable small

amounts of oxygen are observed in product film (seen in Figure 8); we attribute this to termination of the radical chain reaction by adventitious oxygen. PMP contains primary, secondary, and tertiary C-H bonds as shown in Figure 2, so a range of chlorinated product structures are possible; chlorination of small molecule hydrocarbons has been reported to be site specific with a 6.7 : 4.4 : 1 preference for tertiary : secondary : primary carbons. [8] No attempt is made in this thesis to distinguish among them but the reaction is regarded as a simple replacement of hydrogen atoms with Cl atoms. Other aspects of the reaction are inherently complex. The kinetics and surface selectivity (relative rates of reactions at different depths) will depend on both Cl_2 concentration and photointensity in ways not easily predicted. High Cl_2 concentration and high photointensity should yield rapid conversion, but the product may inhibit further reaction by acting as a barrier layer for Cl_2 diffusion.

A series of heterogeneous photochlorinations of a PMP film were carried out using a vacuum/gas manifold as a reactor with which reaction time, chlorine pressure, and photointensity could be conveniently controlled (see figure 3). The reaction time was varied from 15 s to 17 h by opening a valve to start the reaction and evacuating the manifold to stop the reaction. Chlorine pressure was varied from 5 mm to 1 atm using low-temperature baths to control subatmospheric pressures. Photointensity was controlled by four reproducible conditions by wrapping the reactor with black cloth ("dark"), exposing the reactor to ambient hood light, or shining either a medium- or high-intensity UV light source on the sample container. Use of the high-intensity UV light source created a reaction parameter that could not be controlled in the chlorination set-up that was used. Considerable heating of the sample container took place during the exposure to the light source. Figure 9 shows the temperature inside the container as a function of exposure (reaction) time.

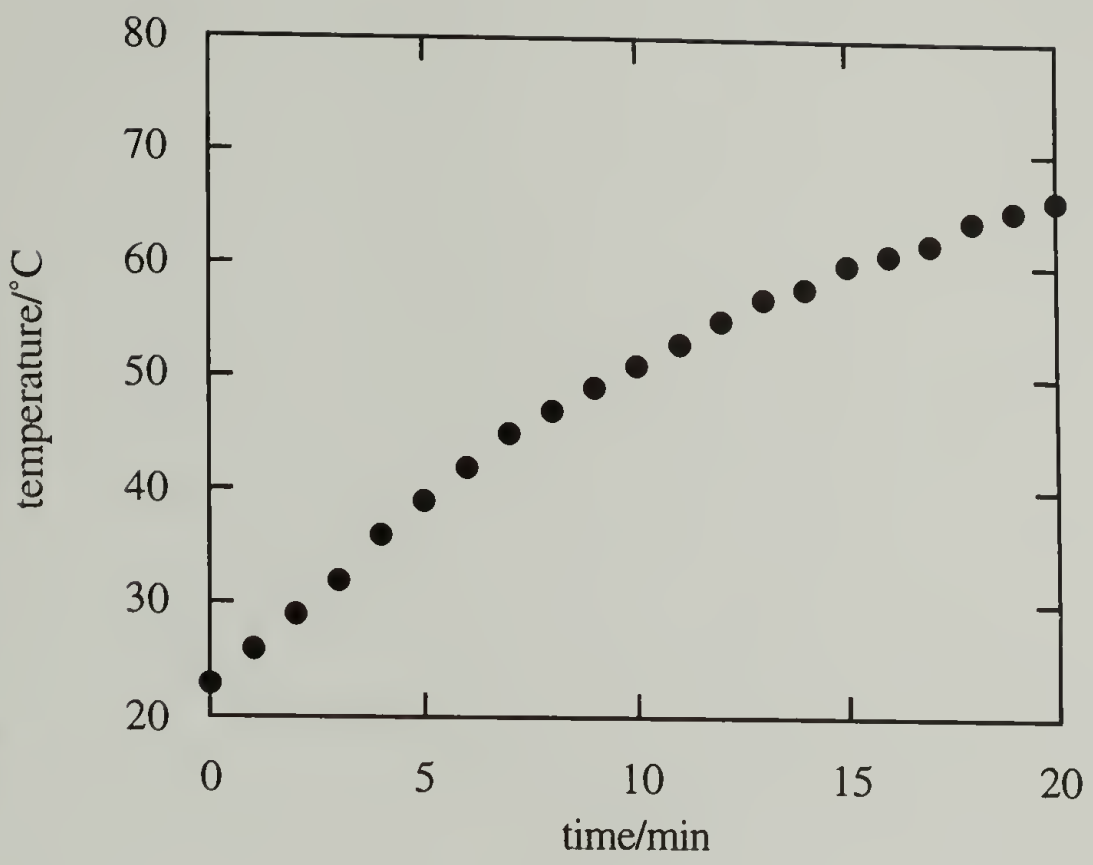

Figure 9. Temperature inside the sample container as a function of time of exposure to high-intensity UV light source.

The elevated temperature increases the mobility of PMP chain segments leading to higher diffusion rates of chlorine into the film giving deeper modifications than at the same reaction conditions at a lower temperature.

The effects of reaction time, chlorine pressure, and photointensity on both the depth of reaction and the density (on the PMP chain) of chlorination were studied with the objective of establishing conditions with which reproducible and independent control over both chlorination depth and chain density could be exercised. Gravimetric analysis and XPS were used as survey analytical methods. XPS yields a precise determination of atomic composition from which Cl:C ratios and chlorination densities can be determined for the outermost 10-40 Å of the film samples. Gravimetric analysis yields the total chlorine content of the film samples from which (along with XPS data) depths of reaction can be estimated.

Atomic composition tables from XPS analysis are presented for chlorinated samples in Tables 4a to 7a. Corresponding chlorine:carbon ratios and gravimetric data tables for the series of modifications are shown in Tables 4b to 7b. All data in these tables were acquired using the following scheme (400 W, 15 kV):

(1) 15° survey spectrum (3 min)

(2) 15° multiplex spectra (5 min)

(3) 75° multiplex spectra (5 min)

(4) 75° survey spectrum (3 min)

X-ray beam damage was shown to take place by rerunning a 15° multiplex after the scheme shown above. For example, the Cl:C ratio for a highly chlorinated sample (20 min/1 atm Cl_2/high-intensity UV light) from the rerun was lowered by approximately 15 % compared to the atomic ratio from the original acquisition (that does not take into account beam damage during the acquisition of the first survey spectrum).

Conditions were then chosen to prepare four prototypical membranes: a highly and deeply chlorinated sample (H&D), a lightly and deeply chlorinated sample (L&D), a highly and shallowly chlorinated sample (H&S), and a lightly and shallowly chlorinated sample (L&S). These prototypes were analyzed in more detail with regard to structure, composition, and their potential as gas separation membranes.

Effect of Chlorine Pressure

The rate of diffusion of chlorine into a PMP film is controlled by the chlorine vapor pressure. The effect of chlorine pressure on the product structure was studied under reaction conditions of ambient, medium-intensity UV, and high-intensity UV light and over a range of reaction times. Representative data that summarize pressure effects are presented here.

Figure 10 shows plots of both mass increase and Cl:C ratio (determined by XPS at a takeoff angle of 15° - indicative of the composition of the outermost 10 Å) versus chlorine pressure for PMP samples chlorinated for 2 min under ambient light conditions. Figure 11 shows the same data for PMP samples chlorinated for 2 min under high-intensity UV conditions.

At Cl_2 pressure above 50 mm for ambient light conditions and at all pressures studied under UV light, the extent of chlorination (density of chlorine atoms on the chain) is independent of pressure. Chlorine:carbon ratios of ~0.4 and ~1 are obtained for ambient and high-intensity UV light conditions, respectively, indicating compositions of $C_{100}Cl_{\sim 40}$ (51 wt % chlorine - 2.4 Cl atoms per PMP repeat unit) and $C_{100}Cl_{\sim 100}$ (73 wt % chlorine - 6 Cl atoms per PMP repeat unit). The mass increases, however, are highly dependent on chlorine pressure. A linear dependence on pressure is observed for the 2 min reactions under ambient light conditions (Figure 10). A PMP sample increased in mass by 0.6 % at 16 mm, and at 760 mm a 3 % increase was observed. A 47.5-fold difference in pressure yielded a 50-fold difference in mass gain. This indicates an approximate first-order rate dependence on chlorine concentration and also that mass uptake can be controlled over a significant range using pressure control. Under UV light conditions, the effect of chlorine pressure on mass increase (Figure 11) is not linear, and a greater pressure dependence is observed at low pressures. At 5 and 16 mm, mass increases of 0.2 % and 0.6 % were observed, indicating an approximate first-order chlorine pressure dependence, but at 760 mm a 3.3 % mass gain occurred - a 5-fold increase with a 47.5-fold pressure difference over the reaction at 16 mm. Nonlinear pressure dependencies of this type were observed for all reactions that produced samples that had XPS ratios greater than ~0.6. This suggests that samples containing a sufficiently high chlorine content in their modified surface region exhibit barrier properties to chlorine gas.

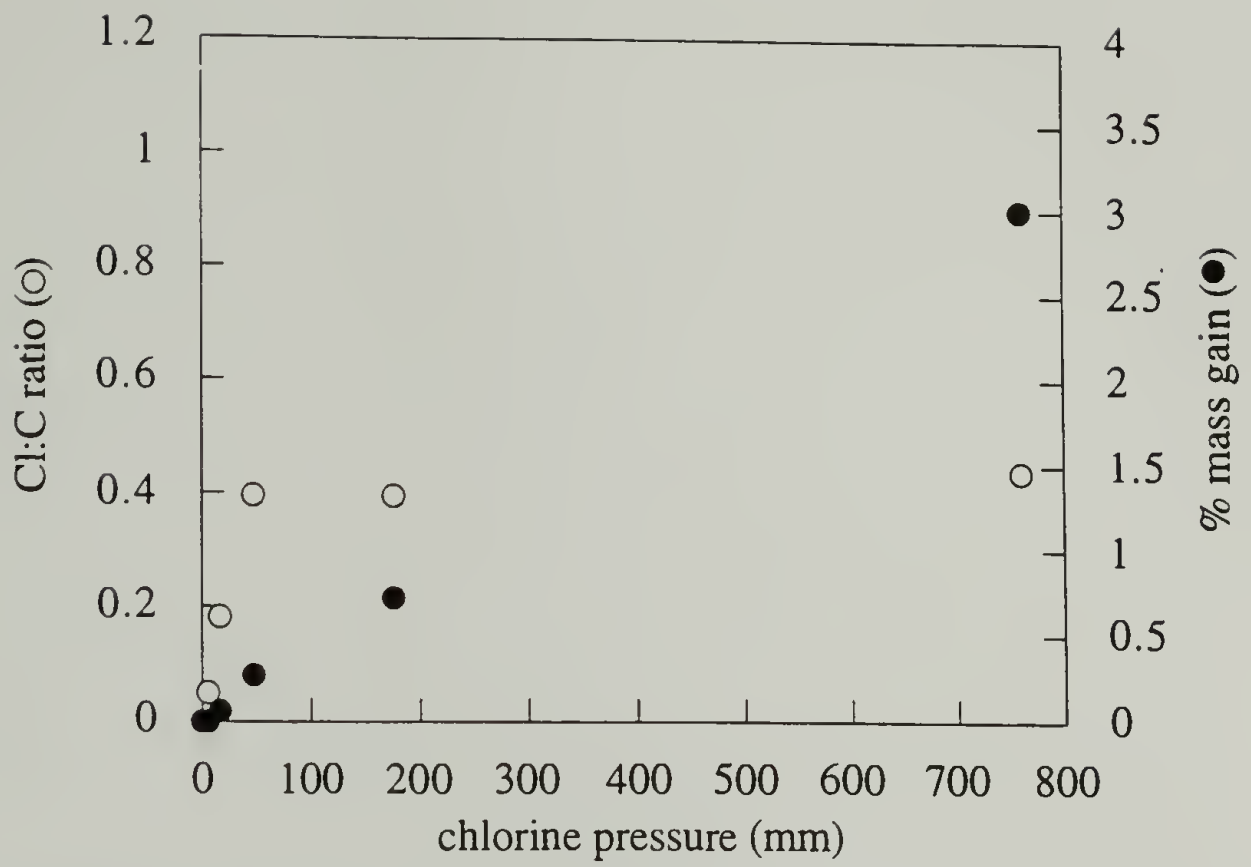

Figure 10. XPS and gravimetric data for PMP samples chlorinated in ambient light for 2 min.

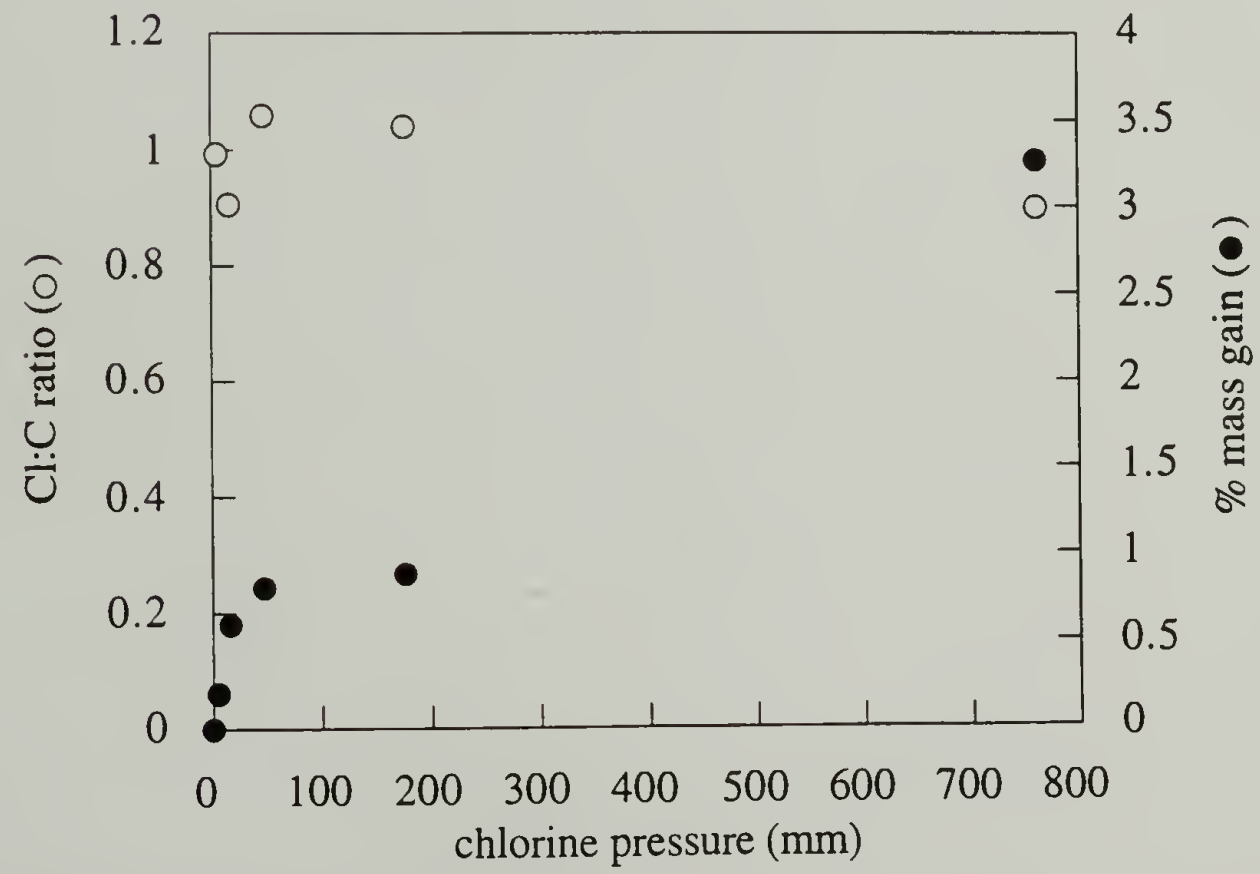

Figure 11. XPS and gravimetric data for PMP samples chlorinated in high-intensity UV light for 2 min.

The dependence of mass uptake and the independence of the Cl:C ratio in XPS data on chlorine vapor pressure allow control of the thickness of the modified layer at a constant chlorine content.

Effect of Light Source Intensity

The photointensity controls the rate of formation of chlorine radicals that initiate radical chain chlorination and thus the concentration of radical species in the PMP film region that chlorine has diffused to during reaction. The higher the photointensity, the higher the probability that chlorine molecules that diffuse into the film will react with PMP chain radicals rather than diffuse deeper into the film sample. Figure 12 indicates that photointensity controls the composition (Cl:C ratio) of the XPS sampling region. Chlorine:carbon ratios are plotted versus reaction time for samples prepared at 1 atm of Cl_2 under the four light conditions studied.

The plots indicate that for the ambient and UV conditions most of the reaction in the XPS sampling depth occurs in the first 2-5 min. Compositions level at Cl:C = ~0.6, ~0.8, and ~1.1 for ambient, medium-intensity UV, and high-intensity UV light, respectively. Reaction in the XPS sampling depth for the dark chlorination is slower and has not leveled at the times shown in Figure 12. Samples chlorinated for 40 and 120 min exhibited Cl:C ratios of 0.1.

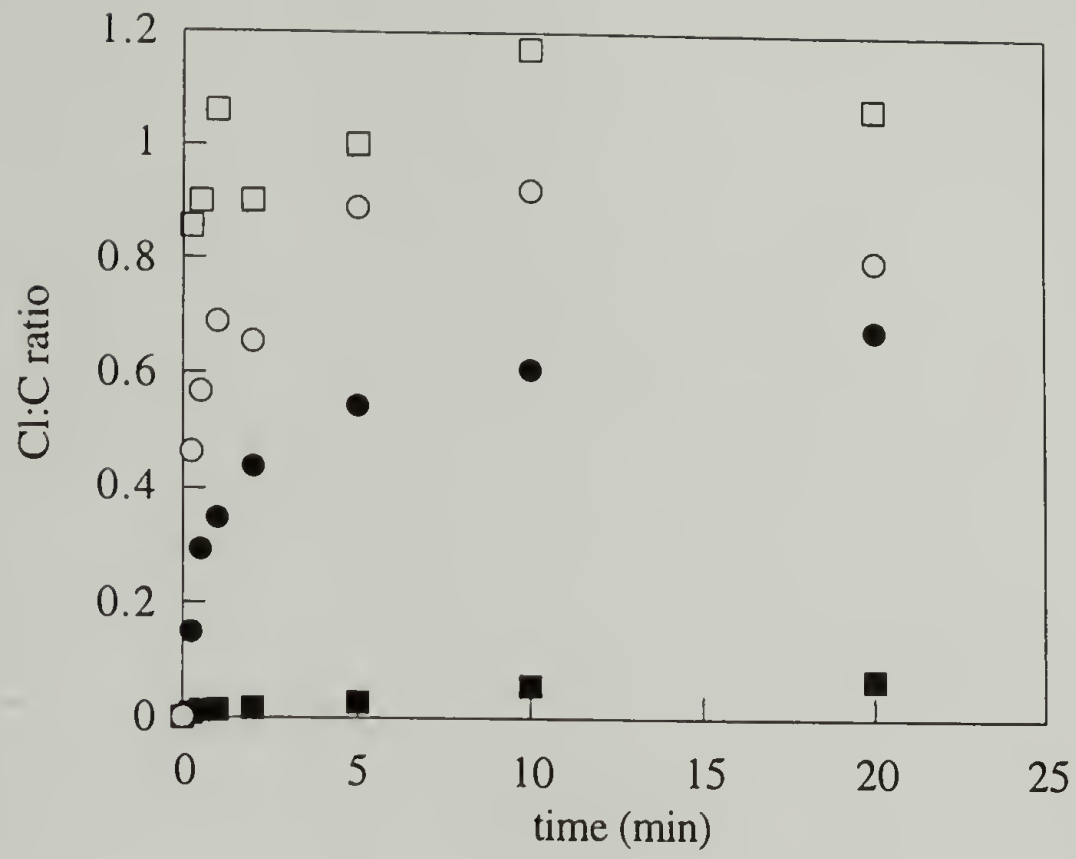

Figure 12. XPS data for PMP samples chlorinated at 1 atm of Cl_2 pressure in the dark (■), in ambient light (●), in medium-intensity UV light (○), and high-intensity UV light (□).

Figure 13 exhibits gravimetric data for the samples described in Figure 12. Samples continue to gain mass with longer reaction times under all photointensity conditions, indicating that good barrier properties toward chlorine are not achieved under any conditions: reactions proceed deep into the bulk of the film.

The differences in mass uptake rate between the ambient, medium-intensity, and high-intensity light conditions indicate that barrier properties are improved with increasing photointensity. The mass increases that occurred between 10 and 20 min of the photochlorination reactions were 5.8 %, 2.6 % and 1.3 % for ambient, medium-intensity UV, and high-intensity UV conditions, respectively. The inverse dependence of rate on photointensity can only be explained by a diffusion rate that decreases with

photointensity. The XPS composition data are consistent with this observation; the more highly chlorinated surfaces function as better barrier layers (compare Figures 12 and 13).

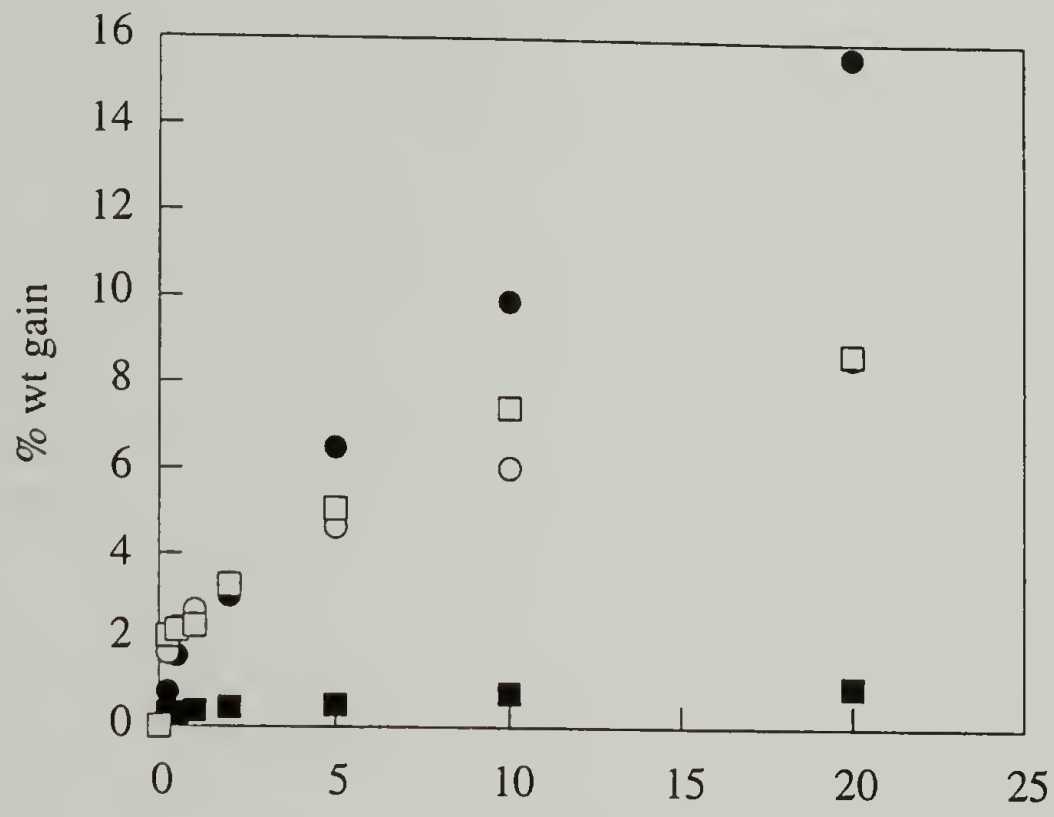

Figure 13. Gravimetric data for PMP samples chlorinated at 1 atm of Cl_2 pressure in the dark (■), in ambient light (●), in medium-intensity UV light (○), and high-intensity UV light (□).

Effect of Reaction Time. Summary of Variable Effects

The data in Figure 12 indicate that, after rather short reaction times, the extent of chlorination in the XPS sampling region is independent of reaction time. This was found to be true, in general, for chlorination reactions at all Cl_2 vapor pressures under all light conditions studied. Controlling chlorination extents with reaction time is thus not practical and, in practice, is more easily accomplished by controlling photointensity. The mass, however, increases regularly with reaction time as indicated by the plots in Figure 13. Reaction time is thus a variable that is as useful as Cl_2 vapor pressure in

controlling mass gain or thickness of the modified layer. We have concluded that the most convenient means of preparing modified PMP samples of desired extents and depths of chlorination is to use an appropriate chlorine pressure and light source and fine tune the modification by adjusting the reaction time.

Determining reaction depths or thicknesses of chlorinated layers is not straightforward. Thickness values can be calculated from the XPS composition and gravimetric data, but the values are meaningful only relatively. If we assume that the composition of the modified layer is that indicated by the XPS data, then the stoichiometry of the reactions can be determined. For example, the samples chlorinated at different pressures in ambient light for 2 min (figure 10) have Cl:C ratios of 0.1 (5 mm), 0.18 (16 mm), 0.40 (47 mm), 0.40 (176 mm), and 0.44 (760 mm). These ratios correspond to compositions of $C_{100}H_{190}Cl_{10}$ (5 mm reaction product), $C_{100}H_{182}Cl_{18}$ (16 mm), $C_{100}H_{160}Cl_{40}$ (47 mm), $C_{100}H_{160}Cl_{40}$ (176 mm), and $C_{100}H_{156}Cl_{44}$ (1 atm). Using estimates of densities for the modified layers (determined from the Cl:C ratio and the densities of PMP and poly(vinyl chloride), thicknesses can be calculated (see Appendix A) that account for the mass increases observed. Thicknesses of 0.06 (16 mm), 0.13 (47 mm), 0.34 (176 mm), and 1.3 μm (760 mm) are calculated. No mass gain was observed for the sample reacted at 5 mm. These thickness estimates are minima and assume a constant chlorine concentration throughout the modified layer. There is most certainly a gradient structure (see below) with less chlorine at greater depths; thus, the true thicknesses are greater than these estimates.

Chlorine vapor pressure and reaction time thus control the depth of modification, and these depths scale with the mass increases (at constant Cl:C ratios). The photointensity also controls thickness by controlling barrier efficiency. For example, the 20 min reactions at 1 atm of Cl_2 (Figures 12 and 13) give samples with structures of $C_{100}H_{93}Cl_{107}$ (high-intensity UV), $C_{100}H_{120}Cl_{80}$ (medium-intensity UV), $C_{100}H_{132}Cl_{68}$ (ambient), and $C_{100}H_{193}Cl_{7}$ (dark). Thicknesses of the type discussed above

for these samples are 1.5 (high-intensity UV), 2.0 (medium-intensity UV), 4.3 (ambient), and 2.6 μm (dark).

Effect of Sample Container Material

The photointensity of the light source was shown above to play an important role in both the extent and the depth of reaction. In an attempt to further enhance the radical formation in the high-intensity UV experiments, identical sample containers were made of glass and quartz. The XPS and gravimetric data table for the quartz experiments shown in Table 8 follow closely those of the chlorinations performed in glass vessel (Table 6) indicating that the sample container material does not affect the course of modification under these conditions. Thus all chlorinations to described below were done in the same glass walled container that was used in the chlorinations reported in Tables 4 to 7.

Prototype Membranes

The preliminary chlorination experiments described above indicate that the depth and extent of reaction can be controlled by adjusting three parameters: reaction time, chlorine vapor pressure, and light source intensity. Four modified sample types were chosen for more detailed surface analysis and gas permeation studies; conditions for their preparation were chosen from the preliminary chlorination data. A highly (high Cl:C ratio) and deeply chlorinated membrane (H&D) was prepared using high-intensity UV light conditions, 1 atm of chlorine pressure, and a 20 min reaction time. A highly and shallowly chlorinated membrane (H&S) was prepared using high-intensity UV light conditions, 16 mm chlorine pressure, and a 2 min reaction time. A lightly (low Cl:C ratio) and deeply chlorinated membrane (L&D) was prepared using 1 atm of

chlorine pressure, a 120 min reaction time, and dark conditions. A lightly and shallowly chlorinated membrane (L&S) was prepared using ambient light, 5 mm chlorine pressure, and a 2 min reaction time.

XPS and gravimetric data for the prototype membranes are summarized in Table 9. Separate XPS samples were used to obtain 15° and 75° takeoff angle spectra (multiplex acquired prior to survey spectrum) to minimize errors in atomic composition data due to beam damage. Each of the data points is the average of four experimental values that are presented in Table 10.

Figure 14 shows XPS C_{1s} region spectra for the four samples: spectra of the highly modified samples show the presence of significant levels of both monochlorinated and dichlorinated carbon species; spectra of the lightly chlorinated samples indicate only light monochlorination.

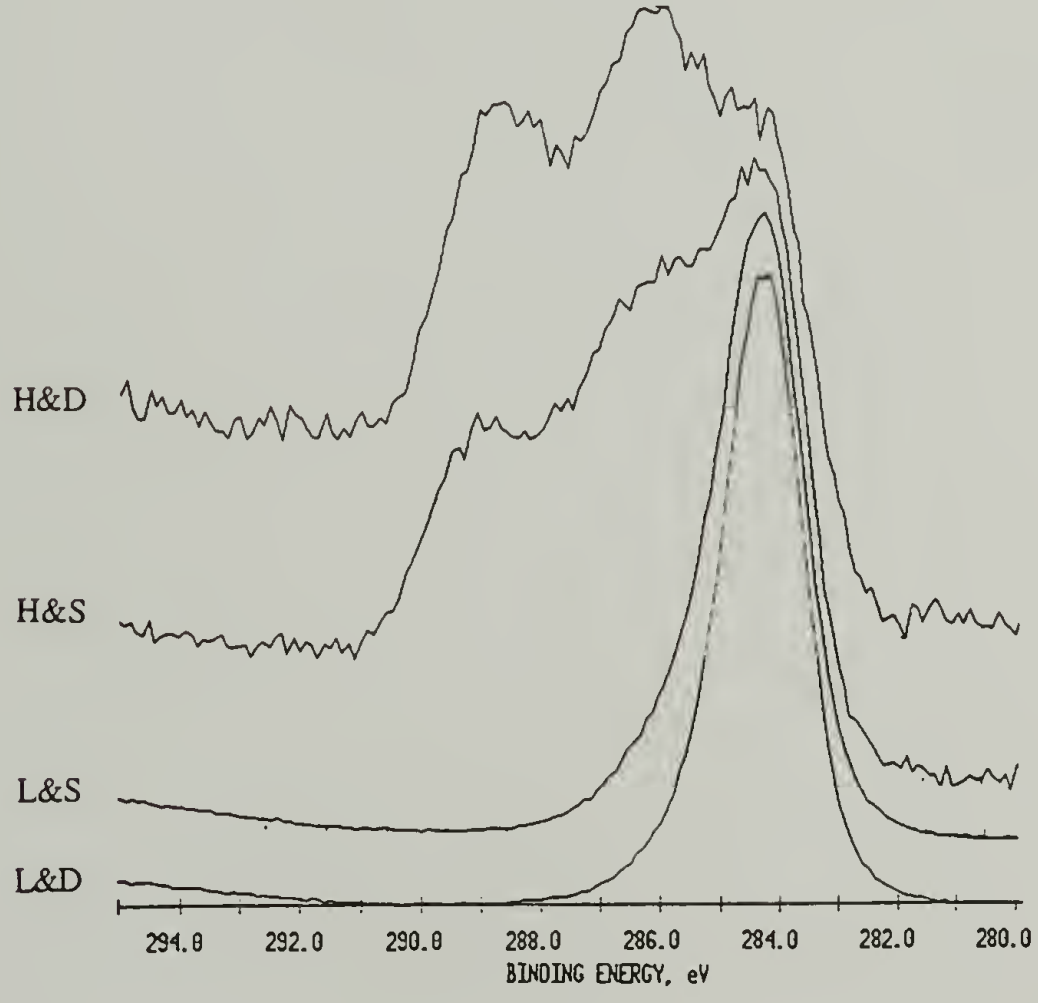

Figure 14. C_{1s} region XPS spectra for the prototype membrane samples.

Figure 15 shows the results from the deconvolution of the spectral features due to unmodified, monosubstituted, and disubstituted carbon atoms in the chlorinated prototype membranes at 15° and 75° takeoff angle XPS analysis.

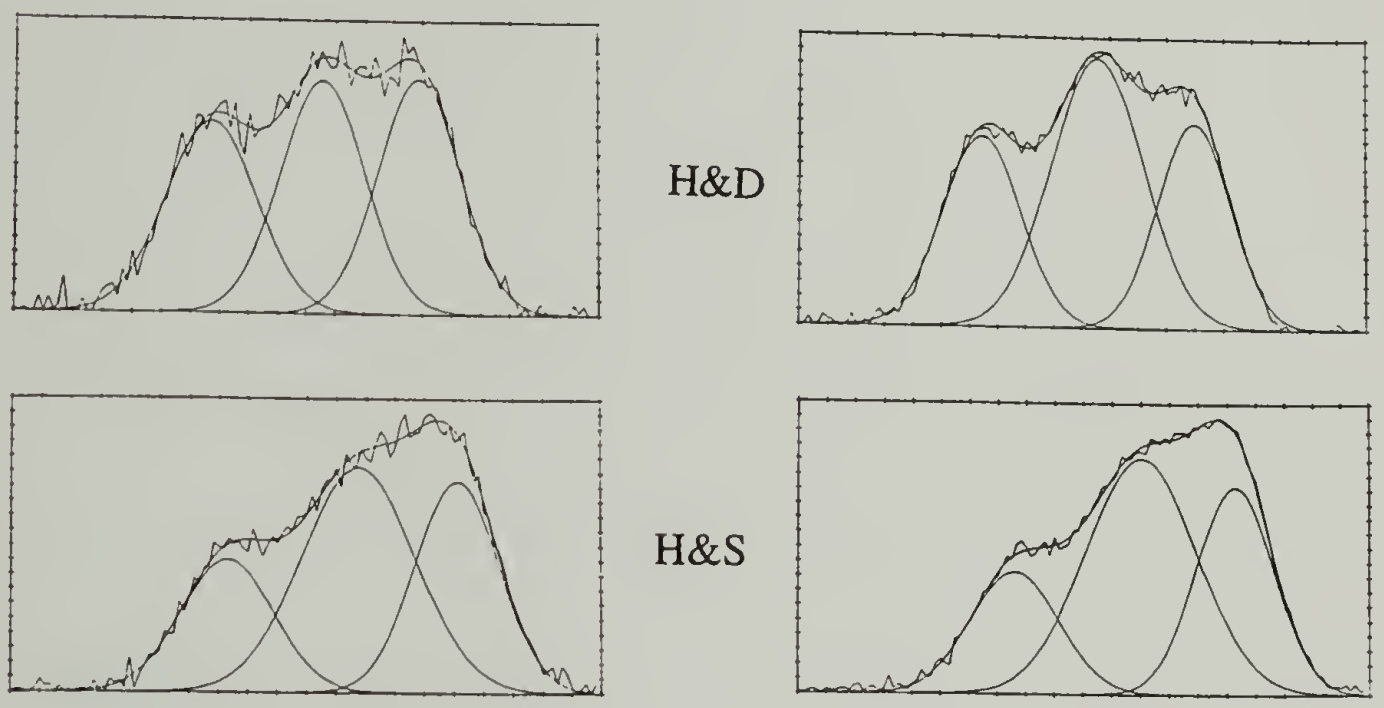

Figure 15. Deconvolution of C_{1s} spectral features from 15° (left) and 75° (right) XPS analysis on the prototype samples.

The relative abundances of unmodified and modified carbon atoms from deconvolution analysis are shown in Table 11 for the selected membranes. C_{1s} spectral features of the lightly chlorinated samples indicate the existence of unmodified and monochlorinated carbon atoms at the XPS sampling depth, whereas the highly chlorinated samples were shown to have a high number of dichlorinated carbon atoms as well. Interestingly, the relative amount of unmodified carbon atoms decreases with increasing sampling depth and the relative amount of monochlorinated carbon atoms increases with the sampling depth, even though the extent or density of chlorination decreases with the sampling depth (see Table 9 for chlorine:carbon ratios). This suggests that as the reaction conditions at the outermost skin lead to a relatively high number of unmodified and dichlorinated carbon atoms, and reaction taking place deeper in the film leads to more uniformly monochlorinated carbon atoms. Reasons for these differences are complicated, but parameters such as local reactant concentration and UV light intensity as well as intermediate and product stability are likely to play an important role in the outcome of the modification.

Chlorinated layer thickness values (estimated by the method described in Appendix 2) are 1.5 μm for H&D, 0.07 μm for H&S and 4.1 μm for L&D. The L&S sample gained no measurable mass. The takeoff angle dependence of the Cl:C ratio, which is observed for all the samples, reveals that the outermost 10 Å of the membranes is more extensively chlorinated than the next deeper 30 Å. This suggests that there is a gradient chlorine density throughout the modified layers of each of the samples and that the calculations underestimate the actual thicknesses. The sharp takeoff angle dependence of the Cl:C ratio for the L&S sample (Table 9) and the gravimetric data (no mass gain) indicate a very shallow modification. The thickness of the modified layer in the L&D sample is understandable as in the absence of a light source the reactivity of chlorine is suppressed but the diffusion of chlorine gas into the film is unaffected.

The four samples were also analyzed by contact angle analysis, ATR IR, and transmission IR, and an H&D sample was analyzed by phase measurement interference microscopy (PMIM). PMIM indicates that no gross topographical changes occur upon chlorination as can be seen in surface roughness profiles in Figures 7 and 16.

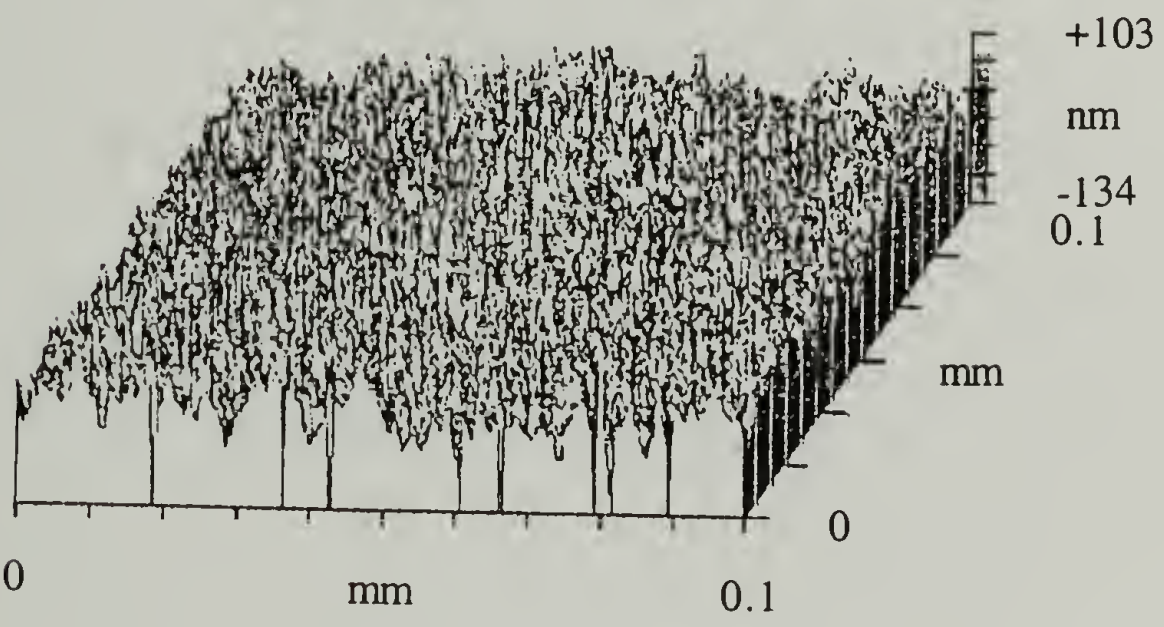

Figure 16. Surface roughness profile for the highly & deeply chlorinated PMP membrane from Phase Measurement Interference Microscopy.

Contact angle measurements (Table 12) were carried out with both water and diiodomethane as probe fluids. Water contact angles do not clearly differentiate between chlorinated samples, but both advancing and receding angles show clear differences with an unmodified film. Measurements with diiodomethane as the probe fluid also show differences within the series of modified samples. Diiodomethane contact angles (that indicate structure in the outermost few ångströms) decrease with increasing chlorine content, as determined by XPS analysis (of a thicker region).

Figure 17 displays transmission and ATR (45° KRS-5 internal reflection element) infrared spectra for virgin PMP and the four prototype membranes. The complexity of the region is a result of the C-Cl stretch interaction with C-C and other stretching and/or bending oscillators. The observed absorption frequencies depend on the actual spatial arrangement of the atoms. C-Cl stretching vibrations are observed at ~740-700 cm^{-1} (a carbon atom is trans to chlorine; a planar C-C-C-Cl zigzag arrangement) and ~660-620 cm^{-1} (a hydrogen atom is trans to chlorine; a gauche C-C-C-Cl arrangement) for all the chlorinated samples and are more intense with increasing depth and extent of modification. The ATR IR sampling depth under the conditions of these analyses is ~2 μm. Comparing the transmission and ATR spectra of the H&D sample reveals that little if any unreacted PMP remains in the ATR IR sampling depth. This suggests that both amorphous and crystalline PMP are chlorinated under these conditions. The transmission spectrum indicates, however, that the majority of PMP in the bulk of the sample is unreacted.

In order to further investigate the depths of selected modifications, ATR IR spectra were also acquired using Ge internal reflection elements (30°, 45° and 60°) as they probe only ~0.2 μm into the bulk of sample at these particular frequencies. The use of Ge crystals gave spectral features similar to those from measurements with KRS-5 element (see Figure 18 for ATR IR spectra acquired using a 45° Ge crystal), suggesting that even the shallow modifications proceed deeper than the sampling depth of Ge crystals, or the technique is not sensitive enough to differentiate between different modification depths.

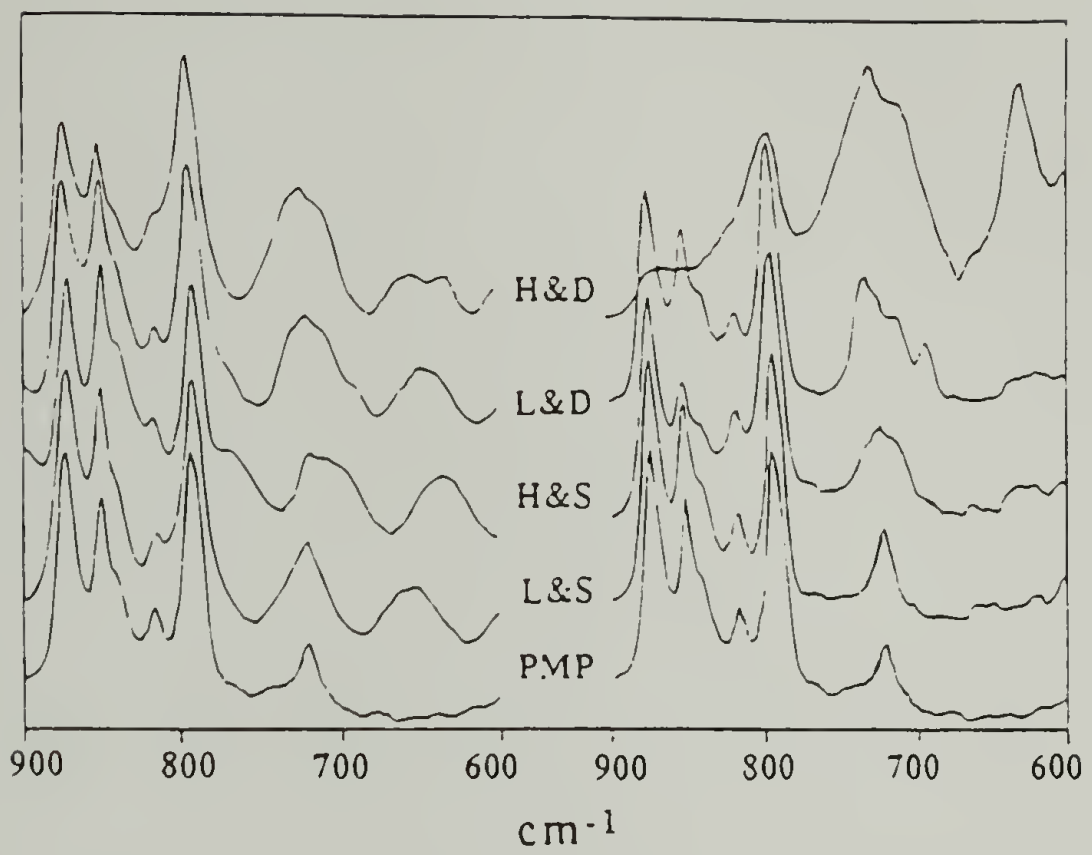

Figure 17. Transmission (left) and ATR (right; 45° KRS-5 internal reflection crystal) infrared spectra for virgin PMP and the prototype membrane samples.

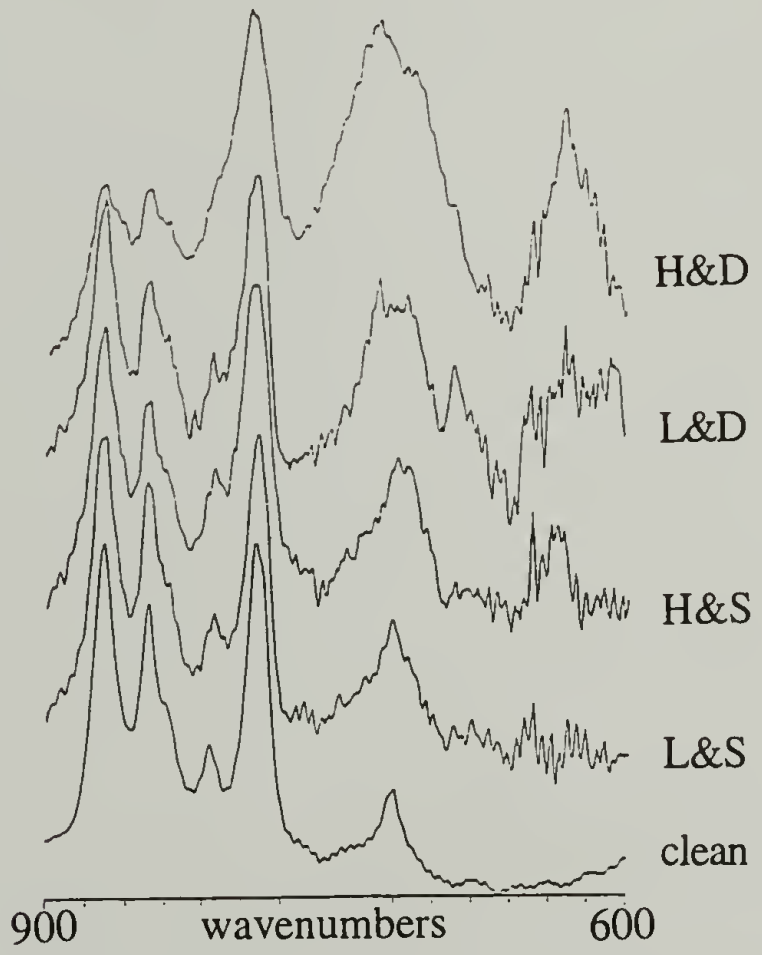

Figure 18. ATR IR spectra for virgin PMP and the prototype membrane samples acquired using a 45° Ge internal reflection crystal.

Gas Permeation Results

Gas permeability data in Table 13 shows that, for the set of gases studied, a high extent of reaction in a deeply modified layer is necessary to change diffusion rates and selectivities. The L&S, L&D, and H&S samples exhibit no differences in permeability compared with virgin PMP within experimental variation. The H&D chlorinated membrane shows decreased permeabilities for all gases studied.

The selectivities between all gas pairs are enhanced in the H&D chlorinated membrane over virgin PMP (Table 14). The largest increase in selectivity is 5.8-fold for the hydrogen/nitrogen pair with a 46 % decrease in hydrogen flux. The need for deep modification suggests that a chlorinated layer of PMP does not have excellent barrier properties; the selective skin on typical asymmetric membranes is 0.1-0.5 μm.

Conclusions

The heterogeneous chlorination of poly(4-methyl-1-pentene) can be controlled by choosing the appropriate combination of chlorine vapor pressure, light intensity, and reaction time. The depth of the reaction can be controlled with the chlorine vapor pressure and/or reaction time, and photointensity plays an important role in the extent and reaction. Gas permeability data as well as the chlorination kinetics indicate that the chlorinated layer does not have excellent barrier properties. Only highly and deeply chlorinated membranes show decreases in gas permeability. The improved selectivities observed demonstrate that rationally controlled surface modification is a viable route to asymmetric gas separation membranes.

Table 3. Chlorine vapor pressures with various cold baths.

temperature	equilibrated P/mm	reaction P/mm
-97	16	5
-83	48	16
-63	140	47
-44	520	176

Table 4. Chlorinations at ambient light condition.
a. XPS atomic composition data.

		15 deg.				75 deg.			
P/mm	time/min	C	Cl	O	Si	C	Cl	O	Si
5	0.25	91.86	0.79	5.06	2.29	98.23	0.19	1.17	0.4
5	0.5	89.17	5.65	4.35	0.84	96.39	2.81	0.61	0.18
5	1	93.78	2.72	2.4	1.1	98.7	0.74	0.47	0.1
5	2	85.77	4.39	6.62	3.21	94.44	3.51	1.48	0.57
5	5	87.23	7.98	4.19	0.6	92.3	6.82	0.8	0.08
5	10	80.6	16.81	1.91	0.68	87.6	11.49	0.79	0.13
5	20	75.09	17.54	2.28	5.09	83.51	13.6	0.8	2.09
16	0.25	90.58	3.14	4.69	1.59	96.2	1.89	1.42	0.5
16	0.5	83.55	12.31	3.47	0.66	92.55	6.73	0.72	
16	1	87.37	10.07	2.56		93.51	6.09	0.4	
16	2	83.52	13.86	2.62		91.58	7.47	0.95	
16	5	70.93	27.06	2.01		79.91	19.6	0.49	
16	10	71.96	24.57	2.36	1.11	81.16	17.75	0.78	0.31
16	20	65.58	29	3.98	1.43	77.55	21.02	1.13	0.3
47	0.25	85.45	13.02	1.53		91.74	7.88	0.38	
47	0.5	87.82	10.52	1.66		94.16	5.39	0.45	
47	1	75.9	22.56	1.54		85.53	13.7	0.77	
47	2	71.14	25.92	1.99	0.96	79.26	19.88	0.67	0.19
47	5	71.9	25.31	2.79		84.46	14.7	0.84	
47	10	66.24	30.14	2.35	1.26	73.91	24.39	1.36	0.34
47	20	60.71	32.3	7		72.27	26.82	0.91	
176	0.25	87.62	9.83	2.55		96.31	3.24	0.45	
176	0.5	76.53	14.13	6.77	2.57	86.04	10.76	2.03	1.17
176	1	72.11	24.74	3.15		80.22	19.32	0.46	
176	2	70.05	27.57	2.38		78.05	21.56	0.39	
176	5	69.03	28.96	2		71.05	27.38	1.57	
176	10	64.68	33.4	1.92		71.91	27.4	0.68	
176	20	63.98	33.35	2.68		70.36	28.79	0.85	
760	0.25	86.23	12.48	1.3		91.8	7.61	0.59	
760	0.5	74.29	19.26	3.86	2.58	83.28	15.62	0.86	0.24
760	1	74.54	23.95	1.51		80.9	18.14	0.96	
760	2	68.4	24.3	4.71	2.59	74.88	23.96	0.82	0.34
760	5	64.15	34.14	1.71		69.42	29.24	1.35	
760	10	60.13	35.97	2.39	1.5	66.05	32.77	0.89	0.29
760	20	58.98	39.45	1.57		64.08	34.72	1.2	

Continued, next page

Table 4, continued
b. XPS atomic ratios and gravimetric data.

P/mm	time/min	15 deg. Cl/C	75 deg. Cl/C	Wt. gain/%
5	0.25	0.00860004	0.00193424	0.0745
5	0.5	0.06336212	0.0291524	0
5	1	0.02900405	0.00749747	0.0476
5	2	0.0511834	0.03716645	0
5	5	0.09148229	0.07388949	0.0804
5	10	0.20856079	0.13116438	0.0228
5	20	0.23358636	0.16285475	0.257
16	0.25	0.03466549	0.01964657	0.0209
16	0.5	0.14733692	0.07271745	0
16	1	0.11525695	0.06512672	0.0646
16	2	0.16594828	0.08156803	0.0621
16	5	0.38150289	0.24527594	0.0852
16	10	0.34143969	0.21870379	0.404
16	20	0.44220799	0.27105093	0.461
47	0.25	0.15236981	0.08589492	0.0442
47	0.5	0.11979048	0.05724299	0.0765
47	1	0.2972332	0.16017772	0.166
47	2	0.36435198	0.25082009	0.269
47	5	0.35201669	0.17404689	0.501
47	10	0.45501208	0.32999594	0.829
47	20	0.53203756	0.37110834	1.325
176	0.25	0.112189	0.03364137	0.0845
176	0.5	0.18463348	0.12505811	0.0933
176	1	0.34308695	0.2408377	0.389
176	2	0.39357602	0.27623318	0.723
176	5	0.41952774	0.38536242	1.498
176	10	0.51638837	0.38103185	2.126
176	20	0.52125664	0.40918135	2.622
760	0.25	0.14472921	0.0828976	0.788
760	0.5	0.25925427	0.18756004	1.627
760	1	0.321304	0.22422744	2.388
760	2	0.35526316	0.31997863	3.007
760	5	0.53219018	0.42120426	6.497
760	10	0.59820389	0.49613929	9.885
760	20	0.6688708	0.54182272	15.67

Table 5. Chlorinations using a medium-intensity UV light source.
a. XPS atomic composition data.

		15 deg.				75 deg.		
P/mm	time/min	C	Cl	O		C	Cl	O
16	10	55.83	41.39	2.78		60.53	36.61	2.86
16	20	50.79	44.5	4.72		55.77	41.19	3.04
47	0.25	67.04	30.84	2.12		75.24	23.45	1.31
47	0.5	65.05	33.17	1.79		73.43	25.13	1.45
47	1	59.35	37.44	3.21		67.22	30.68	2.1
47	2	61.61	35.85	2.54		69.08	29.67	1.25
47	5	57.29	38.83	3.88		67.46	30.85	1.69
47	10	48.03	47.88	4.09		55.43	41.48	3.09
47	20	50.32	45.22	4.46		56.06	39.63	4.31
176	0.25	64.97	33.52	1.51		72.1	27.08	0.82
176	0.5	69.58	28.25	2.17		77.11	22.05	0.84
176	1	58.86	37.79	3.35		66.6	32.07	1.33
176	2	57.86	39.57	2.57		64.01	34.69	1.31
176	5	54.38	40.69	4.93		61.78	36.59	1.63
176	10	55.14	52.48	2.38		61.86	36.34	1.8
176	20	56.41	40.82	2.76		59.51	38.4	2.08
760	0.25	66.47	30.78	2.75		73.34	25.69	0.96
760	0.5	61.83	35.19	2.98		70.49	28.49	1.03
760	1	57.37	39.97	2.66		65.06	33.59	1.35
760	2	59.55	37.84	2.62		65.77	33.11	1.12
760	5	50.97	46.42	2.6		58.31	40.51	1.18
760	10	51.79	46.58	1.62		56.62	41.61	1.78
760	20	54.34	43.21	2.46		60.08	38.86	1.06

Continued, next page

Table 5, continued
b. XPS atomic ratios and gravimetric data.

		15 deg.		75 deg.	
P/mm	time/min	Cl/C		Cl/C	Wt gain/%
16	10	0.74135769		0.60482405	0.289
16	20	0.87615672		0.73856912	1.045
47	0.25	0.46002387		0.31166932	0.14
47	0.5	0.50991545		0.3422307	0.23
47	1	0.63083404		0.45641178	0.223
47	2	0.58188606		0.42950203	0.672
47	5	0.67777972		0.45730803	0.64
47	10	0.99687695		0.74833123	1.031
47	20	0.89864865		0.70692116	1.792
176	0.25	0.51593043		0.37558946	0.43
176	0.5	0.40600747		0.28595513	0.593
176	1	0.64203194		0.48153153	0.81
176	2	0.68389215		0.54194657	0.971
176	5	0.74825303		0.59226287	1.197
176	10	0.95175916		0.58745554	1.701
176	20	0.72363056		0.6452697	2.742
760	0.25	0.46306604		0.35028634	1.695
760	0.5	0.56914119		0.4041708	2.283
760	1	0.6967056		0.51629265	2.679
760	2	0.63543241		0.50342101	3.303
760	5	0.9107318		0.69473504	4.636
760	10	0.89940143		0.73489933	6.026
760	20	0.79517851		0.64680426	8.664

Table 6. Chlorinations using a high-intensity UV light source.
a. XPS atomic composition data.

		15 deg.				75 deg.		
P/mm	time/min	C	Cl	O		C	Cl	O
5	2	52.46	40.58	6.95		57.92	40.41	1.68
5	5	51.62	45.78	2.61		54.94	42.19	2.87
16	2	52.2	44.95	2.85				
16	5	47.92	49.56	2.52		51.03	47.36	1.61
47	2	48.56	48.38	3.06		52.22	46.5	1.28
47	5	45.1	53.11	1.78		48.17	50.15	1.68
176	2	47.61	48.57	3.82		52.06	46.75	1.19
176	5	45.37	51.35	3.29		49.68	48.09	2.23
760	0.25	50.91	43.64	5.44		60.31	37.54	2.16
760	0.5	51.53	45.63	2.84		57.87	40.1	2.03
760	1	48.64	48.81	2.55		52.57	45.63	1.8
760	2	52.36	44.97	2.67		57.5	40.52	1.98
760	5	49.16	48.02	2.82		53.13	44.28	2.59
760	10	46.11	50.08	3.8		49.71	48.15	2.14
760	20	46.75	49.8	3.45		50.31	47.89	1.8

Continued, next page

Table 6, continued
b. XPS atomic ratios and gravimetric data

		15 deg.		75 deg.	
P/mm	time/min	Cl/C		Cl/C	Wt gain/%
5	2	0.77354175		0.69768646	0.204
5	5	0.88686556		0.76792865	0.47
16	2	0.86111111			0.601
16	5	1.03422371		0.92808152	0.401
47	2	0.99629325		0.89046342	0.81
47	5	1.17760532		1.04110442	1.46
176	2	1.02016383		0.89800231	0.888
176	5	1.13180516		0.96799517	2.27
760	0.25	0.85719898		0.62245067	2.1
760	0.5	0.88550359		0.69293243	2.22
760	1	1.00349507		0.86798554	2.34
760	2	0.85886173		0.70469565	3.27
760	5	0.97681041		0.83342744	5.06
760	10	1.08609846		0.96861798	7.42
760	20	1.06524064		0.95189823	8.72

Table 7. Chlorinations in the dark.

a. XPS atomic composition data.

		15 deg.			75 deg.		
P/mm	time/min	C	Cl	O	C	Cl	O
760	0.25	97.15	0.8	2.04	99.31	0.26	0.43
760	0.5	98.42	1.14	0.44	99.13	0.47	0.4
760	1	97.01	1.4	1.58	97.61	0.96	1.43
760	2	97.1	1.72	1.18	98.61	0.88	0.51
760	5	93.67	2.63	3.7	98.34	1.42	0.25
760	10	94.2	5.19	0.61	96.7	2.86	0.44
760	20	91.28	6.03	2.69	96.24	3.18	0.58
760	40	89.31	7.93	2.76	94.23	4.97	0.79
760	60	92.03	6.47	1.5	95.05	4.18	0.77
760	120	90.08	9.2	0.72	93.75	5.65	0.6

b. XPS atomic ratios and gravimetric data

		15 deg.	75 deg.	
P/mm	time/min	Cl/C	Cl/C	Wt gain/%
760	0.25	0.00823469	0.00261806	0.293
760	0.5	0.01158301	0.00474125	0.308
760	1	0.0144315	0.00983506	0.36
760	2	0.0177137	0.00892404	0.456
760	5	0.02807729	0.0144397	0.504
760	10	0.05509554	0.02957601	0.779
760	20	0.06606047	0.03304239	0.96
760	40	0.08879185	0.05274329	1.52
760	60	0.07030316	0.04397685	1.25
760	120	0.10213144	0.06026667	2.25

Table 8. Chlorinations in a quartz vessel using a high-intensity UV light source.

a. XPS atomic composition data.

		15 deg.			75 deg.		
P/mm	time/min	C	Cl	O	C	Cl	O
760	0.25	52.7	44.18	3.13	59.73	39.17	1.09
760	0.5	52.11	46.64	1.25	56.12	42.43	1.35
760	1	54.47	44.27	1.26	58.63	40.01	1.36
760	2	50.55	47.39	2.05	55.13	43.21	1.65
760	5	49.82	47.66	2.52	53.41	44.87	1.72
760	10	46.2	50.96	2.84	50.49	46.97	2.53
760	20	47.25	49.19	3.56	51.92	45.5	2.57

b. Chlorine:carbon atomic ratios and gravimetric data.

		15 deg.	75 deg.	
P/mm	time/min	Cl/C	Cl/C	Wt gain/%
760	0.25	0.83833017	0.65578436	1.517
760	0.5	0.89502974	0.75605845	1.785
760	1	0.81274096	0.68241515	2.123
760	2	0.93748764	0.78378378	3.139
760	5	0.95664392	0.84010485	3.896
760	10	1.1030303	0.93028322	6.528
760	20	1.0410582	0.87634823	8.409

Table 9. XPS and gravimetric data summary for the prototype membranes.

sample	Cl:C (15°)[a]	Cl:C (75°)[a]	mass gain/%
H&D	1.1	1.0	8.4
H&S	0.9	0.8	0.4
L&D	0.05	0.04	2.0
L&S	0.1	0.07	0.0

[a] XPS takeoff angle.

Table 10. Experimental variations in the XPS and gravimetric data for the selected membranes.

sample	Cl:C (15°)[a]	Cl:C (75°)[a]	mass gain/%
H&D	1.020	1.067	7.691
	1.096	1.070	8.858
	1.212	1.002	8.215
	1.119	1.017	8.697
H&S	0.842	0.799	0.563
	0.893	0.832	0.498
	0.864	0.753	0.415
	0.968	0.882	0.304
L&D	0.040	0.027	1.671
	0.070	0.050	2.329
	0.066	0.036	2.283
	0.043	0.030	1.817
L&S	0.101	0.075	0.0866
	0.084	0.089	0
	0.116	0.049	0
	0.115	0.048	0

Table 11. Relative abundance of different carbon atom types from deconvolution of C_{1s} peaks in XPS analysis at 15° and 75° takeoff angles.

sample	% CH_2		% CHCl		% CCl_2	
	(15°)[a]	(75°)[a]	(15°)[a]	(75°)[a]	(15°)[a]	(75°)[a]
H&D	34	27	35	46	31	27
H&S	32	30	46	49	22	21
L&D	91	89	9	11	-	-
L&S	79	89	21	11	-	-

[a] XPS takeoff angle

Table 12. Contact angle data.

sample	H_2O		CH_2I_2	
	θ_A	θ_R	θ_A	θ_R
PMP	122	95	77	38
H&D	93	65	25	0
H&S	94	64	15	0
L&D	108	68	60	14
L&S	93	68	47	2

Table 13. Gas Permeability Data.

sample	$P(N_2)$[a]	$P(O_2)$[a]	$P(CO_2)$[a]	$P(H_2)$[a]
PMP	1.3	5.4	11.5	22.0
H&D	0.12	0.90	2.3	11.8
H&S	1.3	4.5	11.9	20.5
L&D	1.3	4.4	10.7	18.2
L&S	1.1	4.0	11.7	21.1

[a] 10^{-9} cm^3 (STP) cm/cm^2 s cmHg

Table 14. Gas Selectivity Data

sample	O_2/N_2	H_2/N_2	CO_2/N_2	CO_2/O_2	H_2/O_2	H_2/CO_2
PMP	4.1	16.5	8.6	2.1	4.1	1.9
H&D	7.3	95.9	18.9	2.6	13.1	5.1

References

(1) Cross, E.; McCarthy, T. J. *Macromolecules* **1992**, *25*, 2603.

(2) Elman, J. F.; Gerenser, L. J.; Goppert-Berarducci, K. E.; Pochan, J. M. *Macromolecules* **1990**, *23*, 3922.

(3) Csernica, J.; Rein, D. H.; Baddour, R. F.; Cohen, R. E. *Macromolecules* **1991**, *24*, 3612.

(4) Chiao, C. C. *U.S. Patent 4,828,585, 1989.*

(5) Mohr, J. M.; Paul, D. R.; Pinnau, I.; Koros, W. J. *J. Membr. Sci.* **1991**, *56*, 77.

(6) Mohr, J. M.; Paul, D. R. *Polymer* **1992**, *33*, 57.

(7) Mohr, J. M.; Paul, D. R.; Mlsna, T. E.; Lagow, R. J. *J. Membr. Sci.* **1991**, *55*, 131.

(8) Sykes, P. *A Guidebook to Mechanism in Organic Chemistry;* 5 ed.; Longman Group Limited: Essex, 1981, pp 397.

CHAPTER 3

GAS PERMEABILITY OF POLYELECTROLYTE MULTILAYERS SELF-ASSEMBLED ONTO SURFACE-OXIDIZED POLY(4-METHYL-1-PENTENE)

Introduction

Thin polymer films are used in integrated optics, sensors, friction reducing coatings and surface oriented layers. [1] For example, by using an appropriate conjugated polymer one can create thin film devices such as multilayer light emitting diiodes and high capacity thin film dielectrics. [2] Deposition of various conducting polymers onto certain layers in a multilayer heterostructure can give novel electrical and optical properties that are not accessable by simple composite lay-ups. [3]

Control of preparation of multilayered structures at the molecular level is thus of both academic and industrial interest. Traditionally ultrathin multilayered films have been prepared by four methods:

(1) solution casting of preformed bilayer aggregates

(2) annealing of spin coated films of copolymers

(3) Langmuir-Blodgett (LB) techniques

(4) chemisorption/grafting

These methods have deficiencies in numerous aspects of use; they may lead to intermixing of layers (solution casting and annealing), have restrictions in the sample size (LB), or require 100% reaction yields in order to maintain the functionality density at the surface (chemisorption).

Decher et al made use of earlier experimental [4,5] and theoretical work [6,7] on interactions between polyelectrolytes and charged surfaces, and introduced "layer-by-

layer deposition of polyelectrolytes" as a novel method for preparing ultrathin multilayered films. [8] The method is based on electrostatic attraction between anionic and cationic polymer species.

A poly(4-methyl-1-pentene) (PMP) film can be used as a substrate for polyelectrolyte depositions when the PMP surface is functionalized in such a way that polyelectrolytes can interact with the surface in a nonreversible manner. Oxidation under selected conditions is likely to incorporate ionizable functionalities at the PMP surface that can act as anchors for thin polyelectrolyte layers deposited onto the substrate. Control of structures at the molecular level to build up highly anisotropic, densely packed multilayered heterostructures supported by a PMP film is expected to depress gas permeabilities through the asymmetric membrane to an extent that cannot be reached by conventional membrane technology.

Surface Oxidation of Polyolefins

Polyolefin surfaces have been oxidized commercially in order to improve adhesion and wettability properties. Lane and Hourston divide the oxidation techniques into dry and chemical processes in their review. [9] On an industrial scale the fast, economical and easily automated dry processes based on corona discharge and plasma treatments are mostly used, but they give a poor control over the chemistry taking place. Examples of polyolefin surface oxidations using corona discharge treatment (CDT) and chemical modifications are given below.

Corona Discharge Treatment

Corona discharge ionizes active (air, O_2) or inert (N_2, Ar, He) gases between electrodes. Most commonly, industrial pretreatments utilize air which, as a mixture of

gases, yields a number of functionalities at the oxidized surface. Even in the case of CDT oxidation with pure oxygen, the peroxide groups initially formed by reaction between a carbon radical and an oxygen molecule will undergo numerous chemical reactions to give carboxylic acid, ketone, aldehyde and ether functionalities, and various unsaturated stuctures. The ether group is the most abundant functionality at polyethylene surfaces after oxygen CDT.

Even though high levels of oxidation can be achieved (10 - 20 % oxygen at the XPS sampling depths), much of the oxidized polyethylene can be easily washed away due to chain scission occuring during the treatment. Corona discharge treatment is thus a fast and economical method to increase adhesive properties of polyolefin films and fibers, but because of extensive surface degradation and lack of control over the course of reaction, the technique it is not suitable for preparing well defined surfaces.

Chemical Oxidation

Chemical oxidations are likely to yield more well defined structures at polymer surfaces. Because polyolefins are chemically resistant, one has to use highly reactive oxidants. With semicrystalline polyolefins this leads to etched surface structures due to preferencial attack at the amorphous regions.

Oxidants such as permanganic and chlorosulphonic acids have been used to modify polyolefin surfaces, but they yield highly corroded surfaces. Chloric acid has been used successfully to oxidize reduced polytetrafluoroethylene,[10] and chromic acid oxidation of polyethylene, on the other hand, gives a moderately rough, featureless surface that has been shown to contain a large number of carbonyl-group containing functionalities. [11]

By choosing appropriate reaction parameters, one can use oxidation reactions to functionalize the surface instead of just burning it off. The use of an aqueous solution

restricts the modification to the skin of the film as the solution would prefer not to wet the unmodified hydrocarbon surface.

Layer-by-Layer Deposition Technique

Decher et al began to utilize the interactions between polyelectrolytes and charged surfaces to prepare ultrathin multilayered films in 1991. [8] The method uses electrostatic attraction as the driving force for self-assembly of ionic polymer molecules.

An ultrathin layer is formed simply by dipping a substrate with a charged surface into a solution containing a polyelectrolyte of an opposite charge (Figure 19). After a monolayer of the polyelectrolyte is deposited onto the substrate, the original surface charge is reversed and repulsive ionic forces prevent further deposition from taking place. The chain conformation of the deposited molecule, and thus also the layer thickness, are determined by the pH, ionic strength and the polyelectrolyte concentration of the dipping solution. Submerging the new surface in a solution of an oppositely charged polyelectrolyte causes another monolayer to deposit, and multilayers can be formed by alternating the dipping solutions.

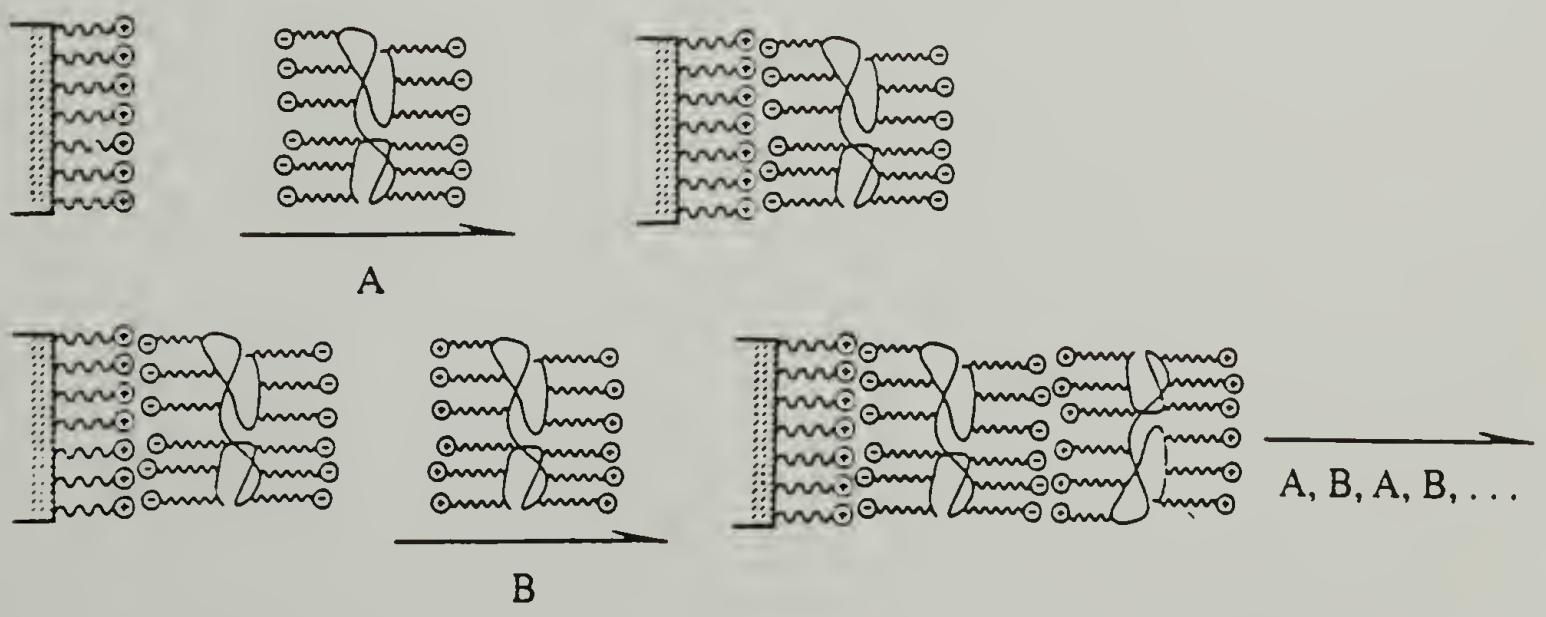

Figure 19. Layer-by-layer deposition of polyelectrolytes onto charged surfaces. [12]

In addition to polycations and polyanions, a similar method has been shown to work for neutral polymers, where hydrogen bonding is the driving force for adsorption.[13] In addition to the flexibility in the choice of polymers, there are no restrictions in the sample size or the number of layers, and thus automation of the process can be easily achieved (as a comparison the LB technique requires the use of surface-active substances, and has practical limitations for the sample dimensions). The layer-by-layer self-assembled structures have been shown to be highly ordered with minimal mixing between the adsorbed layers. Some essential deposition parameters are discussed below by reviewing studies reported by other laboratories.

Deposition solutions

Dipping solutions for layer-by-layer depositions typically consist of a water-soluble polymer in an aqueous solution at an appropriate pH value. In some cases, such as conducting polymers, one may have to use a cosolvent to enhance solubility. [13,14] Salts can also be added to the deposition solution in order to change the configuration of the adsorbing polymer, or to change the properties of the solvent. [5]

Examples of previously reported adsorption solutions are:

(1) *polyanion;* 30 mg poly(sodium styrene sulfonate), 1 ml of 0.1 N HCl, 2.03 g $MnCl_2 \cdot 4\ H_2O$ and 10 ml water.[12]

(2) *polycation;* 12.5 mg poly(allyl amine hydrochloride), 1.0 ml of 0.1 N HCl and 9.0 ml of Milli-Q water.

(3) *conducting polymer of low solubility in water;* 10 vol% of a polyaniline (PAn) solution in dimethylacetamide (DMAc) (no more than 20 mg PAn in a ml of DMAc stirred overnight, and sonicated for 8-10 hours; remaining particles filtered with 2 and 0.45 μm porous filters) dissolved in 90 vol% water. The pH was adjusted to 2.5 with methane sulfonic acid to dope the PAn (polycation) and the solution was filtered

through a 0.45 μm filter giving a PAn concentration of 0.005 M (in terms of repeat units). [13]

Choice of Polymers

Since the driving force for self-assembly in this technique is electrostatic interaction between oppositely charged molecules, one can use any polymer that can be charged to build up multilayered structures. One can alternate between two polyelectrolytes to create a set of bilayers, or use a number of different polymers for the heterostructure.

The most extensively used polyelectrolytes in layer-by-layer studies are sulfonated polystyrene [2,3,12] and polyallylamine, [1-3,12] but also polyaniline, [13] poly(vinyl sulfate), [1,12] poly(4-vinylbenzyl-(N,N-diethyl-N-methyl)-ammonium iodide, [12] polydiallyldimethylammonium chloride, [15] DNA, [16] Carnation Mottle virus, [17] poly(L-lysine), [18] poly(thiophene-3-acetic acid), [2,3] sulfonated polyaniline [3] and poly(2-N-methyl pyridinium acetylene) [3] have been used for layer-by-layer deposition studies. In related adsorption, doping and composite formation studies the use of poly(styrene sulfonate), [5,19,20] polyaniline [19,20] and poly(acrylic acid) [4] have also been reported.

The technique has also been used to incorporate exfoliated sheets of synthetic hectorite (a mica-type layered silicate), [15] and α-$Zr(HPO_4)_2$ -derived sheets [21] into multilayered organic-inorganic hybrid structures. Versatility of the technique is shown by creating alternating layers of polyelectrolytes and small molecules such as dyes, [18] and photopolymerizable bolaform amphophile monomers, [22] and by combining the self-assembly method with Langmuir-Blodgett techniques. [23]

The effect of molecular weight on the amount polymer adsorbed has not been studied extensively. There appears to be no significant MW dependence within

experimental error when the interaction between the adsorbing molecule and the surface is strong. [5]

Polymer concentration

When the interaction between a polyelectrolyte and a charged surface is strong, the total amount of polymer adsorbed increases linearly with polymer concentration. As the intensity of the ionic interaction is lowered by using polyelectrolytes and surfaces of lower charge density, or by screening the charges with added salt (see below), the amount of adsorbed polymer still increases, but non-linear, more "rounded" (low affinity) adsorption isotherms are obtained (Figure 20).

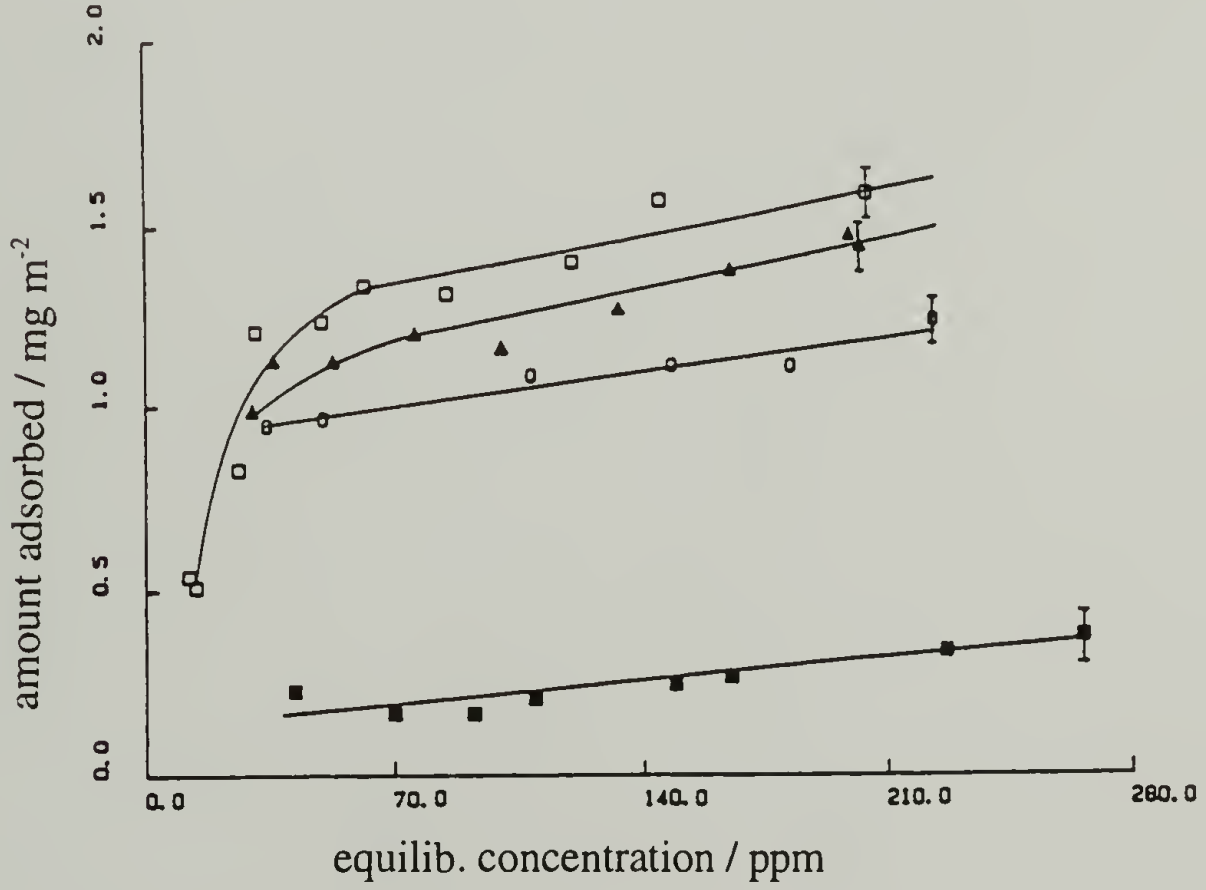

Figure 20. Adsorption isotherms for poly(styrene sulfonate) (M_w 780,000) on a positively charged surface at various ionic strengths: 1.0 M NaCl (open square), 0.5 M NaCl (triangle), 0.1 M NaCl (circle) and 0 M NaCl (filled square). [5]

Ionic strength

The ionic strength of the dipping solution affects the deposition process by changing the solvent strength and the extent of intra- and intermolecular ionic interactions of the polyelectrolyte and the substrate. At all ionic strengths the charges at the surface of the substrate have to be compensated by salt ions or the polyelectrolyte. [4] Changes in solvent strength and polyelectrolyte chain conformations can be used to adjust the amount of polymer adsorbed and the layer thickness. Typical values for bilayer thickness are 10-50 Å. [2] The actual adsorption and packing of the polyelectrolyte chains to form a monolayer is a complex process that is affected by the interaction of charges on the chain and the surface. At low ionic strengths polyelectrolytes adsorb in a flat conformation whereas at high salt concentrations the ionic effects are screened and the polyelectrolyte behaves like a neutral species depositing in a random coil configuration. [24] If the ionic strength of the solution is changed after the initial deposition, the layer structure is not changed to a great extent indicating considerable irreversability of the layer formation process. [25]

Two opposing trends for the effect of ionic strength on layer thickness have been reported. Cosgrove et al [5] studied the configuration of poly(styrene sulfonate) at functionalized polystyrene/solution interfaces and concluded that the net effect of increasing the ionic strength is a decrease in layer thickness whereas many other laboratories have reported the opposite trend, for example Lvov et al [1] for a poly(vinyl sulfate)/polyallylamine system on glass slides. The systems these two groups studied were different and the opposing conclusions may be due to differences in the actual adsorption parameters such as surface charge density. A few remarks on both papers are presented below.

According to Cosgrove et al increasing the ionic strength of a dipping solution decreases the solvent strength and favors adsorption. An increased amount of adsorbed molecules tends to lead to extended tails of polymer chains and thicker layers due to

crowding at the surface. As the increase in ionic strength decreases the solvency and leads to greater layer thickness as described, it also causes the polymer molecule to assume a more random coil like conformation that has a smaller radius of gyration than the extended chains at lower ionic strengths. Thus the trend of increasing layer thicknesses at high salt concentrations due to a increase in the amount adsorbed is actually offset by the collapse of the extended chain conformations due to screening of charges along the polymer chain leading to a decreased layer thickness.

Lvov et al, on the other hand, reported that both the layer thickness and the surface roughness increase in a nonlinear fashion with ionic strength of the adsorption solution (Figure 21). At very high ionic strengths the polymer molecules remain as globular systems and cause the formation of rough surface structures.

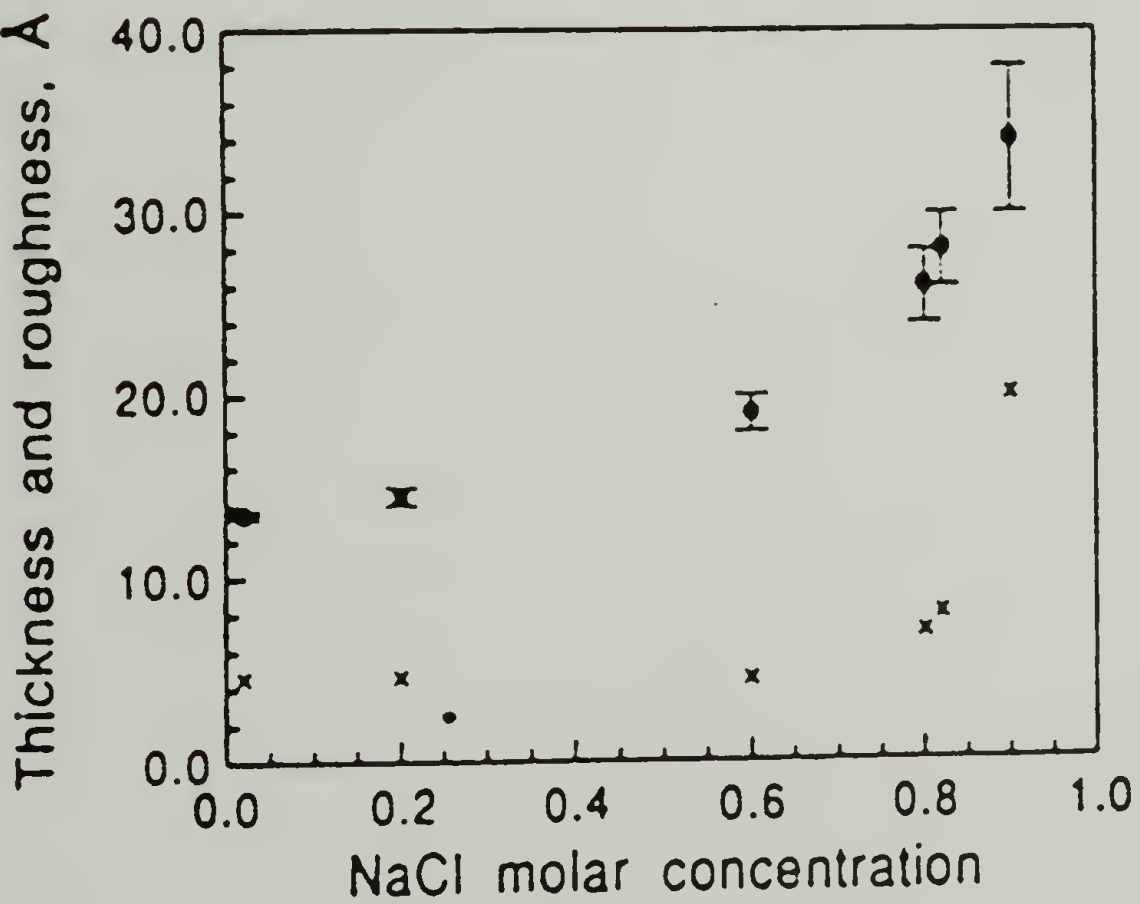

Figure 21. Dependence of poly(vinyl sulfate) / polyallylamine layer pairs thickness (points), and film surface roughness (crosses) on molar concentration of NaCl in polymer solution (Lvov et al [1]).

pH

Each polymer has an optimum pH range for the adsorption to which the solution is adjusted with an acid (such as HCl) or a base (such as NaOH). When the plateau values of the adsorption isotherms are plotted as a function of pH (Figure 22), the maximum amount adsorbed is obtained at a pH that is approximately 1 unit below the pK_o of the polyelectrolyte. This maximum is a trade-off between two opposing trends: for a polyanion, a lowering of pH results in an increase in the electrostatic contribution in the adsorption energy favoring deposition, but simultaneously electrostatic repulsions between similar charges along the polymer chains become stronger and oppose the accumulation of the polyelectrolytes near the surface.

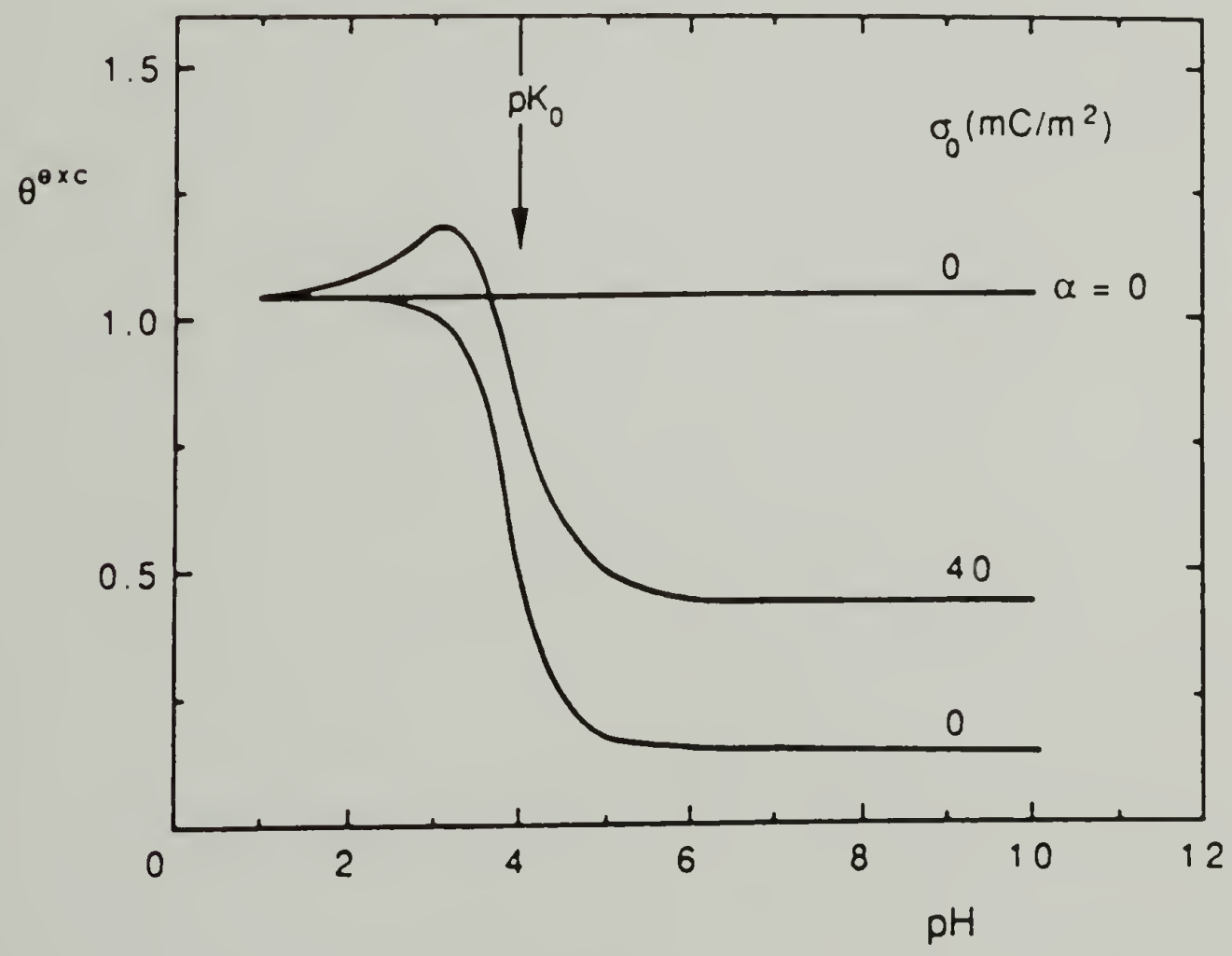

Figure 22. Excess adsorbed amount as a function of the pH for a neutral polymer and weak polyelectrolyte at different surface charge densities. [4]

In addition to the polyelectrolyte, the electrostatic state of the surface contributes significantly to the course of self-assembly, packing of molecules in the layers and interfacial strength between layers. One may have to compromise between the ideal conditions for the polyelectrolyte and the surface, in order to maximize the ionic interaction for a the particular polymer/surface combination.

Substrate

Layer-by-layer depositions have been reported on a number of pure and surface-modified substrates. Depending on the nature and the extent of surface-modification, one can create neutral, or positive and negative surfaces of various charge densities. With strong polyelectrolytes the amount adsorbed on the oppositely charged surface depends on the surface charge density. [4] The charge density can also affect the configuration that the adsorbing polyelectrolyte will have. Highly charged surfaces generally give flat configurations with relatively short loops and thus low adsorbed amounts. At low surface charge densities the electrostatic attraction between the surface and the oppositely charged segments of the polyelectrolyte is reduced resulting in extended tails. [5]

Glass slides have been used in the hydrophilic form (unmodified), as hydrophobic surfaces (gas phase treatment of glass with 1,1,1,3,3,3-hexamethyldisilazane) and as positively charged surfaces (hydrophilic slides treated with a N-2-aminoethyl-3-aminopropyl-trimethoxysilane solution [2,3], plasma treated, [26] and after treatment with boladication solution [1]).

Decher et al have used fused quartz and silicon single crystals reacted with 3-aminopropyldimethylethoxysilane, [8,12] whereas Lee et al used silicon single crystals and gold. [27] Polystyrene latex with positive or negative charges at the surface have also been used in related polyelectrolyte adsorption studies. [4,5]

Time

The length of deposition of a polyelectrolyte onto the substrate or the previously self-assembled layer has to be sufficient in order to ensure that the final state of adsorption has been reached and consequently the surface charge has been reversed. The rate limiting factor in forming uniform layers is the conformational changes of the chain upon adsorption. [1] The final state has been reached with relatively short deposition times of 10 min,[2,3] 15 min [13] and 20 minutes. [1,8,12]

One can also synthesize the polymer in situ instead of dissolving a preformed polymer. [28] The in-situ process deposits a layer whose thickness can be controlled by the length of the time that the substate is submerged in the solution. By using preformed polymers, on the other hand, one can deposit a highly uniform monolayer of polymer on the substrate. [2]

Characterization of deposited layers

The emphasis in the analysis of layer-by-layer deposited heterostructures has so far been in the determination of layer thickness and surface roughness. Decher et al [8] have reported that defects sometimes exist within a 2 mm margin around the edges of the substrate and this has to be taken into consideration when choosing the sampling area for the analytical method in use. Possible sources for the defects are many and the reported value for the edge effect is based on the worst case scenario. [29]

Layer-by-layer structures have been studied by UV-VIS spectroscopy, [2,3,8,12,13] small angle X-ray scattering, [1,12] profilometry and ellipsometry [3], photon correlation spectroscopy, [5] small angle neutron scattering, [5] X-ray [30] and neutron reflectivity, [31] and light microscopy. [13]

Mechanical and atomic composition studies of the multilayered structures are practically nonexistent in the literature. Initial surface force measurements have shown

the multilayer films to be quite fragile, especially for the first few layers. [32,33] Angle-resolved XPS has been shown to be useful in determining the deposition orientation of non-symmetrical small molecules (straight-chain mercaptoaleanoic acids) within self-assembled layers. [34]

Deposition of layers of conducting polymers

Typical polyelectrolytes used in layer-by-layer depositions have localized charges on the polymer chain or in the pendant groups, that interact with the localized charges on the previously adsorbed layer or the original substrate surface. The doping process of conducting polymers creates delocalized positive or negative charges along the chain that can be used as well to create ionic interaction that leads to deposition of polymer molecules onto a charged surface. Thus one can deposit these conjugated polymers even in their nonderivatized highly conducting forms. [3]

An additional aspect of using conducting polymers in the layer-by-layer deposition process is the poor solubility of these polymers in water or commonly used organic solvents. With the appropriate choice of a polymer/dopant/solvent/cosolvent system one can, however, create an electrostatic interaction between the charges on the polymer and the dopant in such a way that their interaction with the solvent yields a solvated polymer in its doped form. [35] The polymer concentrations in a dipping solution thus achieved are high enough for layer-by-layer studies as the method deposits monolayers onto the substrate.

Interaction of polyaniline with poly(sodium styrene sulfonate)

Large molecule sulfonic acids have been used as PAn dopants to render the doped polymer soluble in many organic solvents. PAn/5-sulfosalicylic acid/DMSO is a

ternary system in which the doped polymer is soluble to the extend of 11 g/l. [35] The use of small molecule dopants leads to poor stability of conductivity due to ready migration of the dopant out of the system, especially at elevated temperatures. Polymeric dopants such as poly(styrene sulfonate) by their nature do not have this problem and result in improved stability. [19]

Polymeric dopants occupy a greater volume fraction and thus lead to lowered polaron density as compared to equivalent small molecule dopants. Poly(styrene sulfonic acid) also has a lower ionic strength than for example HCl and both of these factors result in lowered conductivity. In a PAn/100% sulfonated polystyrene blend, the component ratio of 1:3 has been shown to give the highest conductivity. A high sulfonic acid functionality density on the PS chain is needed since a 6% sulfonation level did not give a doping effect. [20]

PAn can be dissolved in the dipping solution as described above, or synthesized in situ following the method by Chiang and Macdiarmid, [36] using an aqueous solution of $(NH_4)_2S_2O_8$to polymerize aniline to give emeraldine hydrochloride (the emeraldine form has an equal number of reduced [-(C_6H_4)-NH-(C_6H_4)-NH-] and oxidized [-(C_6H_4)-N=(C_6H_4)=N-] repeat units).

Gas permeability of PAn

The gas permeability of conducting polymers is lowered upon doping as the dopant molecules fill the void space in the polymer structure. The polymer chains also become stiffer and thus are less likely to facilitate gas diffusion through the material. The effect of doping and undoping cycles on gas permeability polyaniline can be seen in Table 15.

The best improvements in gas selectivities of polyaniline have resulted from doping/undoping recycling treatment. This procedure changes the morphology of the

conducting polymer as the doping and undoping creates size-selective pores. The dimensions of the pores can be adjusted by using dopant molecules of appropriate size.[37]

Layer-by-layer deposition of polyaniline (and polyallylamine) with poly(styrene sulfonate) is expected to result in highly ordered systems that are likely to have gas permeability properties quite different from thin films prepered by conventional techniques such as casting.

Experimental Section

General Procedures

PMP film (50 μm Mitsui TPX) was extracted in refluxing dichloromethane for 1h under nitrogen and dried at reduced pressure at room temperature to constant mass. Potassium chlorate ($KClO_3$, 99% min., Alfa Products) and chromium(VI)oxide (CrO_3, 99.9 %, Aldrich) were used as received and dissolved in sulfuric acid solutions (36 N H_2SO_4, Fisher Scientific; used neat or diluted with distilled water). Nitric acid (15.8 N, Fisher Scientific), 2-propanol (HPLC grade, Fisher Scientific), tetrahydrofuran (HPLC grade, Fisher Scientific), methanol (HPLC grade, Fisher Scientific) and dichloromethane (OPTIMA grade, Fisher Scientific) were used as received.

Aniline (98+%, Aldrich) was vacuum distilled prior to use (105 - 108 °C/50 mm). Ammonium persulfate (98+%, Aldrich), hydrochloric acid (1 N, Fisher Scientific) and N,N-dimethylacetamide (99%, Acros Organics) were used as received.

Poly(allyl amine hydrochloride) (M_n 50,000 - 65,000, Aldrich) and poly(sodium styrene sulfonate) (M_n 70,000, Aldrich) were used as received. Hydrogen peroxide

(30%, Fisher Scientific), 4-aminobutyldimethylmethoxysilane (United Chemical Technologies) and toluene (HPLC grade, Fisher Scientific) were used as received.

XPS spectra were obtained with a Perkin-Elmer Physical Electronics 5100 spectrometer using Mg Kα excitation (400 W, 15.0 kV). Spectra were routinely recorded at a takeoff angles of 15° and 75° (measured between the film surface plane and the entrance lens of the detector optics). Atomic composition data were determined using sensitivity factors obtained from samples of known composition: C_{1s}, 0.250; N_{1s} 0.420; S_{2p} 0.540; O_{1s}, 0.628; Cl_{2p}, 0.655. Attenuated total reflectance infrared (ATR IR) spectra were recorded using an IBM 38 FTIR at 4 cm^{-1} resolution with a 10 x 5 x 1 mm 45° Ge internal reflection element. Gravimetric measurements were made with a Sartorius 1612MP-1 analytical balance. Dynamic advancing (θ_A) and receding (θ_R) contact angles were measured with a Ramé-Hart telescopic goniometer and a Gilmont syringe with a flat-tipped 24-gauge needle as probe fluid was added (θ_A) or withdrawn (θ_R) from the drop. Phase interference microscopy was performed using a Zygo Maxim 3D Model 5700.

Surface Oxidation of Poly(4-methyl-1-pentene)

Surface oxidations were run on both sides of a PMP film (30 mm x 30 mm) in an open reaction vessel covered with aluminum foil, under laboratory atmosphere. The solution was agitated during the oxidation with a magnetic stirbar encapsulated in glass and clean PMP samples were kept submerged in the solution with glass rods. After the prewash in water, the oxidized samples were stirred (for 2 minutes) in alternating water and 2-propanol baths for 5 cycles. The samples were dried to constant mass (overnight)

under reduced pressure (20 mtorr) at room temperature prior to analysis or use in deposition studies.

Polyaniline Synthesis

5.0 ml (0.0549 mol) of aniline was dissolved in 200 ml of 1 N HCl in a three-neck round bottom flask equipped with dropping funnel, condenser and stopper. The reaction vessel was purged with nitrogen and kept below 5 °C using an ice/water bath.

15.653 g (0.0686 mol) ammonium persulfate was dissolved in 200 ml of 1 N HCl, purged with nitrogen and cannulated into the dropping funnel. The ammonium persulfate solution was added dropwise over 75 minutes to the aniline solution while vigorously stirring the solution with a stirbar. The mixture was allowed to react for another two hours while continuing stirring and keeping the mixture under 5 °C. The deep green solid particles of polyaniline were washed with 1 N HCl solution using a Bühner funnel and dried at reduced pressure at room temperature to constant mass (5.356 g).

Surface Modification of Silicon Wafers

Silicon wafers were cleaned by reacting the surface for 15 minutes in 30 vol% H_2O_2 (30%) solution in concentrated sulfuric acid. Wafers were then washed with running water for 15 minutes, dried in a stream of air and placed in a closed reaction vessel while still in the clean room (Electrical Engineering Department, University of Massachusetts Amherst).

Wafers were purged with nitrogen and prewashed using a cannula in methanol (3x), 1:1 methanol/toluene mixture (3x) and toluene (3x). The wafers were amino-functionalized by reacting both surfaces of the sample in 1 vol% 4-aminobutyl-

dimethylmethoxysilane solution in toluene for 16 hours. After the coupling reaction the samples were washed with the same series of solvents, but in reverse order. The silane-coupled silicon wafers (Si-NH_2 surface) were used for layer-by-layer deposition experiments immediately or after storing overnight at reduced pressure.

Layer-by-Layer Depositions

Poly(allylamine hydrochloride) (PAH) and poly(sodium styrene sulfonate) (PSS) deposition solutions were prepared by dissolving 0.250 g PAH and 0.750 g PSS, and in some experiments NaCl salt, in 250 ml Milli-Q™ water (resistivity better than 18.2 MΩ cm) and adjusting pH to the desired value.

Polyaniline deposition solution was prepared as follows: After vigorously stirring 0.92 g PAn in 50 ml N,N-dimethylacetamide (DMAc) for two days, the flask was equipped with a condenser and the system was purged with nitrogen. The PAn/DMAc mixture was stirred while heated, keeping the temperature of the oil bath at 130 °C for 2 hours before raising the temperature to 150-160 °C for four hours. The mixture was stirred and let cool overnight before filtering through a 0.22 μm teflon filter (Cameo 25 F syringe filter, Micron Separations Inc.). This treatment resulted in a dark greenish/blueish PAn stock solution and undissolved residue. 6.0 ml of the PAn/DMAc stock solution was added dropwise while stirring into 50 ml of pH 4 adjusted Milli-Q™ water giving a purple solution of pH 3.6. Three solutions prepared this way were adjusted to pH 2, 4 and 6.

Fresh deposition solutions were made for each day of adsorption. The first layer was deposited onto surface-oxidized PMP film on the day following the oxidation. PMP film samples were submerged vertically in the deposition solution in a scintillation vial. Between depositions the samples were washed twice in Milli-Q™ water and once

in Milli-Q™ water that was adjusted to the pH of the following deposition solution. A maximum of ten layers were deposited before drying the samples in a stream of nitrogen and at reduced pressure at room temperature overnight.

Determination of Multilayer thickness

Total layer thicknesses were determined by Dr. Xiaoqun Zou for a series of PAH/PSS multilayers on silicon wafers. The samples were kept at reduced pressure in the test chamber for 24 hours prior to the X-ray reflectivity measurement (1.54 Å, Cu target) under vacuum to determine dry thickesses.

Selected multilayer samples were also exposed to various levels of relative humidity by purging the sample chamber with a stream of moist air. The humidity level of the air was adjusted by mixing streams of dry and water-saturated air in appropriate portions using flow controllers. Multilayers were allowed to equilibrate at a particular humidity level for 6 hours before starting the 5-hour-measurement for thickness.

Gas Permeation Rate Measurements

Gas permeation studies were run one gas at a time with hydrogen, oxygen, and nitrogen at 40 °C with an upstream pressure of 6 atm and a downstream pressure of 0 atm. After reaching a steady-state flux of gas, a pressure increase of 0.50 mm in a known volume on the downstream side was timed. A home-built pressure/vacuum manifold shown in Figure 5 (Chapter 2) was built around a Millipore 25 mm membrane cartridge and a Celesco DP 31 differential pressure transducer (See Appendix 1 for detailed description of the instrumentation and the permeability measurement).

Results and Discussion

The goal of oxidizing the PMP film surface was to create a surface with a high concentration of carboxylic acid functionalities and thus a high charge density at the skin for polyelectrolyte depositions. As shown with initial screening tests below, potassium chlorate oxidations lead to surface contamination. Subsequently, the applicability of chromic acid was studied in more detail. Results of both types of oxidation reactions are presented below.

Commonly used organic solvents were screened for use in conjunction with water for removing oxidant residues from the surface. 2-Propanol was chosen for its good wetting and reasonable swelling properties, whereas tetrahydrofuran, dichloromethane and methanol were discarded as the oxidized PMP was shown to be somewhat soluble in them.

Oxidations Using Potassium Chlorate

XPS and gravimetric data for potassium chlorate oxidations are presented in Table 16. For a given sulfuric acid concentration and reaction time, potassium chlorate concentration had no noticable effect on the extent of oxidation in the final sample within the experimental variation. For example for 1-minute-reaction sets at room temperature (Table 17) in 10 and 100 vol% H_2SO_4 solutions, a ten-fold increase in $KClO_3$ concentration lead to no changes in the overall oxygen content at the XPS sampling depth.

Oxidations in 10 and 50 vol% H_2SO_4 solutions at all oxidant concentrations studied, lead to oxygen contents of 2 to 5 % in the outermost 10 Å (sampling depth in XPS analysis at 15° take-off angle). In terms of an ideal oxidation in which all oxygen atoms are incorporated into carboxylic acid functionalities, this level of oxidation translates to approximately only one carboxylate functionality in ten PMP repeat units.

Oxidation solutions prepared in concentrated sulfuric acid, on the other hand, resulted oxygen contents up to 11 - 13 %, with accompanying chlorine contamination (Table 16) that could not be removed by the washing procedure.

The maximum level of oxidation was reached early in the reaction. For oxidations in a 0.0809 M $KClO_3$ solution in 50 vol% sulfuric acid, the reaction was shown to take place within the first 10 minutes (Figure 23). In stronger oxidizing solutions the maximum level was reached even earlier. Increases in reaction temperature (see Table 16) increased the oxygen content at the XPS sampling depth, but also lead to elevated chlorine contamination levels.

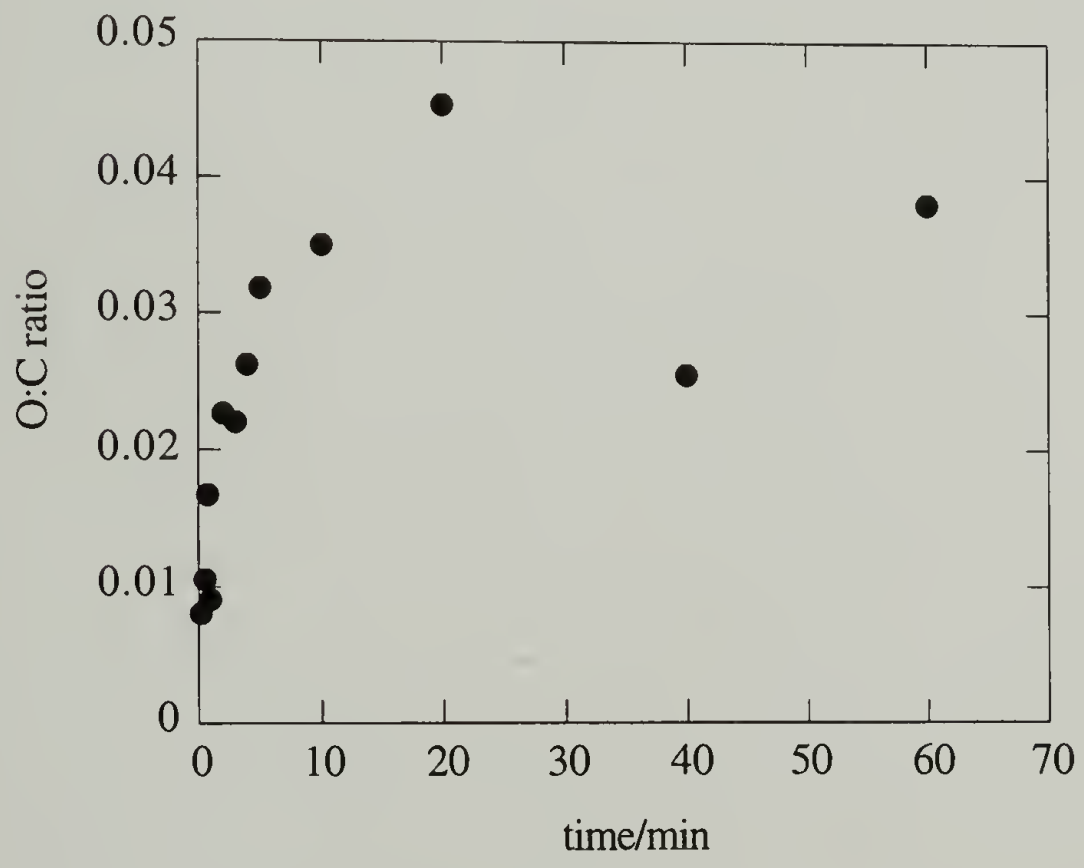

Figure 23. Reaction kinetics of potassium chlorate oxidation (0.0809 M $KClO_3$ solution in 50 vol% sulfuric acid at room temperature, 15° XPS analysis).

The majority of potassium chlorate oxidations yielded low levels of oxygen at the surface of PMP (typically 2 to 5% at the XPS sampling depths). The extent of oxidation was unacceptably low to give reasonably high surface charge densities for polyelectrolyte depositions. Only in the case of oxidant solutions made in concentrated sulfuric acid, were higher extents of reaction reached (up to 13 % oxygen). The high oxygen content was always accompanied with chlorine contamination and thus some portion of the oxygen signal may originate from oxidant residues at the film surface. Because of the contamination problems no further attempt was made to use elevated temperatures or higher oxidant concentrations (0.8 M $KClO_3$ solution is saturated in 50 vol% sulfuric acid) and the oxidation conditions were not studied beyond the scope of the screening tests that are summarized above.

Oxidations Using Chromic Acid

XPS and gravimetric data for the chromic acid oxidations are presented in Table 18. Samples oxidized at high oxidant concentrations, were shown to be contaminated with chromium (%Cr typically 0.4 to 0.7 %). Most of this contamination was shown to be removed with a hot nitric acid bath (70 vol% nitric acid at 50 to 55 °C for 30 minutes) after the oxidation. The post-treatment was shown to decrease the oxygen content typically by 20 to 30 % compared to the samples with no post-treatment, likely due to dissolution of both oxidant residues and oxidized PMP of low molecular weight at the skin of the film. This was desirable, as oxidation products of low molecular weight may lead to a mechanically weak interface. Thus the nitric acid bath was included in the sample treatment procedure for the kinetics and temperature dependence studies in saturated chromic acid solutions.

The extent of oxidation was shown to increase linearly with chromic acid concentration (Figure 24). A 5 molar chromic acid solution is saturated in 28 vol% sulfuric acid and was chosen as the concentration for further studies of kinetics and the temperature dependence of oxidation as presented below.

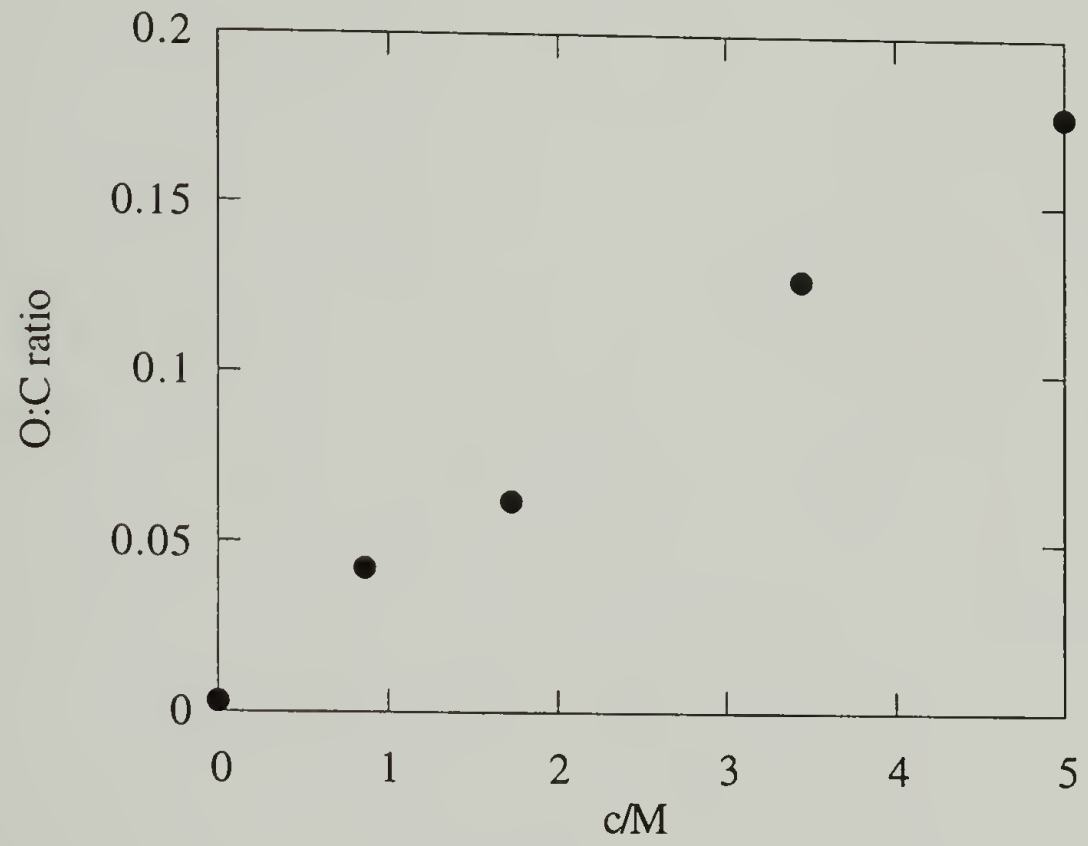

Figure 24. Extent of oxidation as a function of chromic acid concentration (5 min reaction at room temperature in 28 vol% sulfuric acid, 15° take-off angle XPS analysis).

The extent of oxidation increased almost linearly with reaction temperature (Figure 25). No attempt was made to raise the temperature of oxidation higher than 80 °C as this temperature still allowed the reaction to be run in an aluminum foil covered beaker and sample handling in any closed systems would have been difficult as PMP is less dense than the oxidation solution and would prefer to float on top of the solution without the use of glass rods.

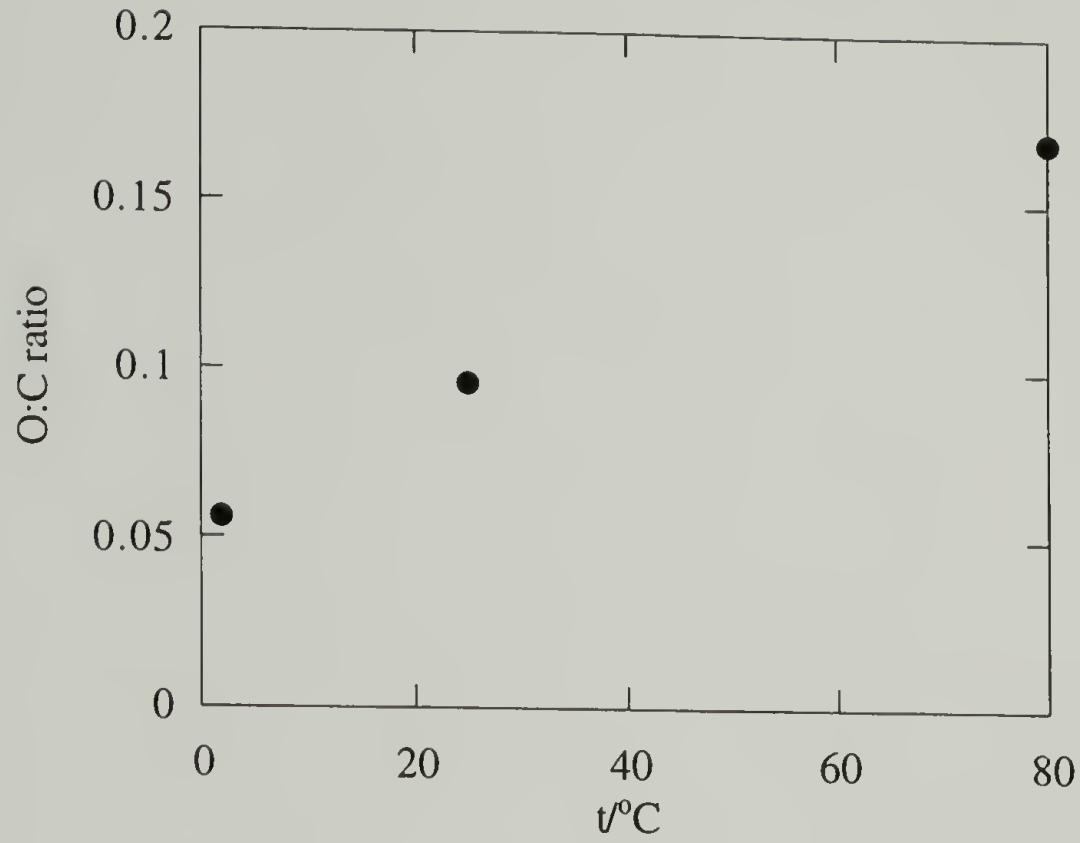

Figure 25. Extent of oxidation as a function of temperature (5 min reaction at room tempererature, 5 M chromic acid solution in 28 vol% sulfuric acid, 15° XPS analysis).

The maximum extent of oxidation at the XPS sampling depth was reached within the first minute of reaction using a saturated CrO_3 solution in 28 vol% sulfuric acid at 80 °C (Figure 26). Gravimetric data for this reaction set reveal that after reaching the oxygen:carbon ratio of about 0.18 (one carboxylate functionality in two repeat units), prolonged oxidation does not change the extent of oxidation but results in weight loss. As a carboxylate functionality at the surface is further oxidized to carbon dioxide, a new reaction site is formed and the reaction proceeds deeper into the bulk of the film.

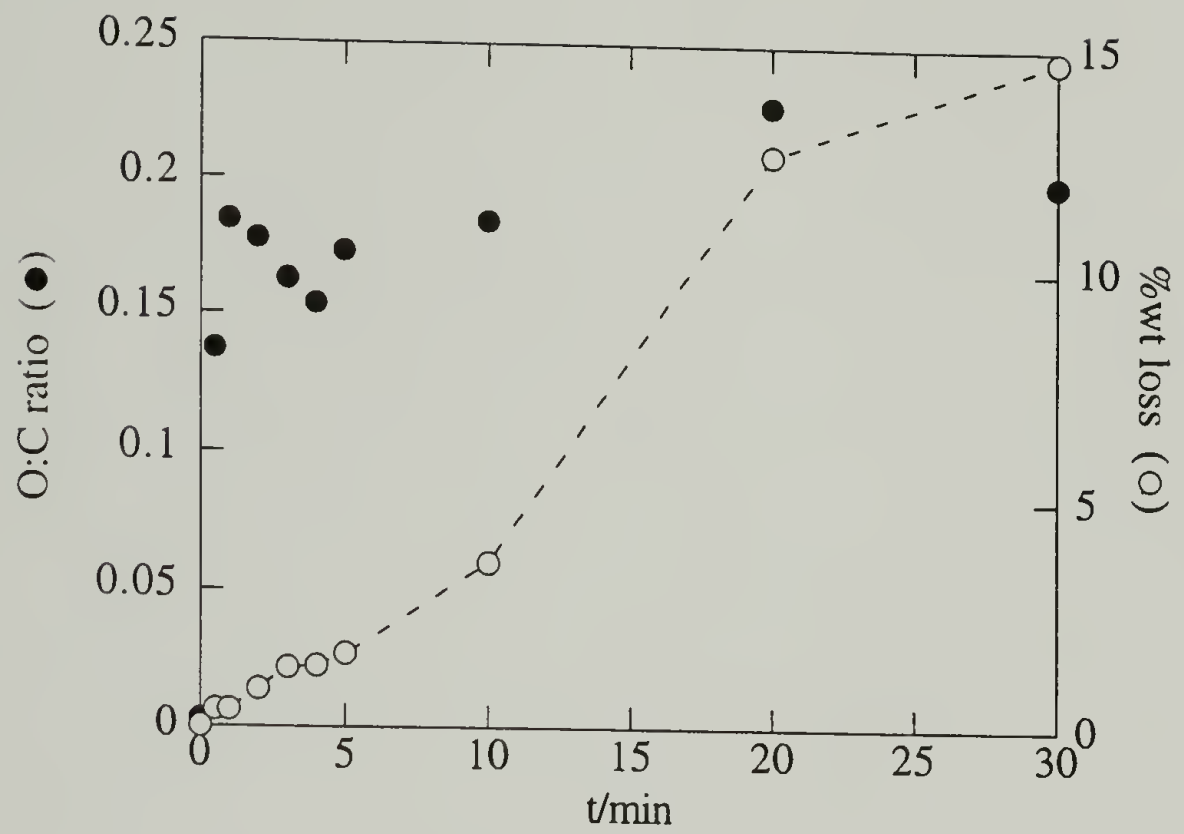

Figure 26. Kinetics for oxidations using 5 M CrO_3 solution in 28 vol% sulfuric acid at 80 °C (oxygen:carbon ratio from 15° XPS analysis).

In order to maximize the extent of oxidation, and to minimize the degradation during the reaction, oxidation for 2 minutes at 80 °C in a 5 M CrO_3 solution in 28 vol% sulfuric acid was chosen. A typical XPS survey spectrum of a PMP sample oxidized at these conditions is presented in Figure 27. Oxygen content in the top 10 Å was typically 15-16% (15° XPS take-off angle), and 13% in the top 40 Å (75° take-off angle). The carbonyl streching band in an ATR FTIR spectrum (acquired using a 45° Ge internal reflection element) in Figure 28 reveals that at least some of the oxygen atoms were incorporated in carbonyl containing functionalities. No other peaks due to oxygen containing functionalities could be detected in the spectrum.

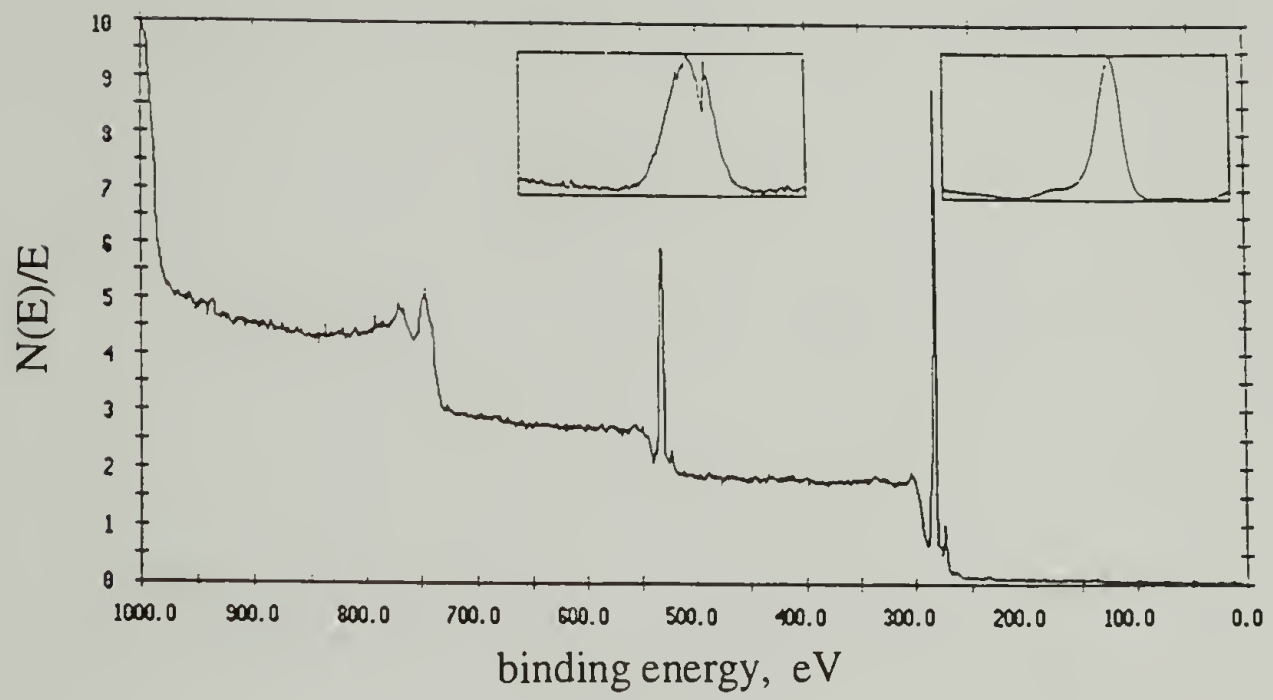

Figure 27. XPS survey spectrum (15° take-off angle) of PMP oxidized for 2 minutes at 80 °C in 5 M CrO_3 solution in 28 vol% sulfuric acid.

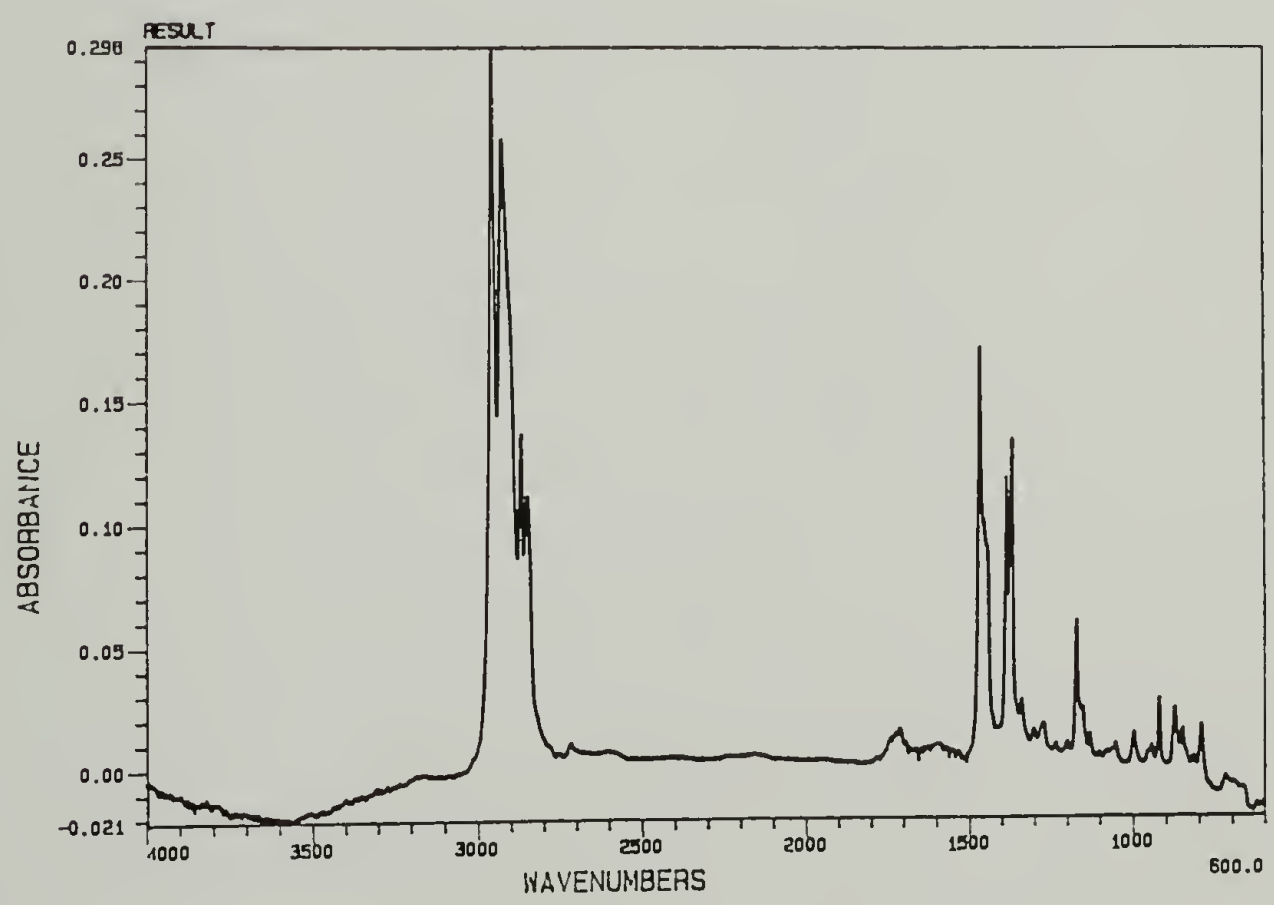

Figure 28. ATR FTIR spectrum of PMP oxidized for 2 minutes at 80 °C in 5 M CrO_3 solution in 28 vol% sulfuric acid (45° Ge internal reflection element).

Comparison of the pH dependence of advancing water (buffered solutions) contact angle for unmodified and surface oxidized PMP samples (Figure 29) confirms that a considerable fraction of the carbonyl groups are carboxylic acid functionalities as the wetting behavior of the oxidized surface changes as a function of pH.

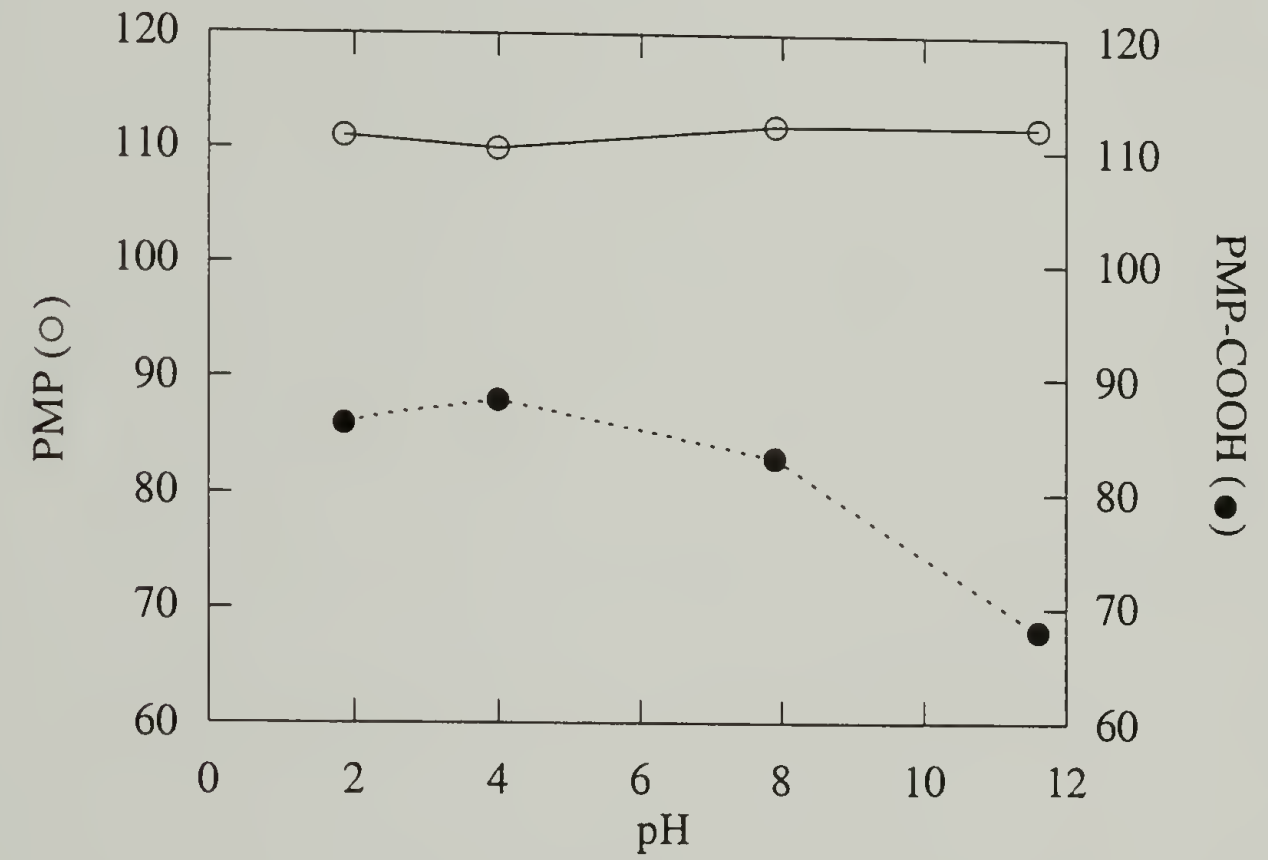

Figure 29. pH dependence of advancing water contact angle for unmodified and surface-oxidized PMP.

Comparison of profilometer roughness profiles of clean PMP (see Figure 7 in Chapter 2) and surface oxidized PMP (Figure 30) shows that the degrative oxidation does not result in any changes in surface roughness detectable by this analytical technique.

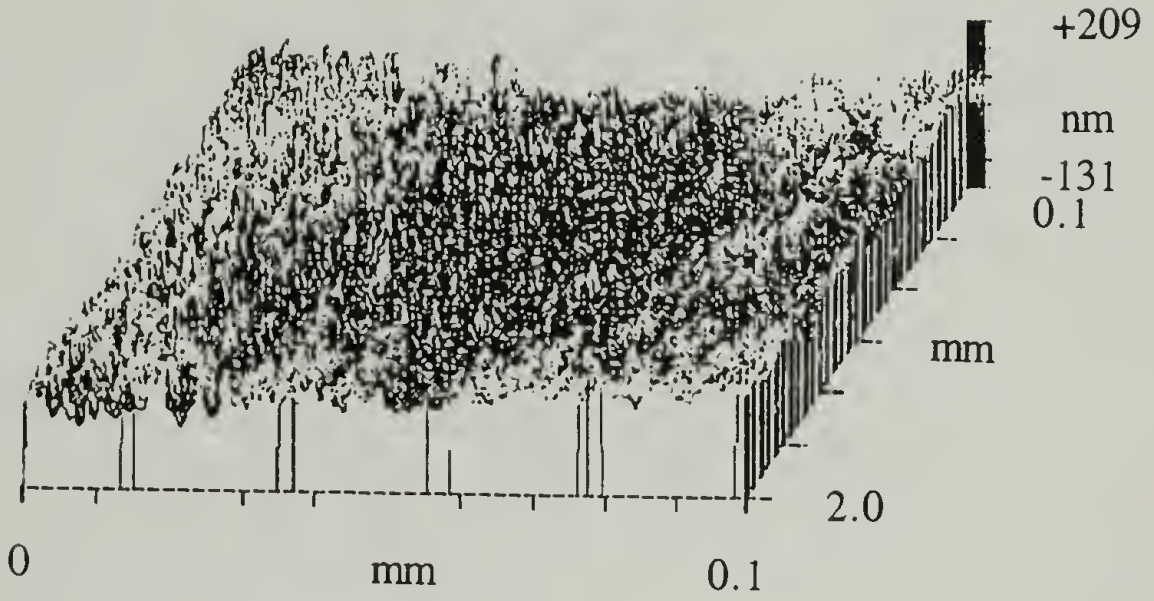

Figure 30. Roughness profile of oxidized PMP surface from phase interference microscopy.

Based on the above analysis, the PMP surface is carboxylated upon oxidation to the extent of having one ionizable carboxylic acid functionality in two repeat units. In two dimensions this gives a high surface charge density and a strong ionic interaction between the surface and the polyelectrolyte in the deposition of the first layer as shown below. The oxidized PMP surface will be referred to as PMP-COOH from this point on.

Layer-by-layer deposition of polyelectrolytes onto PMP-COOH

The preparation of multilayered structures on PMP-COOH surface was devided into two parts. In the first part of the work, poly(allyl amine hydrochloride) (PAH) and poly(sodium styrene sulfonate) (PSS) were used as the polyelectrolytes, whereas in the second part, PAH was replaced by polyaniline (PAn). The polyelectrolyte concentrations were chosen to be high enough that exhaustion of polyelectrolyte from the deposition solution was not a concern in the course of multiple depositions. Thus the possible effect of a limiting polyelectrolyte concentration on deposition characteristics was not studied.

Deposition of PAH and PSS onto Oxidized PMP

0.016 M PAH stock solution was prepared by dissolving 250 mg PAH in 250 ml Milli-Q water and 0.015 M PSS stock solution was prepared by dissolving 750 mg PSS in 250 ml Milli-Q water. PAH, PSS and and predeposition washing solutions were adjusted to the desired pH using HCl and NaOH solutions.

The PMP-COOH substrate was prepared as described above and used for the deposition studies after drying at reduced pressure and room temperature overnight. Freshly oxidized PMP samples were used for each adsorption series in order to eliminate differences in the starting substrate due to surface-reorganization over the length of storage time. Self-assembled polyelectrolyte layers were deposited by dipping the substrate into the polyelectrolyte solution in a 20 ml scintillation vial. The deposition kinetics and pH dependence was studied for PAH deposition onto the PMP-COOH surface, PSS deposition onto the PMP-COOH/PAH surface and PAH deposition onto the PMP-COOH/PAH/PSS surface. Multilayered structures were prepared by depositing alternating PAH and PSS monolayers onto the PMP-COOH substrate.

The polyelectrolyte depositions are likely to lead to changes in the atomic composition data from XPS analysis, as the oxidized PMP surface, PAH and PSS are labeled by high oxygen concentration, nitrogen, and sulfur atoms, respectively.

Deposition of PAH onto PMP-COOH surface

PAH deposition kinetics were studied using 0.016 M dipping solutions at pH 4, 6, 8 and 10. At each pH level PAH was deposited onto the PMP-COOH surface for 5, 10, 20, 30, 40 and 60 minutes. Elemental compositions for the first layer deposition determined by XPS at 15° and 75° take-off angles are presented in Table 19.

Carboxylic acids typically have pK_a values in the range of 4-5. Even though the acidity of a carboxylic acid functionality located at a surface of a solid particle may differ from that of a group dissolved in a solution, this pK_a range is supported by the pH dependence of advancing contact angle of PMP-COOH presented in Figure 29. Thus it can be used as a guideline in interpreting PAH (pK_a ~10) deposition onto PMP-COOH.

The increases in nitrogen:carbon and nitrogen:oxygen ratios as a function of pH for a series of 60-minute-depositions are presented in Figures 31 and 32, respectively. The values of atomic ratios, and thus the total amount of PAH deposited, increase linearly as the pH is increased from 4 to 8, due to deprotonation of carboxylic acid groups leading to enhanced ionic interaction between the surface and the adsorbing PAH molecule. At the same time a decrease in solvent strength also favors deposition. At pH 10, the ionized amino groups in PAH are at the threshold of being deprotonated to the state of a free amine, and PAH begins to partially precipitate out of the aqueous solution. This can be seen in the high values of N:C and N:O ratios. Depositions were also shown to incorporate very small amounts of chloride counterions onto the surface, but at the low level of one chloride in ten nitrogen atoms, suggesting that most ammonium functionalities have carboxylate groups as counterions.

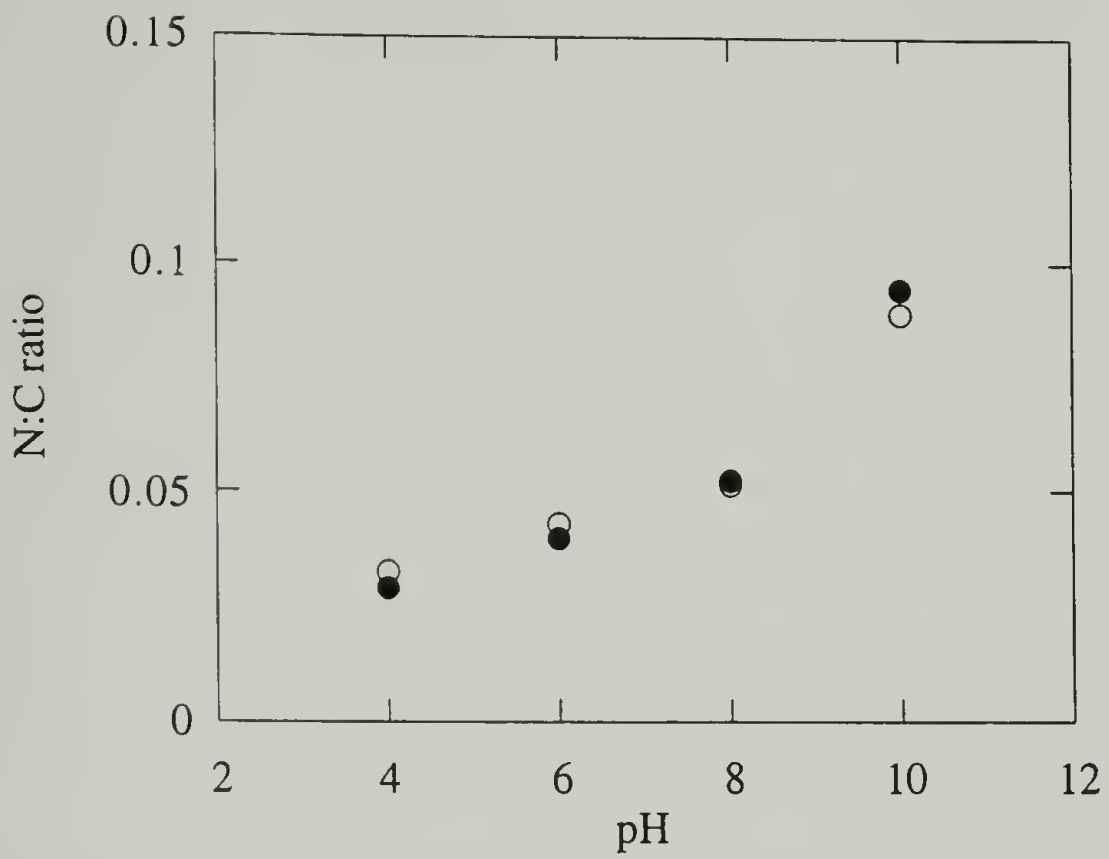

Figure 31. pH dependence of PAH self-assembly onto PMP-COOH. Nitrogen:carbon atomic ratios after 60 minutes of deposition from 15° (○) and 75° (●) XPS analysis.

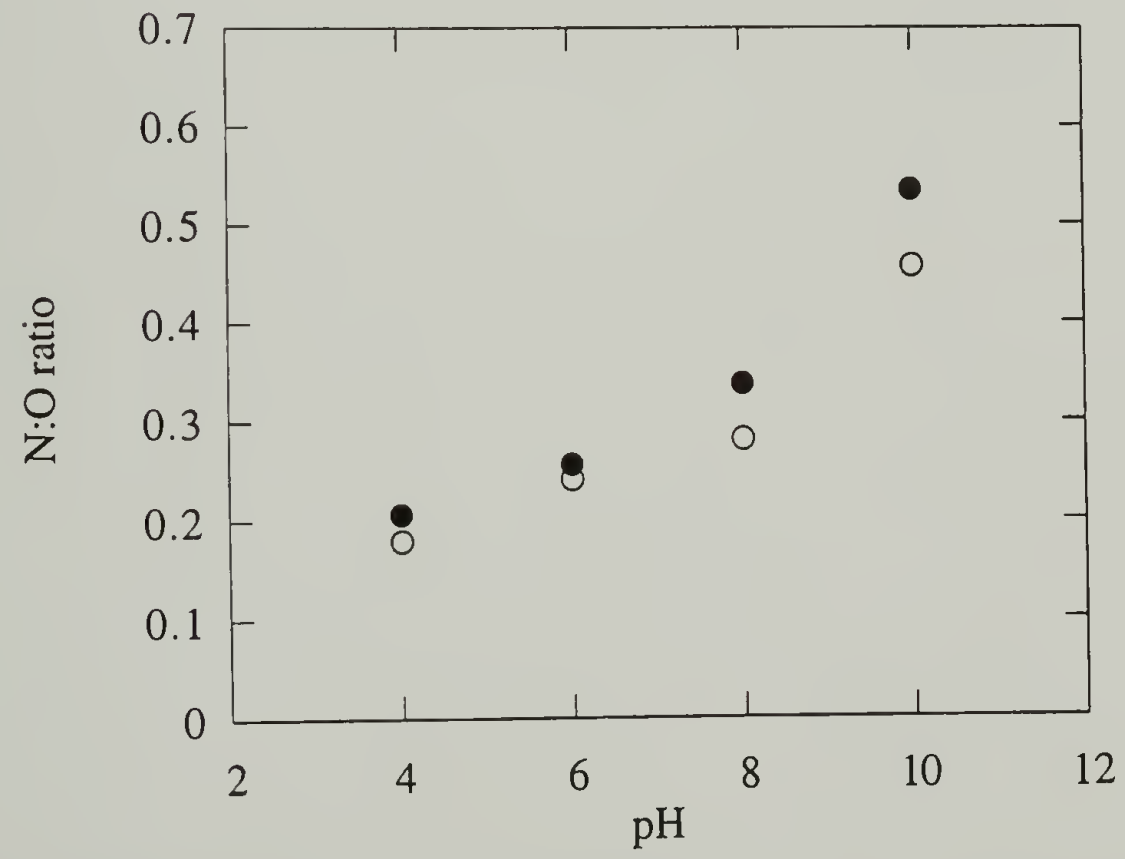

Figure 32. pH dependence of PAH self-assembly onto PMP-COOH. Nitrogen:oxygen atomic ratios after 60 minutes of deposition from 15° (○) and 75° (●) XPS analysis.

Based on XPS analysis, the self-assembly was shown to reach the final state sooner than in 5 minutes at all the pH conditions studied. Deposition kinetics are presented in Figure 33 for the experiments at pH 8. Regardless of the length of deposition, the samples have practically identical atomic compositions within the experimental variation. The variation is larger in the 15° analysis, suggesting that at low take-off angle acquisitions sample-specific parameters such as surface roughness can cause differences between samples in the same series.

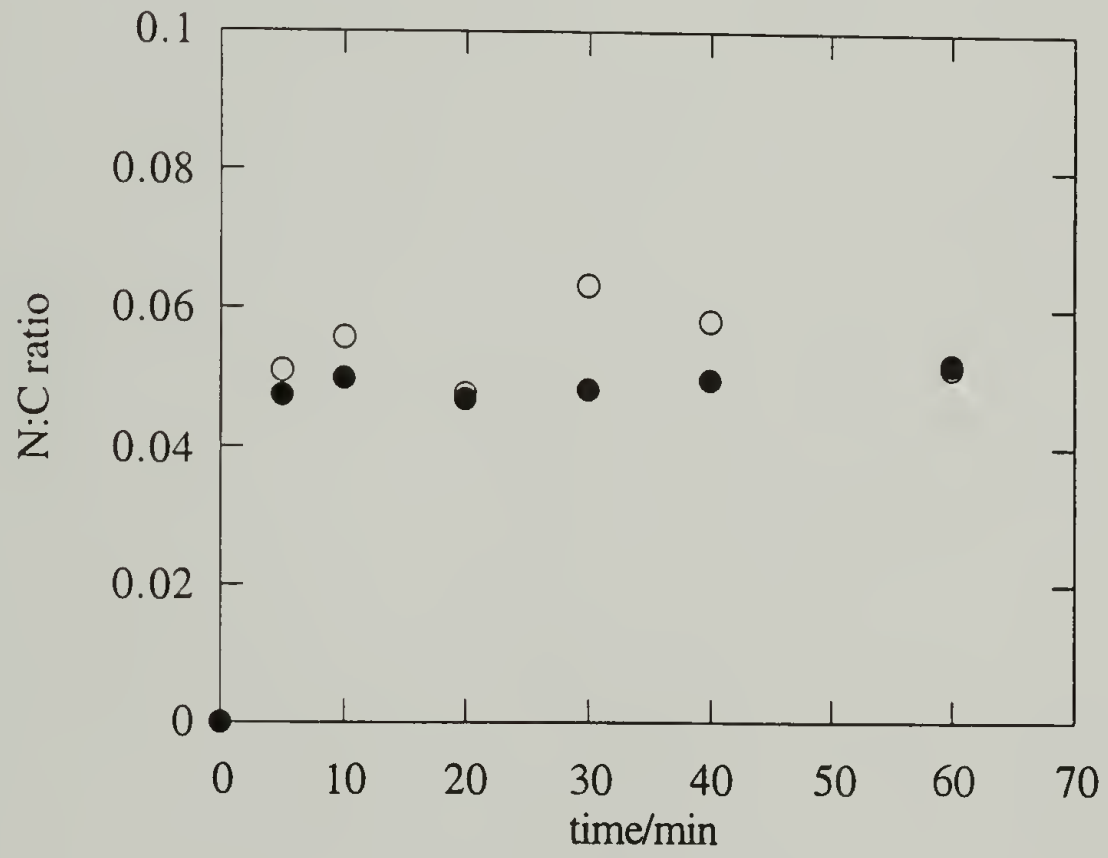

Figure 33. Kinetics of PAH self-assembly onto PMP-COOH at pH 8. Nitrogen:carbon atomic ratios from 15° (○) and 75° (●) XPS analysis.

One of the factors governing the deposition characteristics is the ionic strength of the dipping solution. The effect of added salt was studied by making the deposition solutions one molar in NaCl and using the same pH and deposition time conditions as in

the low ionic strength depositions above. XPS atomic composition data in Table 20, and pH dependence in Figures 34 and 35 reveal that deposition from a high ionic strength solution leads to slightly higher nitrogen:carbon and nitrogen:oxygen ratios in the pH 4 - 8 range, indicative of increased layer thickness. At pH 10, on the other hand, PAH is not precipitated out of the solution as was suggested in the low ionic strength experiment. Nevertheless, the overall level of deposition or deposition kinetics (Figure 36) did not change dramatically upon addition of salt to the dipping solution.

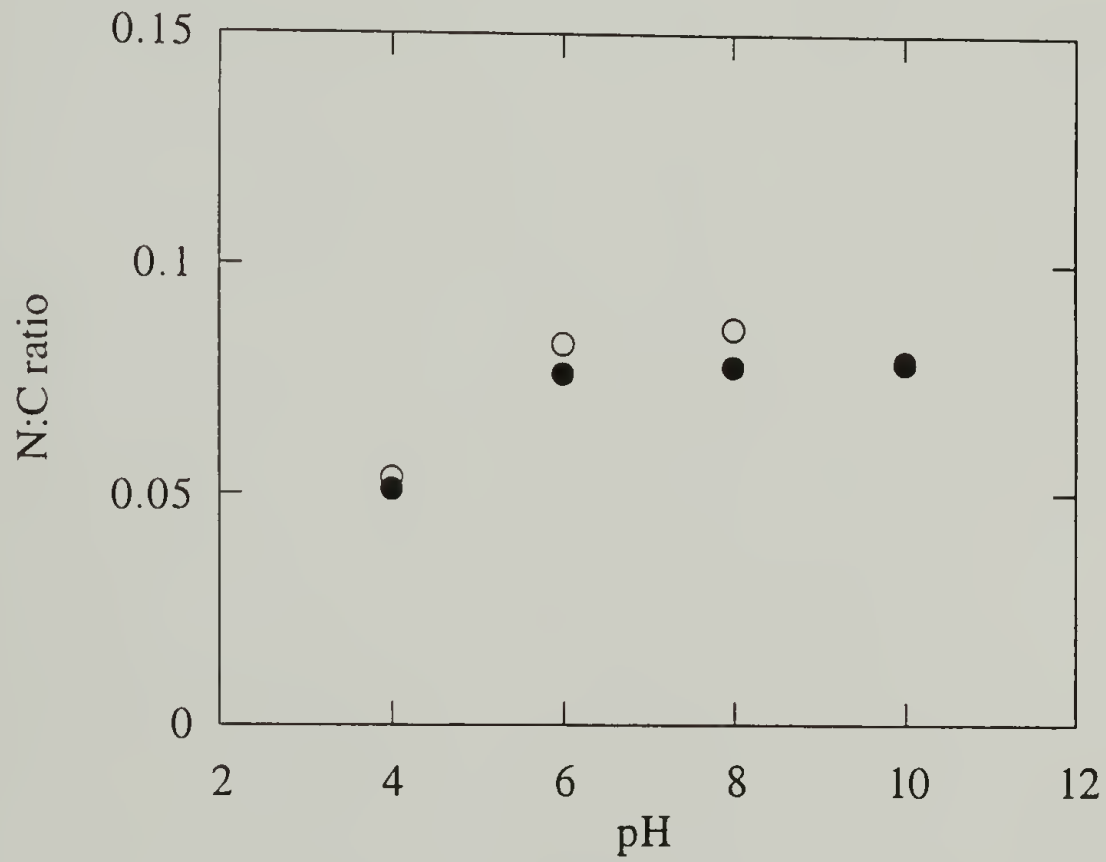

Figure 34. pH dependence of PAH self-assembly onto PMP-COOH (1 M NaCl). Nitrogen:carbon atomic ratios after 60 minutes of deposition from 15° (○) and 75° (●) XPS analysis.

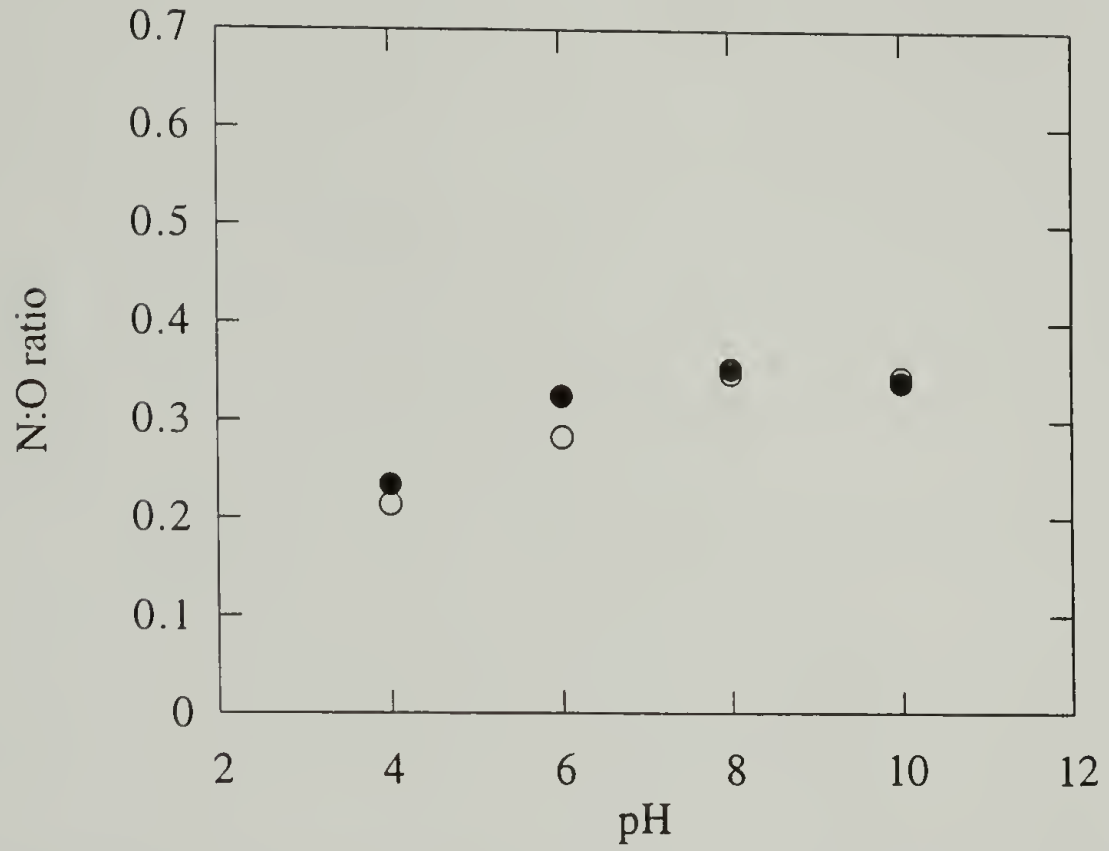

Figure 35. pH dependence of PAH self-assembly onto PMP-COOH (1 M NaCl). N:O atomic ratios after 60 minutes of deposition from 15° (○) and 75° (●) XPS analysis.

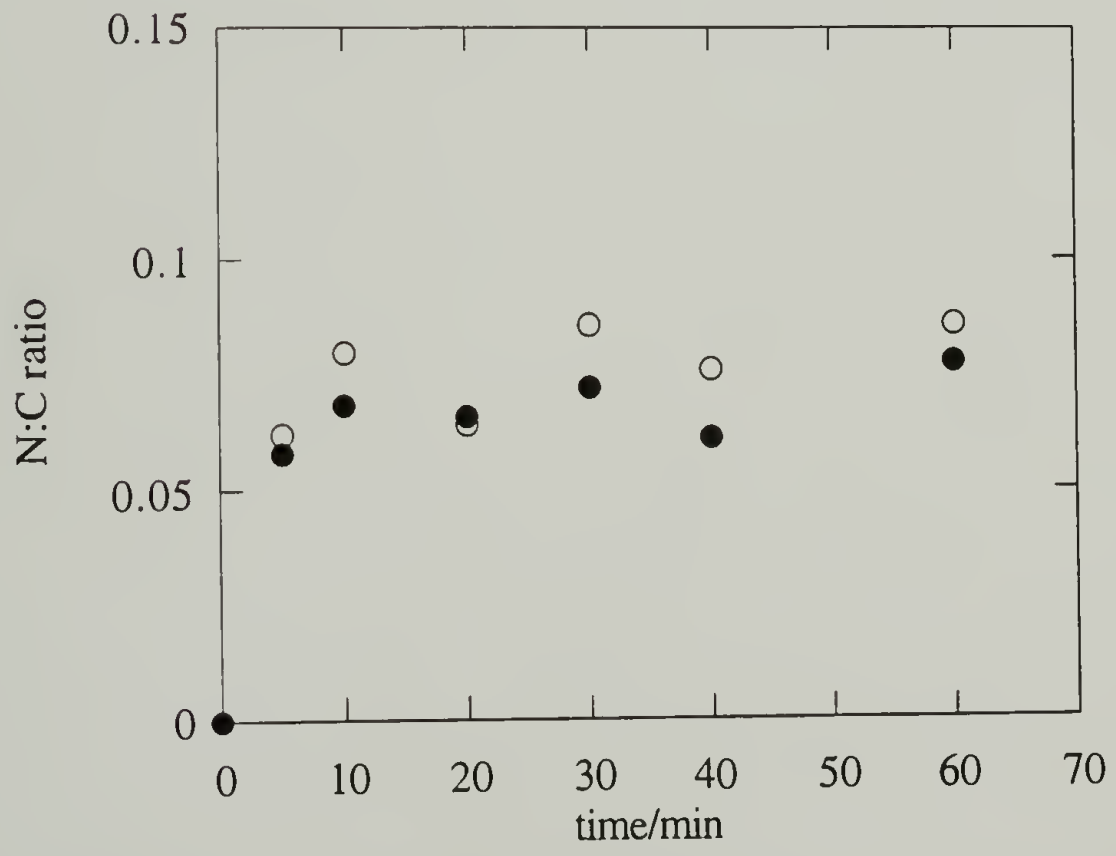

Figure 36. Kinetics of PAH self-assembly onto PMP-COOH at pH 8 (1 M NaCl). Nitrogen:oxygen atomic ratios from 15° (○) and 75° (●) XPS analysis.

In order to eliminate screening of charges along the polymer backbone to ensure that the depositing polyelectrolyte molecules have extended extended coil configuration leading to thin layers, and also to keep the deposition conditions as simple as possible, the use of an added salt was given up at this point. With the PAH/NaCl study it was also shown that use of minimal amounts of HCl and NaOH solutions to adjust the pH of the deposition solutions will not effect the path of deposition to any great extent.

Poly(allyl amine hydrochloride) was chosen to be deposited onto PMP-COOH for 10 minutes from 0.016 M PAH solution adjusted to pH 8. At these conditions, the layer is formed by a self-assembly process. The nitrogen:oxygen ratio of 0.3 suggests, that the polyelectrolyte is adsorbed flat onto the surface with a high number of ionic bonds between ammonium and carboxylate groups. The deviation from ideal nitrogen:oxygen ratio of 0.5 is probably caused by oxygen from carboxylate groups in the region below the substrate-solution interface that is within the XPS sampling depth, but not not accessable to PAH molecule, presence of other oxygen-containing oxidation products that do not contribute to surface charge, and/or incomplete PAH layer coverage. A 10-minute-deposition time was shown to be sufficient to complete the process and was chosen for practical reasons to enable the handling of a number of samples simultaneously in an assembly of scintillation vials.

Deposition of PSS onto PMP-COOH/PAH surface

Deposition of poly(allyl amine hydrochloride) onto PMP-COOH created a positively charged PMP-COOH/PAH surface. Deposition of poly(sodium styrene sulfonate) onto the PAH surface to build the second layer was studied using 0.015 M PSS solutions at pH 4, 6, 8, and 10 with deposition times of 10 to 60 minutes. The XPS data for the second layer deposition series is presented in Table 21.

Sulfonate groups of PSS are ionized under all the pH conditions studied here. Thus any pH dependences of the deposition are caused by changes in the ionic state of the PAH surface. Self-assembly of the first layer (PAH) was shown to take place well within the 10 minutes that was chosen as the dipping time. A 10-minute-deposition of PSS onto PMP-COOH/PAH surface has a pH dependence shown in Figures 37 and 38 for nitrogen:sulfur and oxygen:sulfur ratios, respectively. As the deposition solution becomes increasingly acidic, the ionic interactions are strengthened leading to deposition of a self-assembled layer of PSS. This can be seen in the decrease of N:S ratio as a function of pH. The decrease in the O:S ratio is an indication of a weakening oxygen signal from the carboxylates of the original surface as the uniformity and/or thickness of the PSS layer increases with decreasing pH.

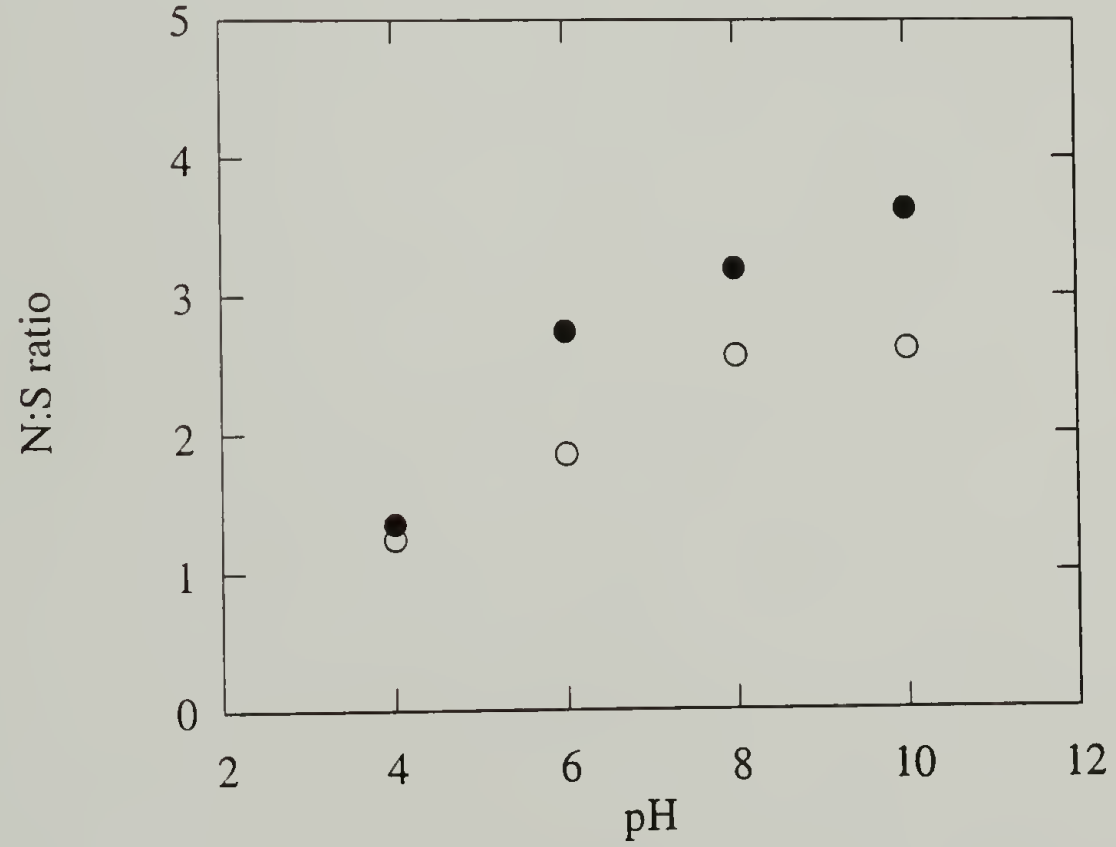

Figure 37. pH dependence of PSS self-assembly onto PMP-COOH/PAH. Nitrogen:sulfur atomic ratios after 10 minutes of deposition from 15° (○) and 75° (●) XPS analysis.

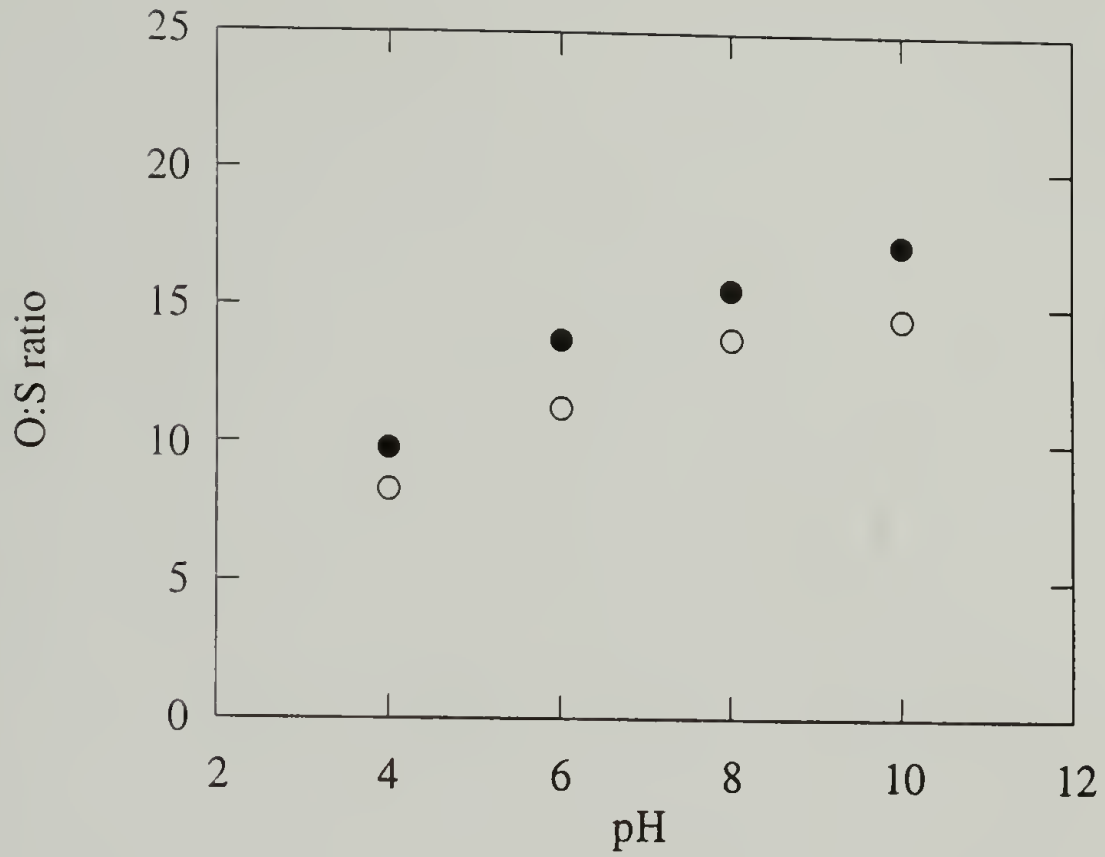

Figure 38. pH dependence of PSS self-assembly onto PMP-COOH/PAH. Oxygen:sulfur atomic ratios after 10 minutes of deposition from 15° (○) and 75° (●) XPS analysis.

Kinetic study of PSS depositions at pH 4 shows that the second layer is also formed rapidly. Similar to the formation of the first layer, the atomic compositions for the samples are practically identical, regardless of the deposition time (Figure 39). Clear deviation of the O:S ratio (Figure 38) from three for the sulfonate groups reveals that the bilayer thickness is thinner than the XPS sampling depth. Based on the atomic composition data for the deposition series, poly(sodium styrene sulfonate) was chosen to be deposited onto PAH surfaces for 10 minutes from 0.015 M PSS solution adjusted to pH 4.

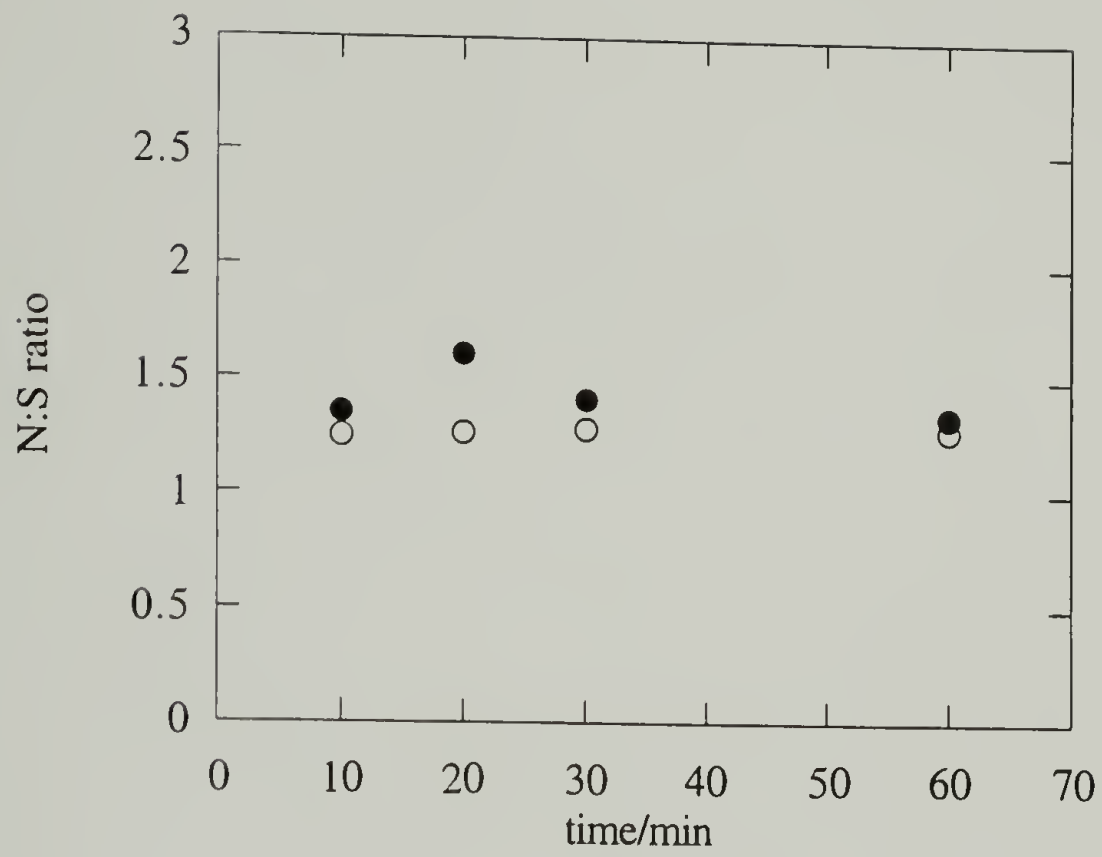

Figure 39. Kinetics of PSS self-assembly onto PMP-COOH/PAH at pH 4. Nitrogen:sulfur atomic ratios from 15° (○) and 75° (●) XPS analysis.

Deposition of PAH onto PMP-COOH/PAH/PSS surface

The third deposition type in this system is the deposition of PAH onto a sulfonate surface. The sulfonate substrate was prepared as described above by depositing PSS onto PMP-COOH/PAH. Deposition of the third layer was studied changing the deposition times from 10 to 60 minutes in 0.016 M PAH solutions adjusted to pH values 4, 6, 8 and 10. XPS data for the third layer depositions is presented in Table 22.

The nitrogen:sulfur ratio in Figure 40 remains almost constant as pH is raised from 4 to 8 as an indication of controlled self-assembly of PAH molecules onto the sulfonate surface. A slight increase in the amount deposited is caused by lowered solvent strength favoring deposition. At pH 10 the solvent strength is dramatically changed and PAH begins to partially precipitate out of the solution and deposits onto the surface. This can be seen in the absolute percentages of nitrogen and sulfur (Table 22) and is even more pronounced in the atomic ratios.

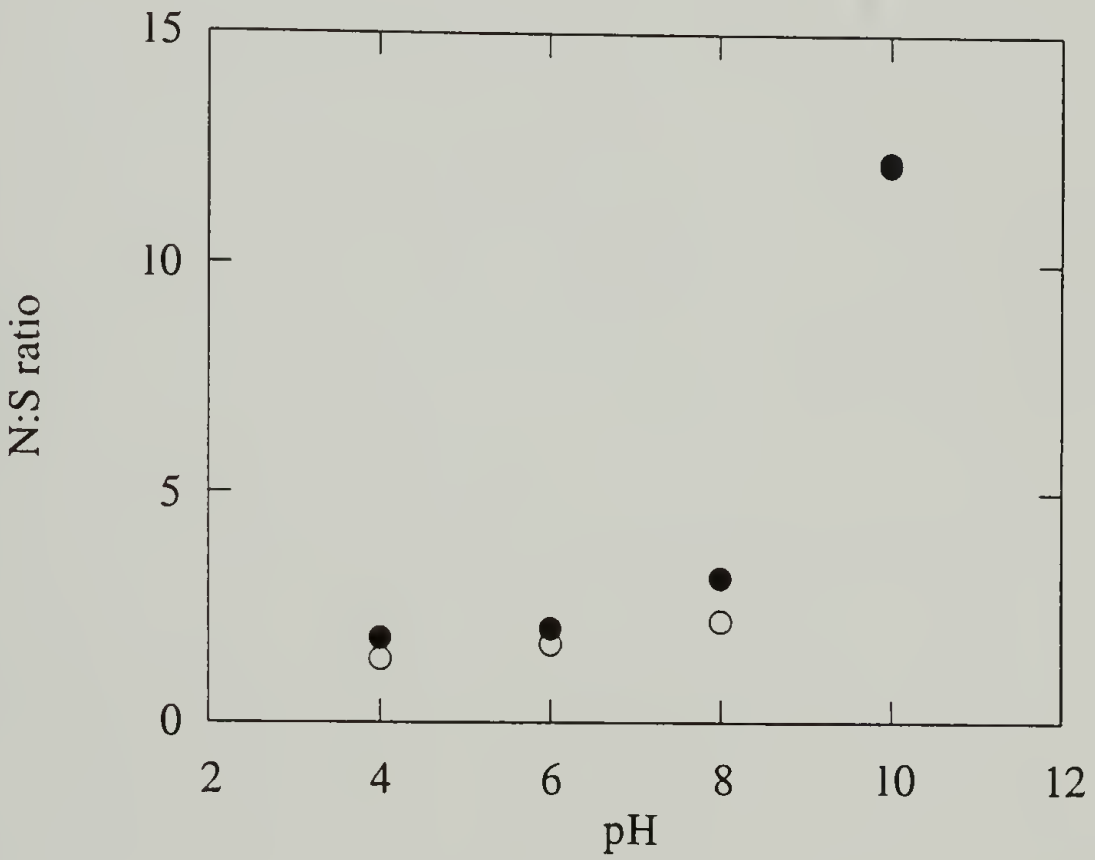

Figure 40. pH dependence of PAH self-assembly onto PMP-COOH/PAH/PSS. Nitrogen:sulfur atomic ratios after 60 minutes of deposition from 15° (○) and 75° (●) XPS analysis.

The peculiarly high oxygen:sulfur ratio at pH 10 (Figure 41) is caused by relative differences in the extent by which the precipitated PAH layer diminishes the strong oxygen signal from substrate and the weak sulfur signal from the thin PSS layer.

Like the preceding self-assemblies, the PAH deposition onto PSS surface was shown to take place rapidly. The nitrogen:sulfur ratio of ~3 (Figure 42) futher indicates that PAH forms thicker layers than PSS under these conditions but the total layer thickness is still thinner than the XPS analysis which probes through the layers into the substrate (high O:S ratio in Figure 41). Thus poly(allyl amine hydrochloride) was chosen to be deposited onto PSS surfaces for 10 minutes from 0.016 M PAH solution adjusted to pH 8.

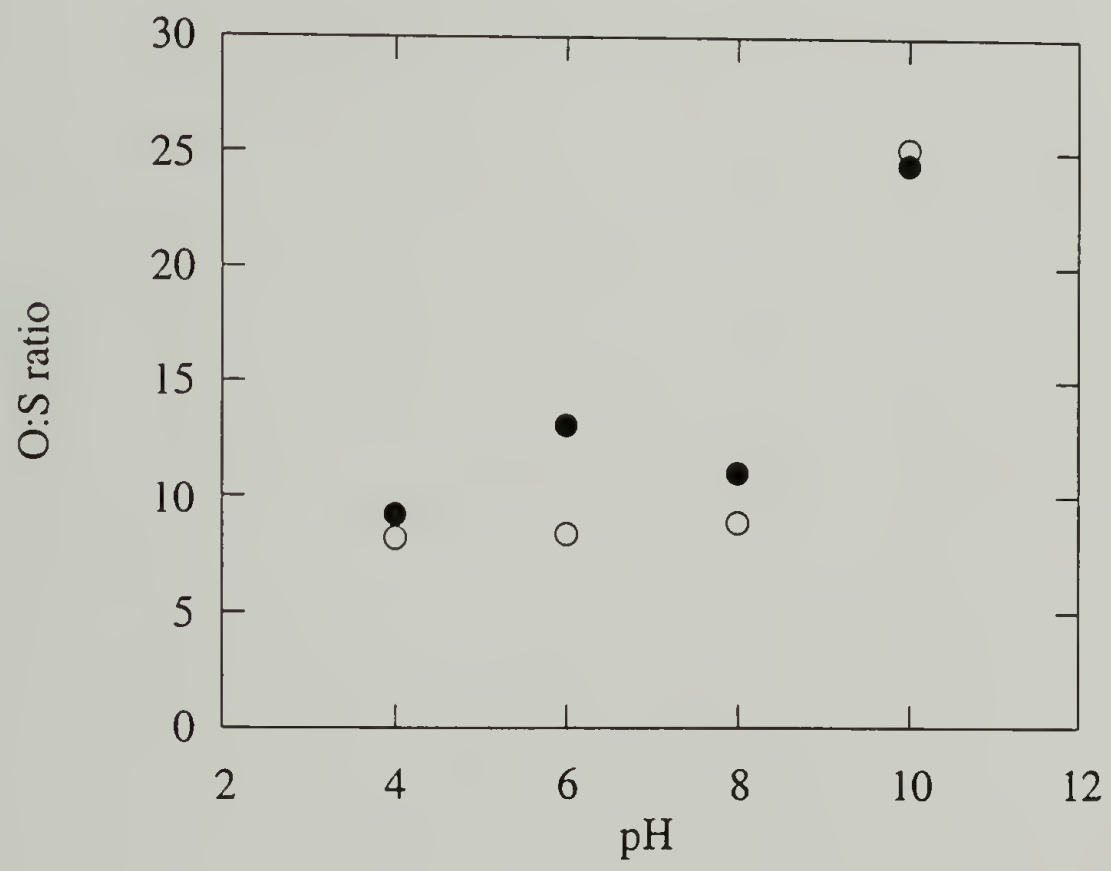

Figure 41. pH dependence of PAH self-assembly onto PMP-COOH/PAH/PSS. Nitrogen:sulfur atomic ratios after 60 minutes of deposition from 15° (○) and 75° (●) XPS analysis.

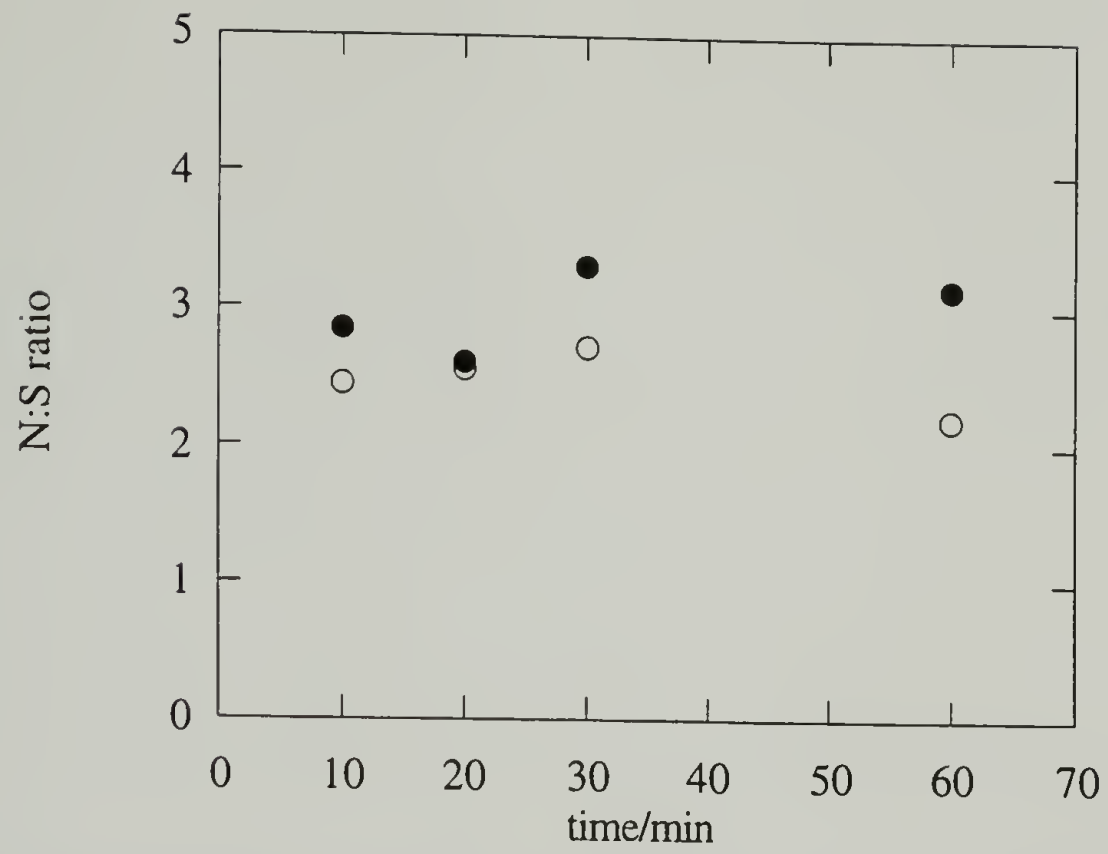

Figure 42. Kinetics of PAH self-assembly onto PMP-COOH/PAH/PSS at pH 8. Nitrogen:sulfur atomic ratios from 15° (○) and 75° (●) XPS analysis.

Layer-by-Layer Deposition of PAH and PSS into Multilayers

PAH and PSS were layer-by-layer deposited onto PMP-COOH to build up multilayered composite structures (PMP-COOH/PAH/PSS) for gas permeability studies. PAH was deposited for ten minutes from 0.016 M solution (aq.) adjusted to pH 8, and PSS was deposited from 0.015 M solution (aq.) adjusted to pH 4, also for ten minutes. Between depositions the samples were rinsed in two Milli-Q water baths and a Milli-Q water bath that was adjusted to the pH of the subsequent deposition solution. The pH adjusted rinse was used to minimize any solution transfer that could change the pH of the deposition solution in the process. After ten depositions the multilayers were air dried and stored under reduced pressure at room temperature overnight before

additional depositions or analysis. Fresh deposition solutions were prepared for each day of deposition.

XPS analysis of multilayers

A typical survey spectrum of a PMP-COOH/PAH/PSS multilayer is presented in Figure 43. The multilayer spectra feature S_{2p} (164 eV) and S_{2s} (230 eV), Cl_{2p} (200 eV) and Cl_{2s} (280 eV), C_{1s} (285 eV), N_{1s} (398 eV), O_{1s} (532 eV) and O(KVV) (745, 767 and 781 eV) peaks, the relative intensities of which depend on the location and thickness of PAH and PSS layers within the XPS sampling depth. Elemental composition data from XPS analysis for the multilayers is presented in Table 23.

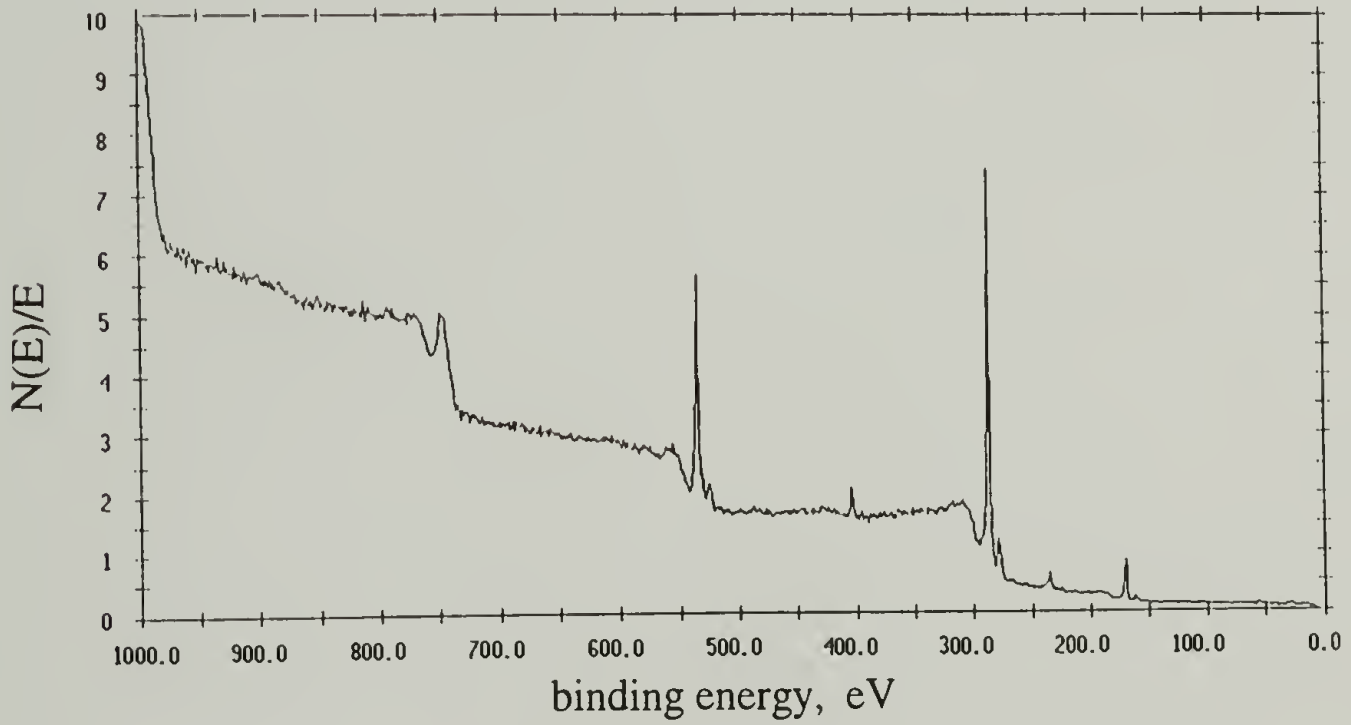

Figure 43. XPS survey spectrum of a PMP-COOH/PAH/PSS multilayer sample with 102 layers.

If the deposited layers are well defined, and there is not extensive mixing between the layers, data from surface-sensitive analytical techniques should strongly

depend on which polyelectrolyte, PAH or PSS, was used in the last deposition step. The three components in the multilayered structures are "labeled" in their atomic composition: in the case of building stratified layers one creates regions that are rich in oxygen (PMP-COOH), nitrogen (PAH) and sulfur (PSS).

The nitrogen:sulfur ratio (from 75° take-off angle XPS data) as a function of number of layers is presented in Figure 44. For samples that had PAH used in the last deposition step, the N:S ratio has a typical value of 1.7 to 1.8. Deposition of PSS onto any of the those samples causes the value of the atomic ratio to be lowered to approximately 1.2 to 1.3. This trend in alternating values for the N:S atomic ratio was shown to be true for a sample series with up to 104 layers (the highest number of layers prepared in this study). This implies that the layered structure is consistently stratified and the PAH layers are thicker than the PSS layers.

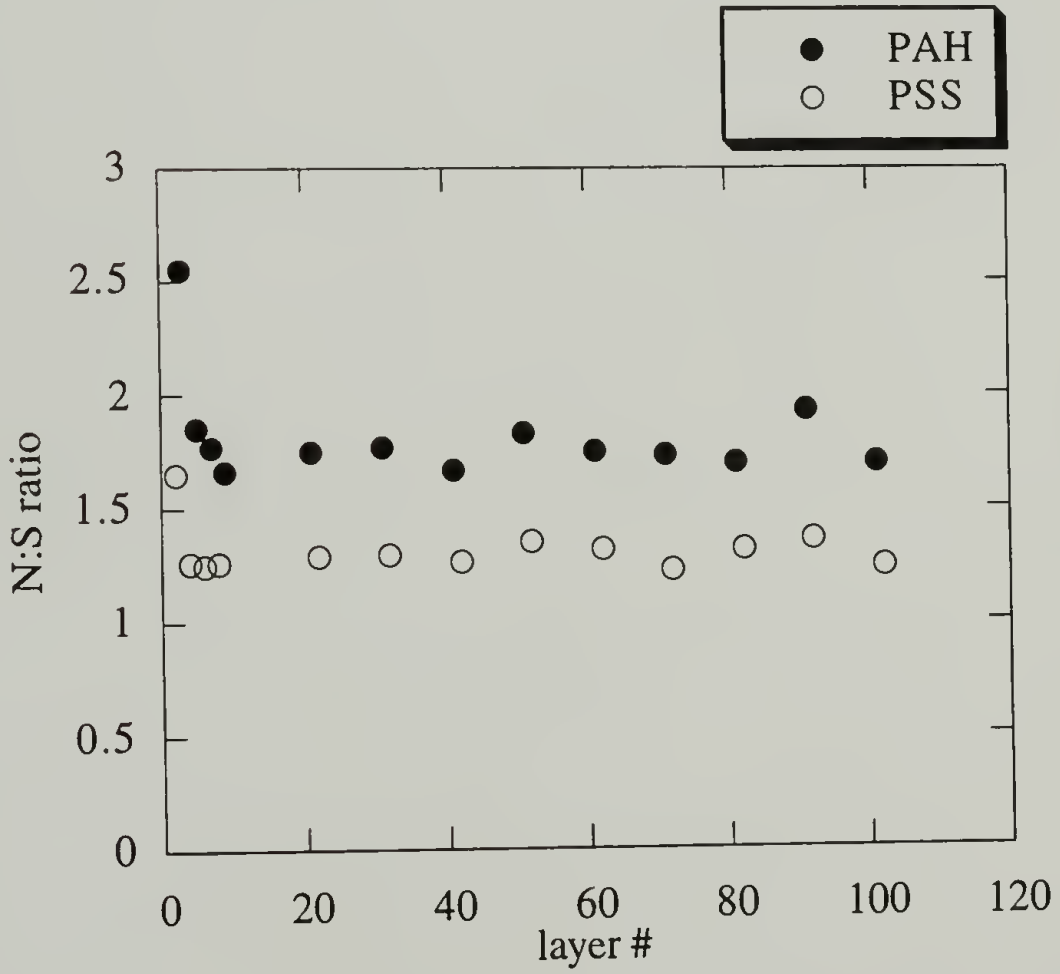

Figure 44. Nitrogen:sulfur atomic ratio (75° XPS data) as a function of number of layers for a series of PMP-COOH/PAH/PSS membranes.

The oxygen:sulfur ratio as a function of number of layers is presented in Figure 45. For samples with only a few layers, the XPS sampling depth reaches the carboxylated substrate resulting in high O:S values. After approximately 8 to 10 depositions the value of the atomic ratio reaches an almost constant level of four. The fact that sulfonate groups contains three oxygen atoms and that the deposition of PAH onto a PSS surface causes the oxygen content to increase slightly, is most likely an indication of presence of water molecules that are strongly bound to the structure (PAH layer in particular) even at the 10^{-9} torr pressures inside the XPS test chamber.

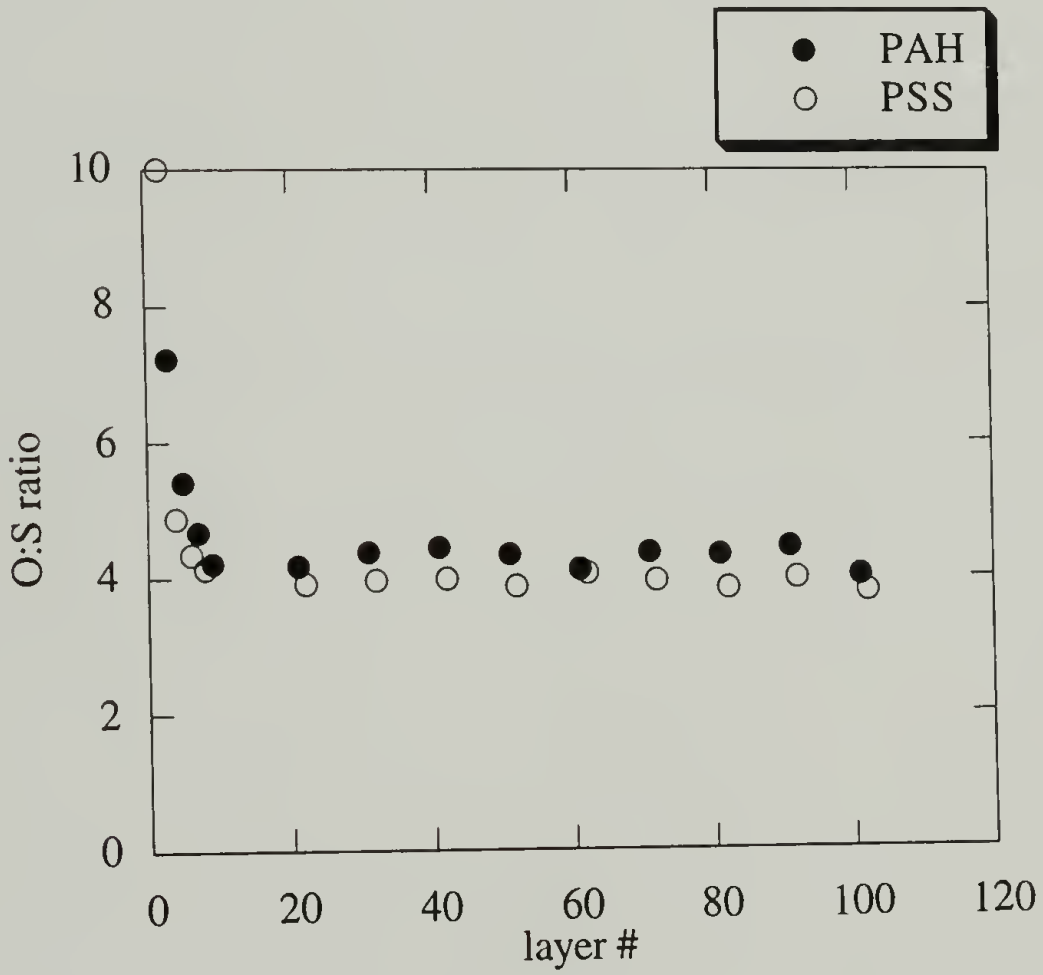

Figure 45. Oxygen:sulfur atomic ratio (75° XPS data) as a function of number of layers for a series of PMP-COOH/PAH/PSS membranes.

Signals from chloride counterions are absent or close to the detection limit in the XPS analysis. Since there is an an excess of ammonium groups over sulfonate groups in the multilayers (see the discussion above), the structure must lose HCl after the self-assembly to form free amine groups from PAH functionalities that are not bound to sulfonate groups on the adjacent PSS layer.

Contact Angle Analysis of Multilayers

In the case of stratified layers, contact angle analysis of the multilayer surface should be sensitive to the wetting properties of the polyelectrolyte used in the last deposition step. The cosine of dynamic advancing contact angle measured using water as the probe fluid (Figure 46) shows that the surface energy of the multilayered samples are greatly dependent on the polyelectrolyte used in the last deposition. Samples with PAH as the last deposited polyelectrolyte gave advancing contact angle of 83° and deposition of PSS onto that surface lowers the angle to 50° indicating that the polyelectrolytes form stratified layers with characteristic wetting properties.

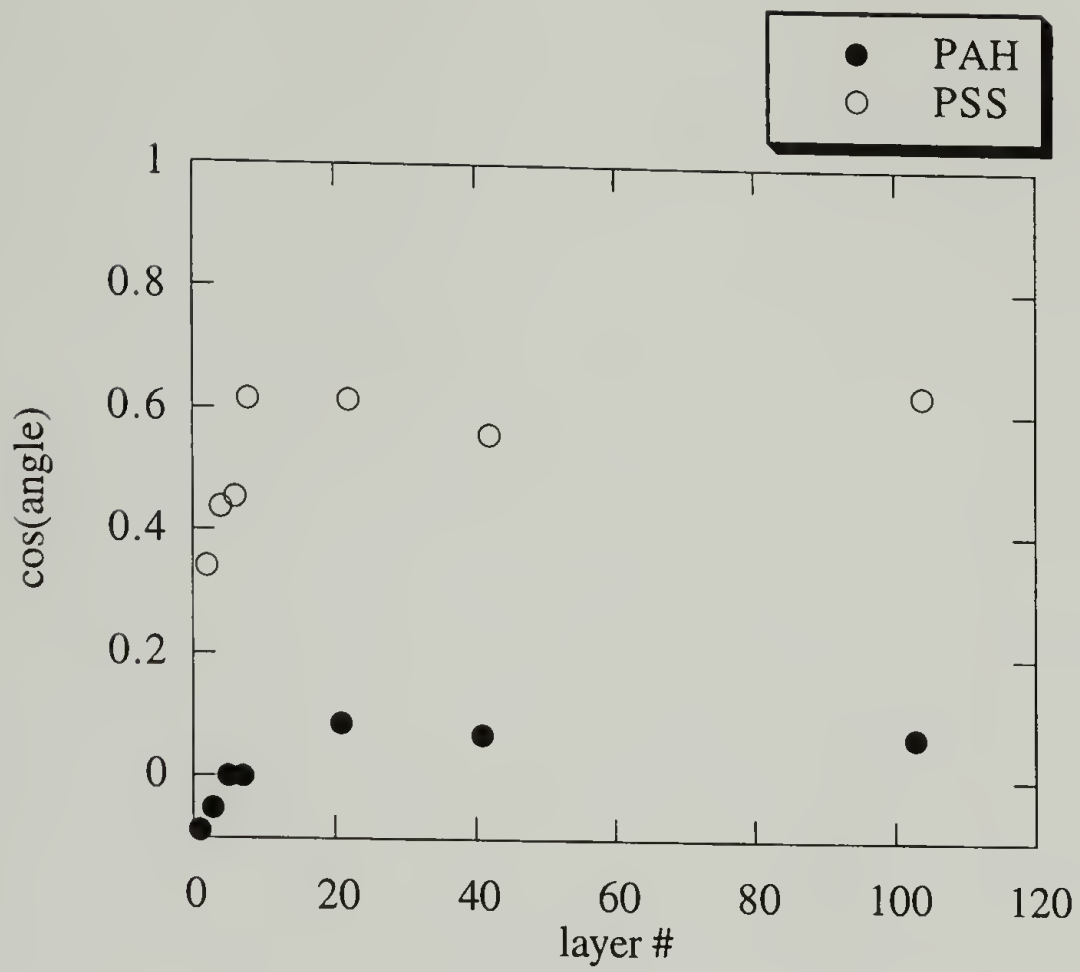

Figure 46. Cosine of the advancing contact angle with water as the probe fluid for a series of PMP-COOH/PAH/PSS membranes.

ATR-FTIR Analysis of Multilayers

An ATR-FTIR spectrum (acquired using a 45° germanium internal reflection element) of a sample with 104 layers is presented in Figure 47. The spectrum shows features of both the substrate and the layers suggesting that even though the multilayer structure is thick enough to give detectable absorption of IR radiation, it is thinner than the sampling depth of ~0.5 μm of a Ge crystal.

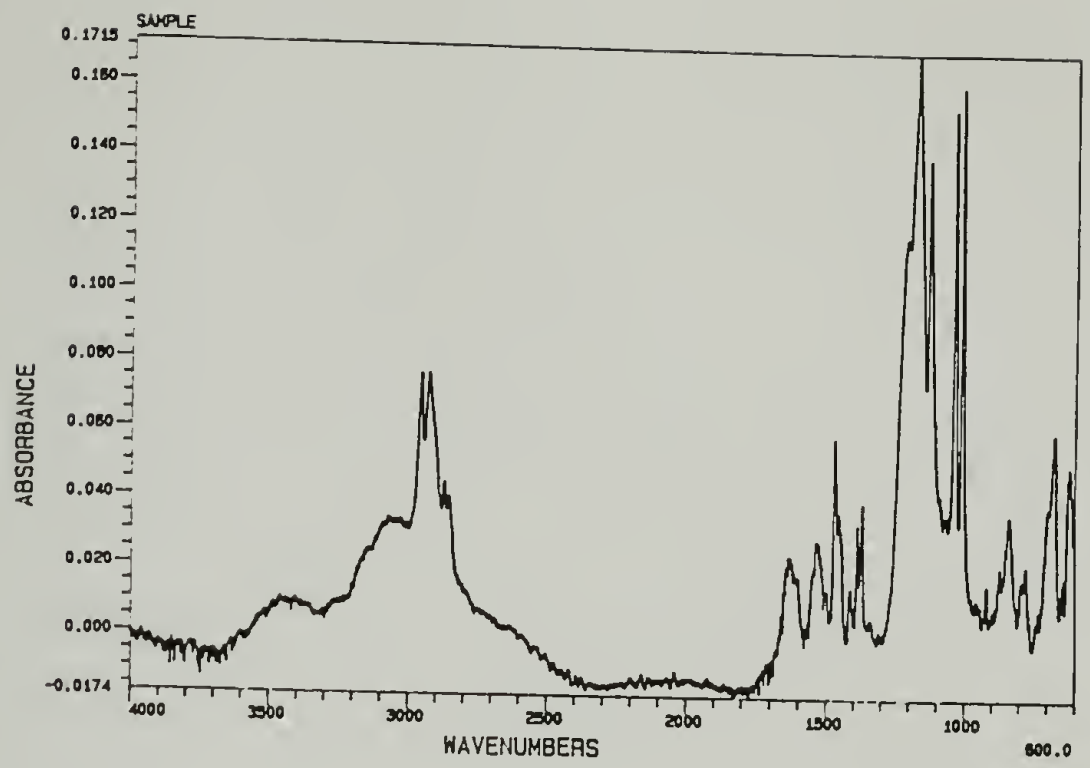

Figure 47. ATR FTIR spectrum (45° Ge internal reflection element) of a PMP-COOH/PAH/PSS membrane with 104 layers.

The double peak at 1380 cm^{-1} is due to -$CH(Me)_2$ deformation and characteristic of the bulk PMP. The carbonyl streching band of the oxidized PMP surface is still visible, even though partly covered by broad peaks due to amino group deformations.

The amino group deformation peaks at 1500 and 1600 cm^{-1} originate from infrared absorption in the PAH layers. The N-H streching band of free amino groups is located at 3400 cm^{-1} and that of ammonium groups gives broadening to the bands in the 3000 cm^{-1} region. The existence of both free amine and ammonium bands in the spectrum supports the assumption made earlier about the loss of HCl from the ammonium groups that are not anchored to PSS layers. The four streching bands characteristic of a sulfonate groups in PSS layers are seen near 1230, 1190, 1130 and 1040 cm^{-1}.

Mechanical Integrity of Multilayers

The mechanical integrity of the PMP-COOH/PAH/PSS multilayers was studied using the pressure sensitive adhesive test. A tape with pressure sensitive adhesive was stuck to multilayer samples with 7 (PAH surface) and 8 (PSS surface) layers and the laminate structure was rolled 20 times with a roller before peeling the tape off at a 180° angle. XPS analysis (Table 24) of the two delaminated surfaces in both experiments revealed that the failure took place in the adhesive leaving a thin adhesive coating onto the PAH and PSS surfaces.

In another qualitative experiment, evaporation of water off a multilayer sample in surface contact with glass gave an adhesive joint strong enough to lead to cohesive failure in the PMP film. Similarly, two multilayer samples (with a total layer number of 103 and 104 with PAH and a PSS surfaces, respectively) were sandwiched in a wet state between glass microscope slides, and forced to flat contact using tightly wrapped rubber bands while drying at reduced pressure. Tearing the structure apart resulted in failure in the bulk of the film or in the glass when applying force with tweezers. At the end the components were not suitable for XPS analysis.

X-Ray Reflectivity Study

Contact angle and XPS studies indicated that the layered structure is highly organized and stratified. In order to determine the average thickness of a layer, alternating monolayers of PAH (10-minute-deposition from 0.016 M PAH solution at pH 8) and PSS (10-minute-deposition from 0.015 M PSS solution at pH 4) were self-assembled onto amino-functionalized silicon wafers for X-ray reflectivity studies. Samples were prepared with a total number of 2, 4, 6, 8, 10, 20 and 30 layers.

The silane coupling layer ($-SiMe_2-CH_2-CH_2-CH_2-NH_2$) alone was too thin to be analyzed by the technique, whereas the reflectivity data for the sample with two layers

could not be fitted to any electron density model indicating a nonuniform coating on the wafer. Dry thickness data for samples with 4 to 30 layers is presented in Table 25. In the table the corrected thicknesses are based on an estimate of 5 Å for the silane coupling layer, the existence of which was proved by XPS analysis as shown below. Figure 48 shows that the total thickness of a multilayer assembly (including the coupling layer) increases almost linearly with the number of layers. For example the difference in thickness of samples with 20 and 30 layers equals that of samples with 10 and 20 layers. The average thickness of a layer depends on its location in the multilayer structure; after about 10 depositions an equilibrium thickness of 10.6 Å is reached, the first layers being considerably thinner.

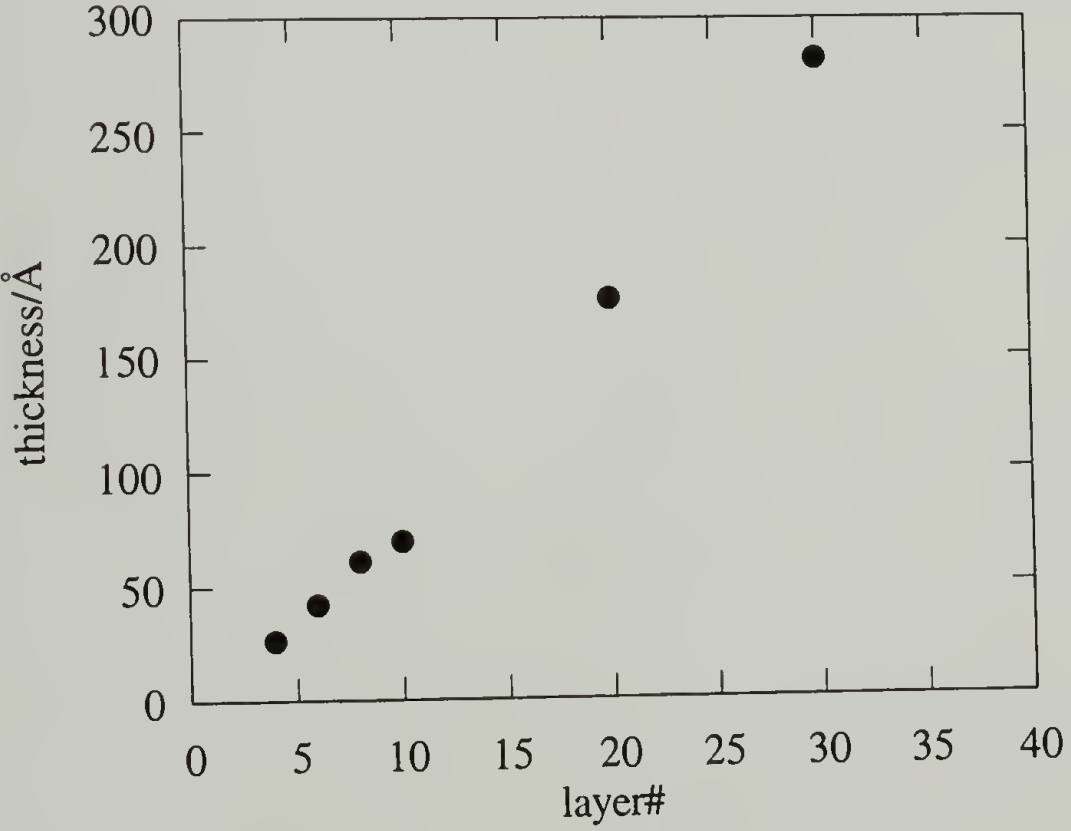

Figure 48. Total thickness of PAH/PSS multilayers on silane coupled silicon wafers.

Samples with 10, 20 and 30 layers were also exposed to various levels of relative humidity. Multilayers were allowed to equilibrate at a particular humidity level for 6 hours before starting the 5-hour-measurement for thickness. This was shown to be sufficient to reach the final extent of swelling. Data for the hydrated thicknesses is also presented in Table 25. The sample with 10 ten layers swelled up 29 % upon hydration (Figure 49), whereas 20 and 30 layers swelled 16 and 13 %, respectively (Figures 50 and 51).

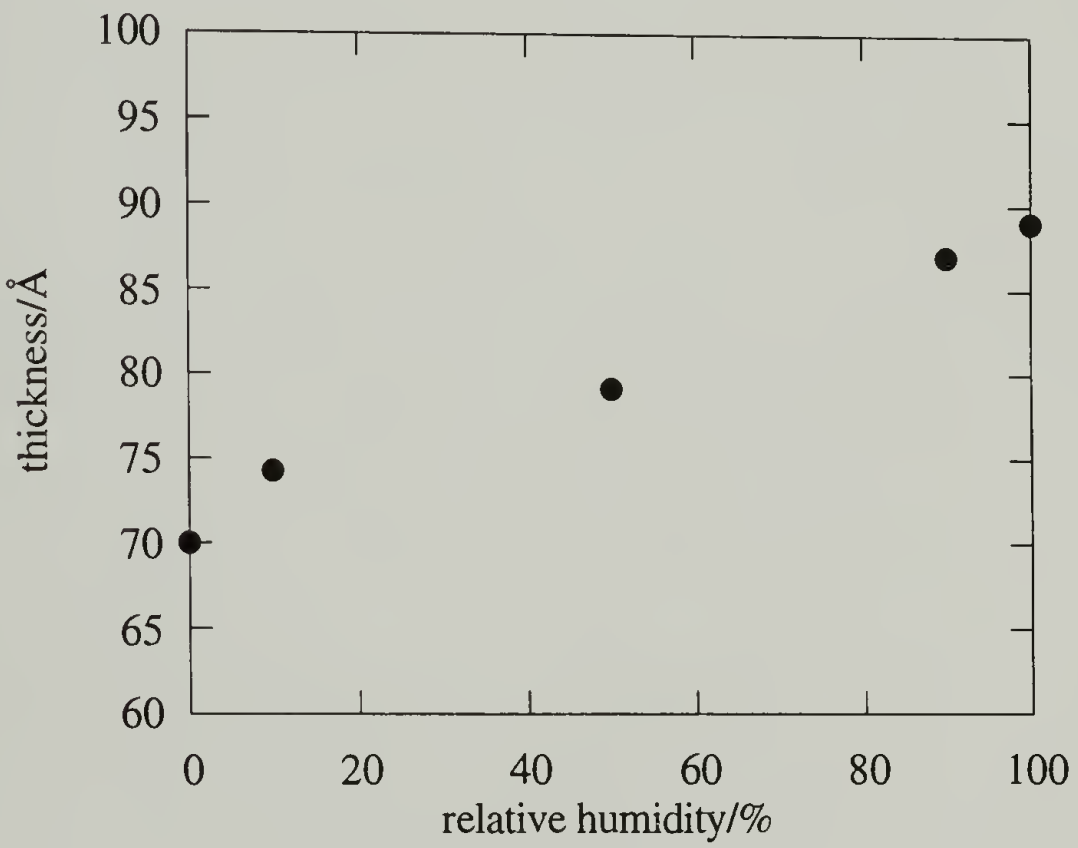

Figure 49. Thickness of 10 PAH and PSS layers on silane coupled silicon wafer as a function of relative humidity.

The swelling experiment suggests that the molecules in the first few layers are fairly loosely packed leaving the layers susceptible to plastication by water molecules, that polar structures such as polyelectrolytes have an inherent affinity to. As the total number of layers increases, the self-healing deposition process gives layers that are uniform in thickness and increasingly swelling-resistant, suggesting efficient packing of molecules within them. The swelling can be further induced by exposure of water vapor at elevated temperatures (Figure 51).

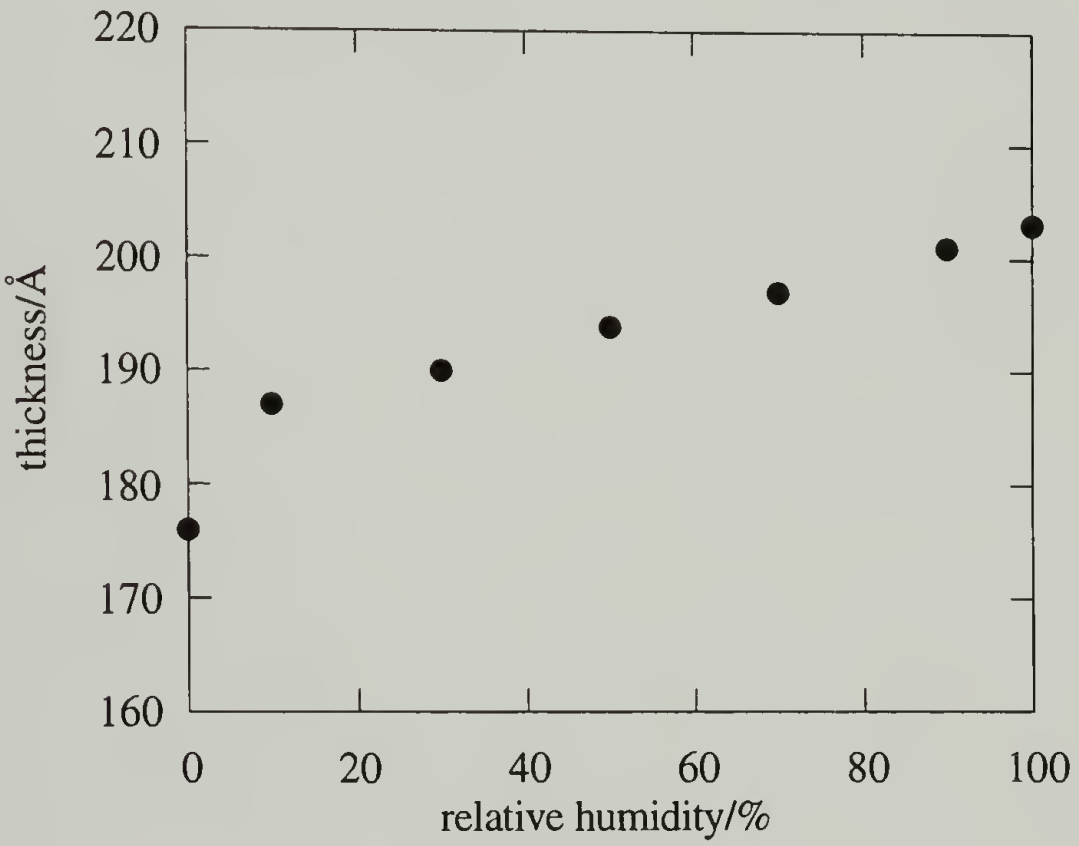

Figure 50. Thickness of 20 PAH and PSS layers on silane coupled silicon wafer as a function of relative humidity.

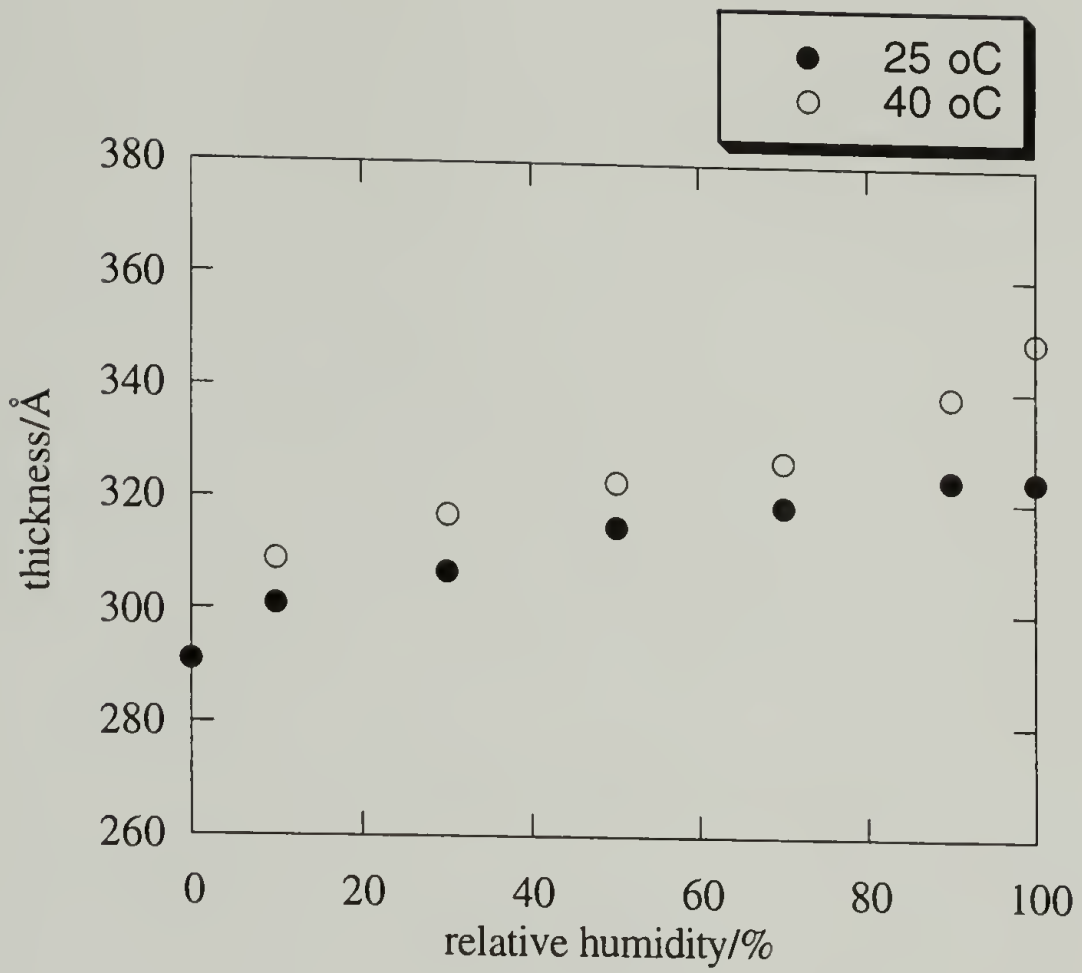

Figure 51. Thickness of 30 PAH and PSS layers on silane coupled silicon wafer as a function of relative humidity.

XPS Analysis of the Si-NH_2/PSS/PAH Multilayers

After the X-ray reflectivity measurements the same samples were analyzed by XPS. Elemental composition data (for the multilayers on the polished surface of the wafer) at 15° and 75° take-off angles is presented in Table 26. The silicon:carbon ratios from XPS analysis and total thicknesses from reflectivity measurements are plotted as a function of number of layers in Figure 52. The silicon signal from the substrate practically disappears after 8 or ten layers in the 75° take-off angle data as was seen earlier for the disappearance of the oxygen signal from the PMP-COOH substrate. This indicates that the layer formation on the two substrates studied is not sensitive to the chemical nature or roughness of the original substrate and the data from different studies can be compared with each other.

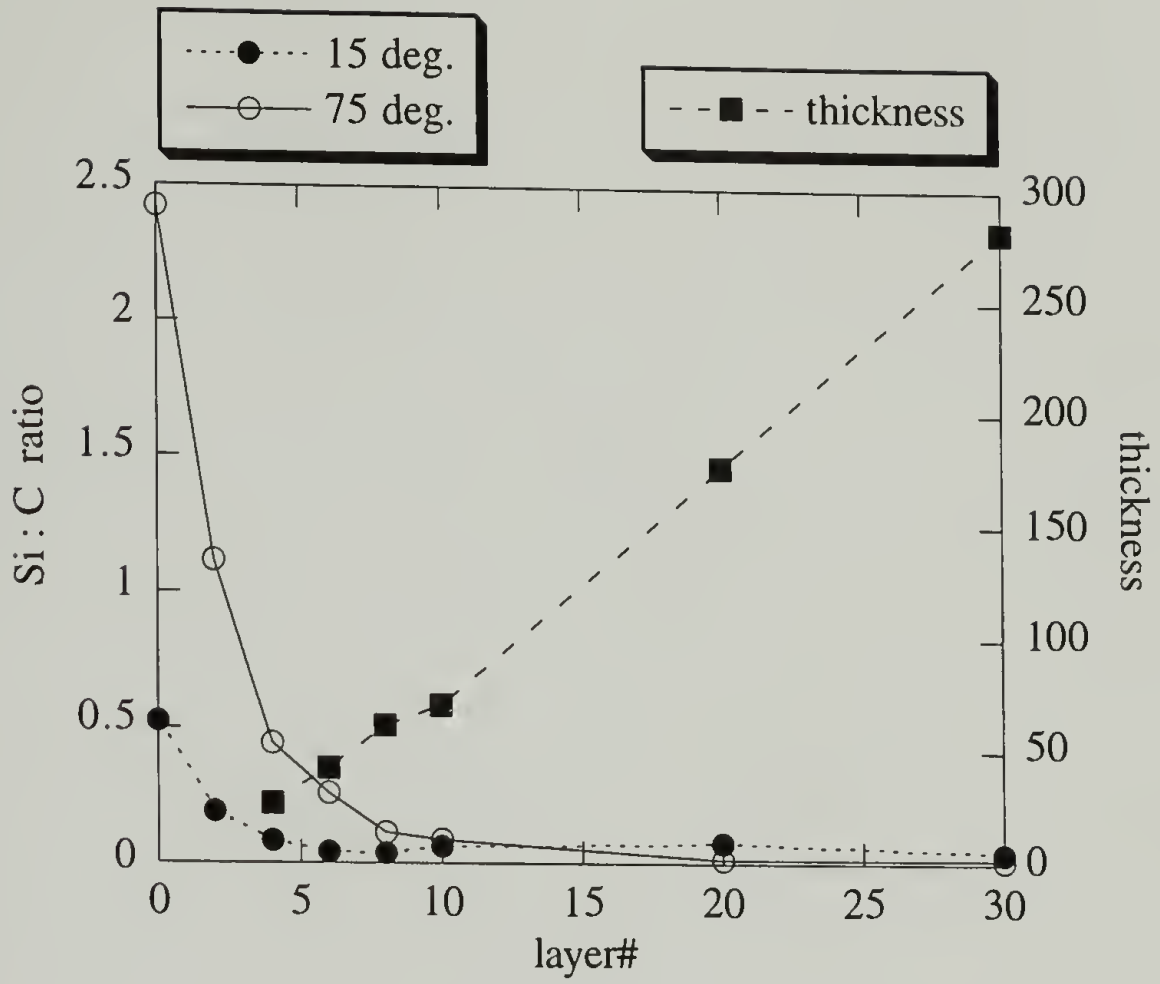

Figure 52. Silicon:carbon atomic ratios form XPS analysis and thickness from reflectivity measurements for a series of multilayers on silane-coupled silicon wafers.

The weak silicon signal that can be detected even in the case of 30 layers (total layer thickness of 281 Å) can be explained by sample edge effect and multilayer damage when cutting the XPS samples leading to some exposed bare silicon wafer. This effect is even more pronounced in the 15° experiment, as can be seen in Table 26.

Gas Permeability of PMP-COOH/PAH/PSS Multilayers

Gas permeabilities of the unmodified PMP, surface oxidized PMP and a series of multilayered membranes were determined to nitrogen, oxygen and hydrogen (Table 27) as shown earlier for the chlorinated PMP membranes. Surface oxidation does affect

the gas permeability of PMP within experimental variation, whereas alternating deposition of PAH and PSS layers lowers the permeability, even in the case of 10 layers. Total number of layers in Table 27 is the sum of number of layers on both sides of the membrane, thus a ten-layer-sample was prepared by five deposition cycles.

Multilayer thickness determinations and swelling experiments suggested that approximately ten deposition cycles were needed to create effectively packed layers of uniform thickness. A comparison of the effectiveness of five layers (a total of ten layers on the membrane) and ten layers (total of twenty layers) to reduce the flux of gas through the membrane supports this picture of packing efficiency as the diffusing gas molecules act as nanoprobes relating the macroscopic permeability properties to differences in packing at the molecular level. Considering the thicknesses of the multilayered structures and the PMP substrate, we can calculate the barrier properties of the multilayered structure using the Equation 2 in Chapter 1. For nitrogen, the multilayered structure is of the order of 18,000 times better barrier than PMP.

Multilayered membranes have improved gas selectivities as compared to bulk PMP. Selectivities calculated from single gas experiments are reported for the composite membrane with 200 layers in Table 28.

The changes in gas permeability indicate that the polyelectrolytes are packed in the monolayers in a very dense and rigid manner. The multilayers can be looked at, in a simplified manner, as assemblies of interfaces where the majority of the repeat unit of the polyelectrolytes are ionically crosslinked to the interface below or above it. The intersegmental distance in the defect-free layers must be comparable to the diameter of the studied gas molecules as considerably larger gaps between chain segments, or defects on a macroscopic scale would not give so extensive reductions in the gas flow through the membrane.

Deposition of PAn and PSS onto PMP-COOH

The layer-by-layer technique under certain conditions can be used to pack the polymer molecules into the layers in a dense and rigid manner to effectively change the gas permeability properties of a composite membrane as was shown above. In order to study the versatility of the layer-by-layer technique, and the role that the chemical structure of the polymer molecule plays in creating the barrier properties in the multilayered structure, poly(allyl amine hydrochloride) was replaced by polyaniline (PAn) in the second part of the project. Polyaniline can be rendered conducting by doping. The ionic sites thus created along the polymer chain can be used to drive the deposition as in the case of traditional polyelectrolytes. With the inherent chain rigidity of PAn in its doped state, further increases in barrier properties in the composite membrane were hoped to be induced, in addition to the dense packing and ionic crosslinking characteristic of the deposition technique used.

In literature polyaniline has been dissolved in N,N-dimethylacetamide (DMAc) by long ultrasonic bath treatments. The ultrasonic dissolution of various polymers is known to lead to extensive chain scission and this is also likely to be the case with PAn dissolution. As lowered molecular weight would lead to defects (increased number of chain ends) in the layers, a thermal dissolution approach was taken to prepare the PAn deposition solutions as described in the Experimental Section.

Adding dropwise 6.0 ml of the PAn/DMAc stock solution into 50 ml of pH 4 adjusted Milli-Q water while stirring, gave a purple solution of pH 3.6. The final pH of three solutions prepared this way were adjusted to 2, 4 and 6.

The pH 2 solution was of clear green color and upon filtering through a 0.22 μm teflon filter it became almost colorless. It was suspected that at pH 2 PAn was highly doped and not truly dissolved. The pH 4 solution was purple before and after filtration. The solution was also easier to filter than the pH 2 solution. A second filtration with a new filter proved that the original filter was not defective, but PAn had remained

dissolved in the solution. The pH 6 solution was blue in color and became almost colorless upon filtration. PAn was suspected to be at a low doping level and the charge density was not high enough to keep the polymer dissolved in an aqueous medium.

Deposition of PAn onto PMP-COOH

All the filtered solutions were used for studying PAn deposition onto PMP-COOH. Only in the case of depositions at pH 4 reasonable amounts of PAn were detected in XPS analysis as can be seen in Table 29. Interestingly, PAn had precipitated out of the pH 2 and 6 solutions overnight, indicating that the suspected solubility problems were real.

Due to the protonated state of the oxidized PMP surface at pH 4, the interaction between PMP-COOH surface and doped PAn is not truly ionic in nature at this pH. There is a slight indication of a decreased rate of deposition (or packing into the final state, see the 15° data in Figure 53) as compared to the previously discussed self-assemblies, thus a deposition time of 20 minutes was chosen for PAn depositions in preparing the multilayered structures.

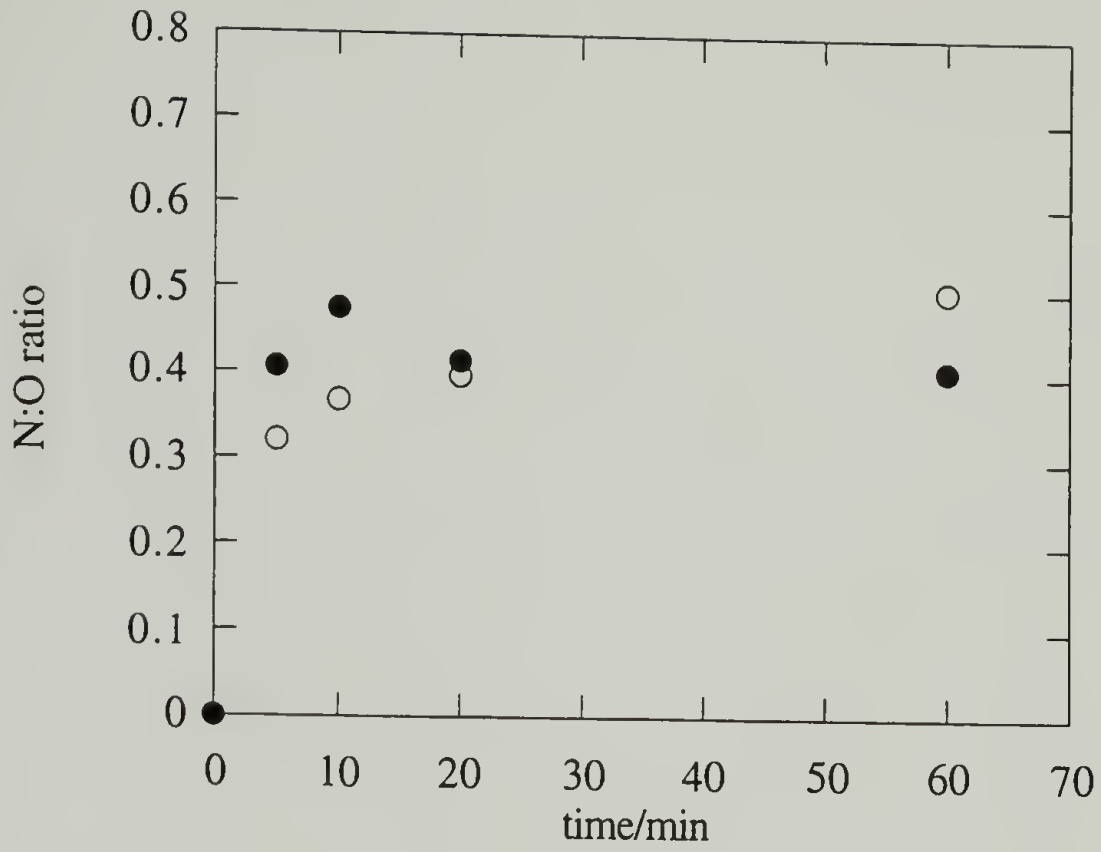

Figure 53. Kinetics of depositing PAn onto PMP-COOH at pH 4. Nitrogen:oxygen atomic ratio from 15° (○) and 75° (●) XPS analysis.

Deposition of PSS onto PMP-COOH/PAn

PSS deposition onto the PAn surface was studied from 0.016 M PSS solutions adjusted to pH 0, 2, 4, and 6. Elemental composition data in Table 30 (and S:N atomic ratio in 20-minute depositions as a function of pH in Figure 54) indicate that depositions at pH 0 gave the strongest interaction between the surface and the depositing PSS molecule. This is caused by increased charge density at the PAn surface in low pH solutions. Based on kinetics study at pH 0, the interaction between PSS and surface is not strongly ionic in nature leading to a linear decrease in nitrogen:sulfur ratio (Figure 55) at a constant sulfur concentration (Table 30). This indicates that the layer thickness increases with deposition time. Deposition time of 20 minutes was chosen for preparing the multilayers as it leads to a reasonable sulfonate concentration in a thin PSS layer.

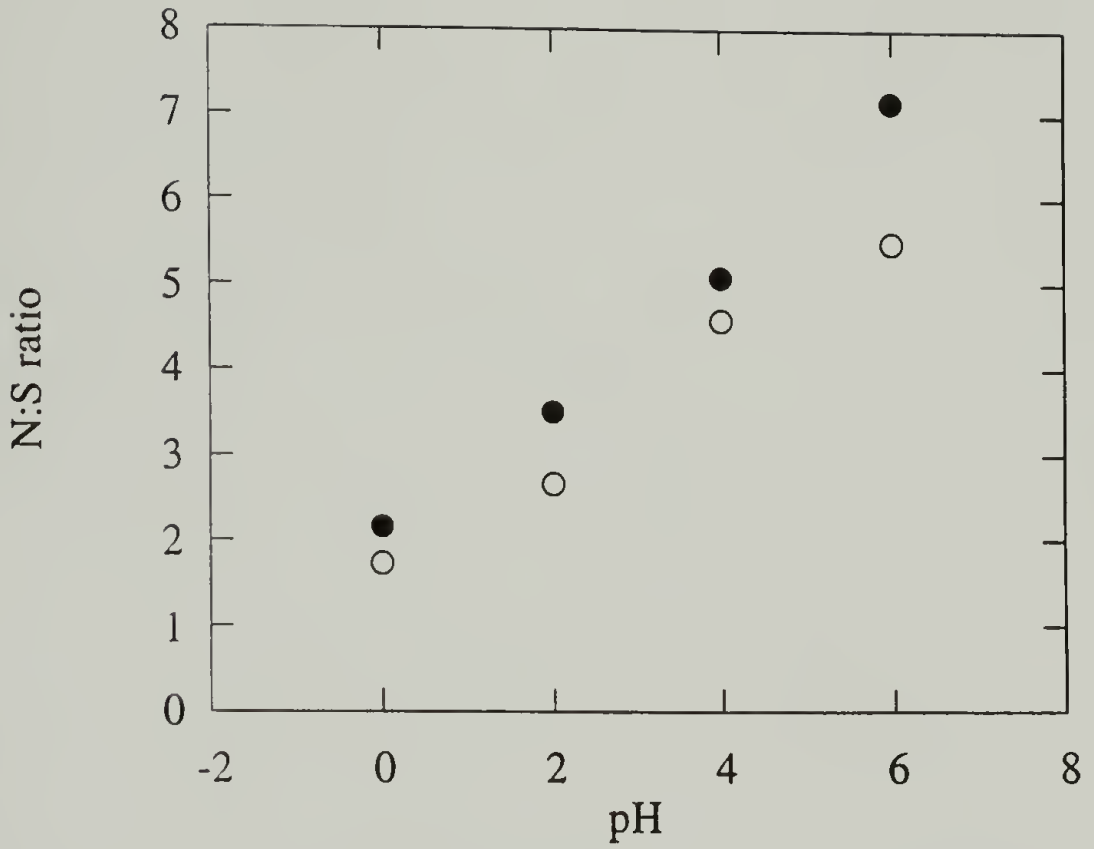

Figure 54. pH dependence of PSS deposition (20 minutes) onto PMP-COOH/PAn. Nitrogen:sulfur atomic ratio from 15° (○) and 75° (●) XPS analysis.

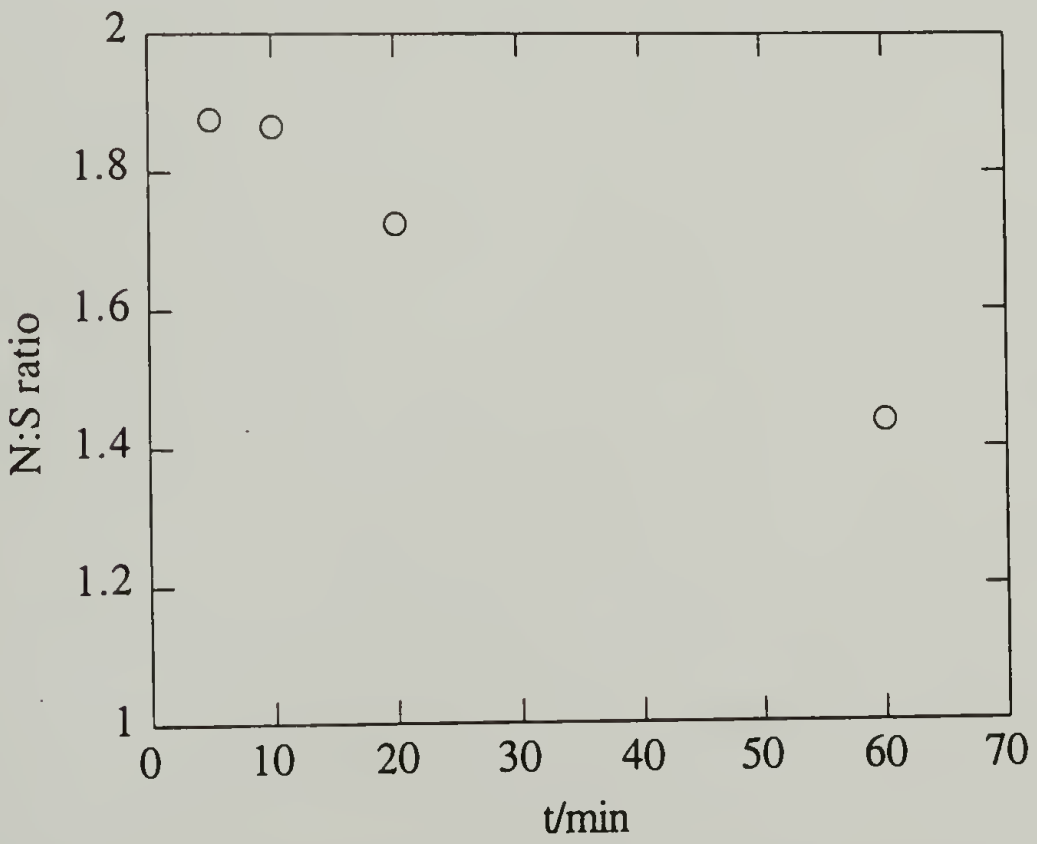

Figure 55. Kinetics of depositing PSS onto PMP-COOH/PAn at pH 0 (15° take-off angle XPS analysis).

PMP-COOH/PAn/PSS multilayers

Multilayers were built up by alternating deposition of PAn (20 minutes at pH 4) and PSS (20 minutes, 0.015 M PSS at pH 0) onto PMP-COOH substrate. A series of samples with the number of layers up to 25 on each side of a membrane was prepared for contact angle, XPS, ATR-FTIR spectroscopy and gas permeability studies. Previous work with the PMP-COOH/PAH/PSS multilayers showed that no more than a total of 50 layers (25 layers on each side of membrane) were needed to see interesting changes in gas barrier properties of the membrane. Thus membranes with 20 and 50 layers were prepared for gas permeability determinations.

XPS elemental composition data for the PMP-COOH/PAn/PSS multilayers is presented in Table 31. The PAn layers are shown to contain Cl^- counterions consistently and in considerably higher concentration than PAH layers in the first multilayer system. This can be caused by a higher relative number of nonanchored charged units along the PAn chain, or by their stability as compared to suggested expulsion of HCl from PAH layers. Figure 56 shows the alternating nitrogen:sulfur ratios as a function of the number of layers indicating a stratified structure also for PAn/PSS layers.

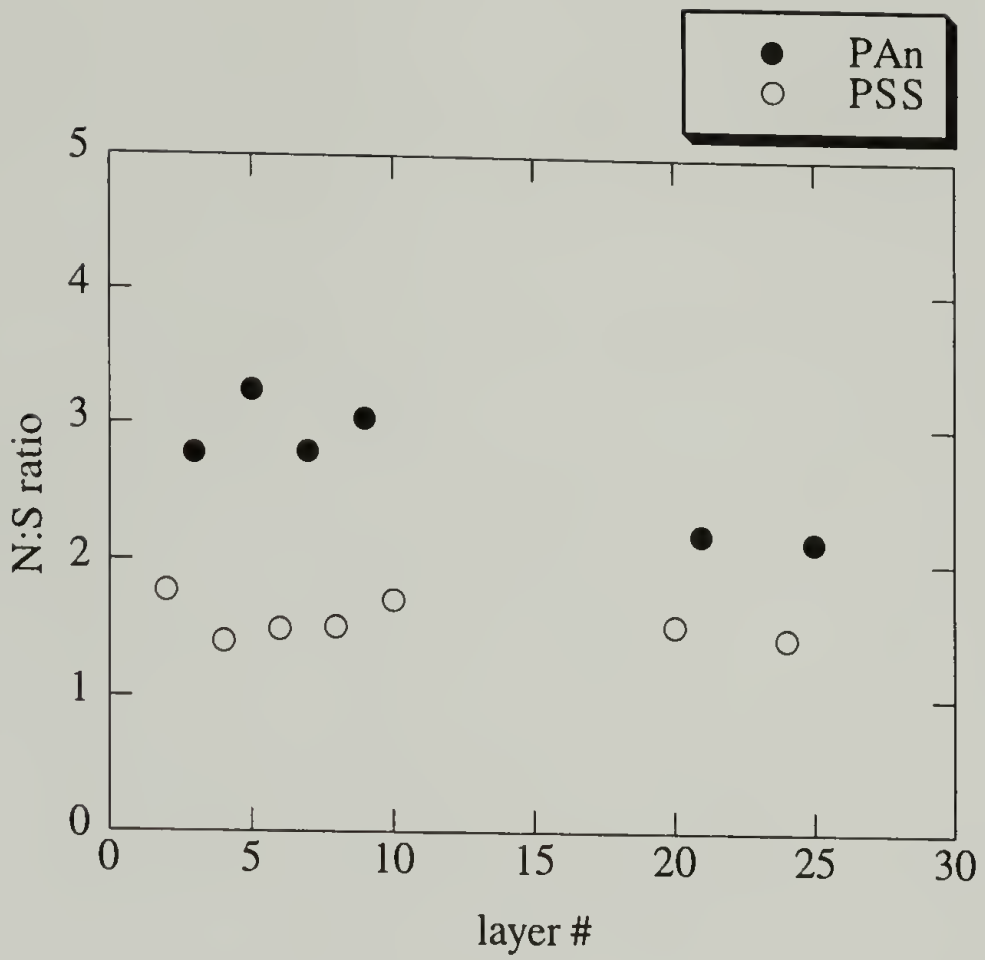

Figure 56. Nitrogen:sulfur atomic ratios for a series of PMP-COOH/PAn/PSS membranes (15° XPS analysis).

Similarly to the PAH/PSS multilayers, deposition of PAn or PSS creates two surfaces distinctly different in their wetting behavior. Figure 57 shows the cosine of advancing contact angle with water as the probe fluid for a series of multilayered samples. PAn as the topmost layers results in an advancing contact angle of 82 whereas deposition of PSS onto that surface will cause the value of the angle to decrease to 62.

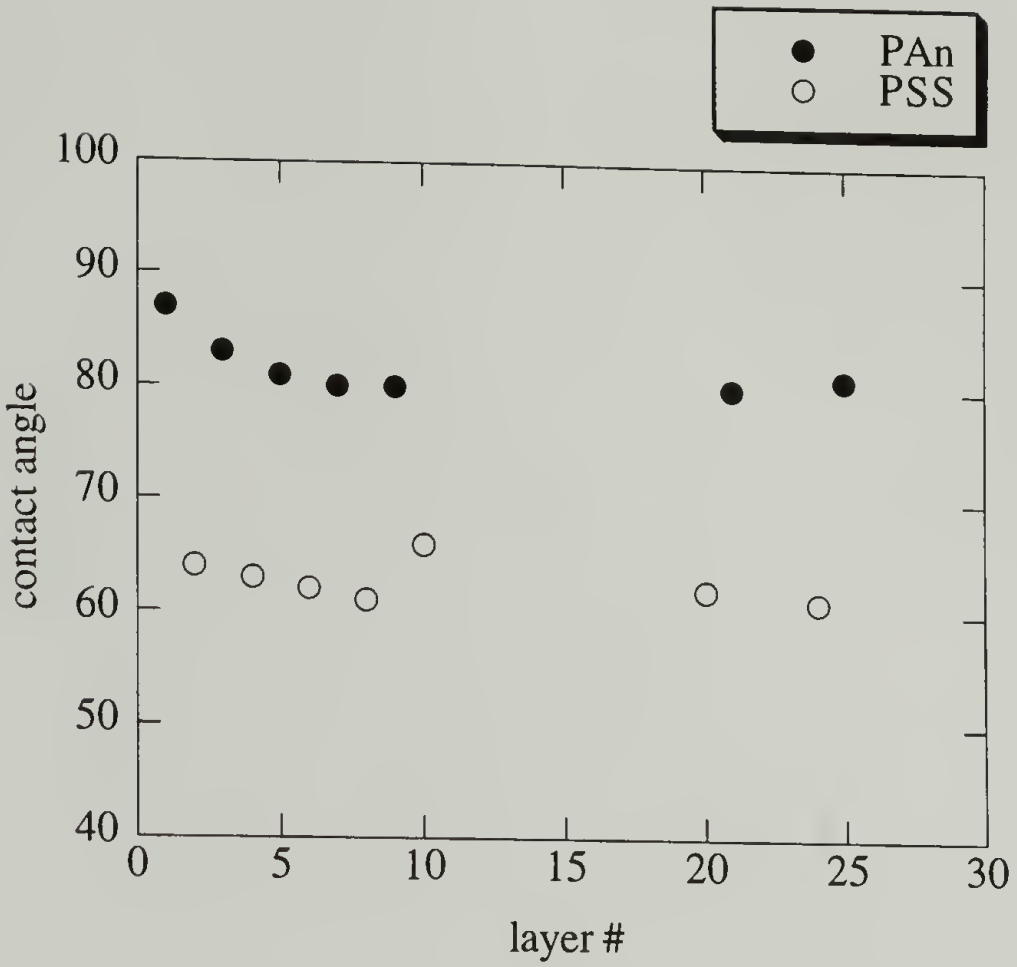

Figure 57. Advancing contact angle with water as probe fluid for a series of PMP-COOH/PAn/PSS multilalyers.

Gas Permeability of PMP-COOH/PAn/PSS Multilayers

Gas permeabilities of PMP-COOH/PAn/PSS multilayered membranes with total number of layers of 20 and 50, were determined to nitrogen, oxygen and hydrogen as described above. It was shown earlier that PAH/PSS assemblies reduce the flux of gas through the membranes dramatically, suggesting close packing and restricted segmental motion of the polyelectrolytes within the layers. Using XPS and contact angle analysis, the PAn/PSS system was shown to assemble into a stratified multilayer structure similar to that of the PAH/PSS system. However, even a 50-layer-assembly of alternating PAn and PSS layers does not affect the gas permeability properties of a PMP membrane. Permeabilities of PMP-COOH/PAn/PSS membranes can be compared to those of unmodified PMP and PMP-COOH/PAH/PSS membranes in Table 32.

The nonexistence of barrier properties in the PAn/PSS assembly suggests that even though the ionic interaction between sulfonate groups and delocalized charges along the PAn chain are sufficiently strong to drive the self-assembly to take place, the intensity of the interaction and/or the density of sites for interaction at the layer interface is not high enough to immobilize the chain segments and thus induce the gas barrier properties.

Conclusions

Self-assembly of polymers into monolayers and subsequent build-up of multilayers was shown to lead to well defined structures and control at a molecular level. Under suitable conditions, the technique enables one to control the thickness of a coating with 10 Ångström increments. For systems of high charge densities and strong ionic interactions, self-assembly results in close packing of polymer chains that are immobilized by ionic crosslinks at charged functionalities in repeat units. High restrictions in segmental motion within the layers leads to interesting macroscopic properties, as was shown for gas permeability in this work.

Table 15. Gas permeabilities (10^{-10} cm^3 (STP)/cm sec cmHg) of polyaniline in its as cast, doped (HCl), undoped and recycled state. [38]

Gas	as cast	4 M doped	undoped	0.01 M doped
He	4.90	2.06	11.5	7.31
H_2	---	1.40	10.6	6.54
CO_2	1.44	< 0.005	1.59	0.732
O_2	0.28	< 0.005	0.172	0.110
N_2	0.0382	< 0.005	0.00323	0.00253
CH_4	---	< 0.005	0.608	< 0.005

Table 16. XPS and gravimetric data for potassium chlorate oxidations.

KClO3	H2SO4	H20		time/		weight	15 deg.			75 deg.		
m/g	V/ml	V/ml	temp.	min	washing	change/%	%C	%O	%Cl	%C	%O	%Cl
0.1	5	45	rt.	1	w & IPA	-0.17	94.68	5.32		96.23	3.77	
0.1	50	0	rt.	1	w & IPA	0	84.63	13.69	1.69	87.26	11.58	1.17
0.5	25	25	rt.	0.25	w & IPA	-0.048	99.2	0.8		99.23	0.77	
0.5	25	25	rt.	0.5	w & IPA	0.066	98.96	1.04		99.41	0.59	
0.5	25	25	rt.	0.75	w & IPA	-0.11	98.36	1.64		99.29	0.71	
0.5	25	25	rt.	1	w & IPA	-0.44	99.1	0.9		99.23	0.77	
0.5	25	25	rt.	2	w & IPA	-0.52	97.78	2.22		98.72	1.28	
0.5	25	25	rt.	3	w & IPA	-0.037	97.84	2.16		98.64	1.36	
0.5	25	25	rt.	4	w & IPA	0	97.44	2.56		98.07	1.93	
0.5	25	25	rt.	5	w & IPA	-0.051	96.91	3.09		97.75	2.25	
0.5	25	25	rt.	10	w & IPA	-0.1	96.62	3.38		97.13	2.87	
0.5	25	25	rt.	20	w & IPA	-0.26	95.66	4.34		97.1	2.9	
0.5	25	25	rt.	40	w & IPA	-0.099	97.51	2.49		97.9	2.1	
0.5	25	25	rt.	60	w & IPA	-0.074	96.33	3.67		97.43	2.57	
0.5	50	0	rt.	1	w & IPA	-0.13	85.79	11.56	2.65	89.13	9.05	1.82
0.5	50	0	rt.	3	w & IPA	-0.46	89.8	7.44	2.76	92.43	5.53	2.04
0.5	50	0	rt.	4	w & IPA	-0.55	88.71	8.48	2.81	92.24	5.87	1.9
0.5	50	0	rt.	5	w & IPA	-0.88	90.01	7.22	2.77	91.12	6.7	2.18
1	5	45	rt.	1	w & IPA	0.29	95.78	4.22		96.94	3.06	
1	25	25	rt.	1	w & IPA	0.021	95.06	4.94		96.41	3.59	
1	50	0	rt.	1	w & IPA	-0.091	85.98	11.25	2.77	87.04	10.74	2.23
1	50	0	rt.	3	w & IPA	-0.8	91.46	6.05	2.5	93.47	5.02	1.52
1	50	0	rt.	4	w & IPA	-1.1	89.16	8	2.84	92.58	5.08	2.34
1	50	0	rt.	5	w & IPA	-1.6	89.57	7.28	3.15	92.83	4.82	2.34
1	50	0	rt.	60	w & MeOH	-8.6	87.2	8.47	4.33	89.56	7.29	3.15
1	50	0	rt.	60	w & CH2Cl2	-9.2	95.52	2.32	2.17	95.83	2.63	1.54
1	50	0	rt.	60	&MeOH&CH2C	-13.5	95.05	3.09	1.86	95.65	2.93	1.43
2	25	25	rt.	3	w & IPA	-0.22	96.14	3.86		98.27	1.73	
2	25	25	rt.	4	w & IPA	0.23	98.08	1.92		98.62	1.38	
2	25	25	rt.	5	w & IPA	0.11	97.21	2.79		98.72	1.28	
2	25	25	65	1	w & IPA	0	95.98	3.32	0.7	97.19	2.44	0.37
2	25	25	65	2	w & IPA	-0.055	94.28	4.56	1.16	95.99	3.3	0.71
2	25	25	65	3	w & IPA	0	95.3	3.41	1.29	96.22	2.96	0.81
2	25	25	65	4	w & IPA	-0.051	94.22	4.19	1.59	95.39	3.54	1.07
2	25	25	65	5	w & IPA	-0.074	93.54	4.61	1.84	95.36	3.41	1.23
2	25	25	65	10	w & IPA	-0.15	93.75	3.83	2.42	94.56	3.64	1.8

Table 17. Oxygen content (15° XPS analysis) in samples oxidized for 1 minute using solutions of various potassium chlorate and sulfuric acid concentrations.

$c(KClO_3)$ / M	$c(H_2SO_4)$ / vol%	% O
0.0162	10	5.32
0.162	10	4.22
0.0162	100	13.69
0.0809	100	11.56
0.162	100	11.25

Table 18. XPS and gravimetric data for chromic acid oxidations.

CrO3	H2SO4	H20	temp./	time/		weight	15 deg.				75 deg.			
m/g	V/ml	V/ml	oC	min	post-treatment	change/%	C	O	Cr	F	C	O	Cr	F
5	16	42	rt.	1		0.018	96.19	3.72	0.09		97.09	2.9		
5	16	42	rt.	5		0.15	95.54	4.05		0.41	97.34	2.45		0.21
5	16	42	rt.	5	50 d. HNO3/15'	0.12	96.22	3.59		0.19	97.04	2.72		0.24
5	16	42	rt.	10		0.1	95.43	4.31		0.26	96.64	3.2		0.16
10	16	42	rt.	1		0	94.73	5.08		0.19	96.29	3.53		0.18
10	16	42	rt.	5		0.13	93.94	5.83		0.23	95.52	4.36		0.12
10	16	42	rt.	5	50 d. HNO3/15'	0.023	93.69	5.89		0.43	96.39	3.59		0.02
10	16	42	rt.	10		0.12	93.27	6.51		0.22	95.21	4.67		0.12
20	16	42	rt.	1		0.16	93.37	6.63			95.55	4.45		
20	16	42	rt.	2		-0.14	91.59	8.41			94.53	5.47		
20	16	42	rt.	5		0.12	88.31	11.25	0.43		92.28	7.52	0.2	
20	16	42	rt.	10		0.09	86.87	12.71	0.42		89.86	9.47	0.68	
20	16	42	rt.	15		0.09	87.13	12.14	0.62	0.11	90.9	8.16	0.53	0.4
20	16	42	rt.	20		0.11	83.89	15.04	0.76	0.31	89.06	10.25	0.54	0.16
29	16	42	2	1	55 d. 70% HNO3/30'	0.083	95.56	4.05		0.39	96.9	2.84		0.26
29	16	42	2	5	55 d. 70% HNO3/30'	0.11	94.39	5.29		0.32	96.2	3.5		0.3
29	16	42	2	10	55 d. 70% HNO3/30'	0.067	94.33	5.18		0.48	96.87	3		0.13
29	16	42	2	20	55 d. 70% HNO3/30'	0.069					96.42	3.42		0.16
29	16	42	2	40	55 d. 70% HNO3/30'	0.047	93.32	6.39		0.29	95.54	4.42		0.03
29	16	42	2	60	55 d. 70% HNO3/30'	0.14	93.16	6.62		0.22	95.08	4.76		0.16
29	16	42	24	1	55 d. 70% HNO3/30'	0.067	93.06	6.69		0.24	95.41	4.34		0.24
29	16	42	rt.	5		-0.18	84	14.84	0.71	0.45	88.76	10.38	0.58	0.29
29	16	42	rt.	5	55 d. 70% HNO3/30'	-0.31	91.24	8.76			94.38	5.62		
29	16	42	rt.	20		-0.16	81.79	17.18	0.53	0.49	86.4	12.62	0.72	0.27
29	16	42	rt.	20	55 d. 70% HNO3/30'	-0.11	87.51	12.49			90.2	9.8		
29	16	42	80	0.5	55 d. 70% HNO3/30'	-0.38	87.91	12.09			88.15	11.85		
29	16	42	80	1	55 d. 70% HNO3/30'	-0.37	84.42	15.58			87.11	12.89		
29	16	42	80	2	55 d. 70% HNO3/30'	-0.82	84.51	15.01		0.49	86.91	12.64	0.16	0.28
29	16	42	80	2	55 d. 70% HNO3/30'	-1.1	83.5	16.28	0.16	0.06	85.67	13.9	0.23	0.21
29	16	42	80	3	55 d. 70% HNO3/30'	-1.3	85.85	13.97		0.18	88.07	11.84	0.06	0.02
29	16	42	80	4	55 d. 70% HNO3/30'	-1.3	86.37	13.29	0.01	0.33	88.74	10.8	0.31	0.15
29	16	42	80	5	55 d. 70% HNO3/30'	-1.6	85.01	14.71	0.03	0.26	86.99	12.71	0.26	0.04
29	16	42	80	5		-2.1	78.78	20.05	0.58	0.6	80.49	18.27	0.95	0.29
29	16	42	80	5	55 d. 70% HNO3/30'	-2.1	85.13	14.36	0.38	0.13	87.09	12.57	0.24	0.11
29	16	42	80	10	55 d. 70% HNO3/30'	-3.6	83.7	15.45	0.44	0.4	86.94	12.44	0.44	0.18
29	16	42	80	20	55 d. 70% HNO3/30'	-12.6	80.62	18.4	0.62	0.35	81.5	17.33	0.92	0.25
29	16	42	80	20		-11.3	85.14	14.58	0.05	0.22	87.99	11.42	0.37	0.22
29	16	42	80	30	55 d. 70% HNO3/30'	-14.8	82.94	16.59	0.4	0.07	86.06	13.69	0.19	0.05

Table 19. XPS data for deposition of PAH onto PMP-COOH
a. pH dependence and kinetics study.

	time/	15 deg.				75 deg.			
pH	min	%C	%O	%N	%Cl	%C	%O	%N	%Cl
4	5	80.01	17.54	2.44		79.63	17.83	2.54	
4	10	83.33	14.06	2.61		86.07	12.21	1.72	
4	20	84.25	13.66	2.09		86.52	11.52	1.96	
4	30	83.16	14.13	2.72		86.07	11.47	2.46	
4	40	84.08	13.49	2.43		85.79	11.9	2.31	
4	60	82.4	14.92	2.69		85.51	12.01	2.48	
6	5	82.78	14.09	3.13		85.2	11.92	2.89	
6	10	84.36	12.93	2.71		86.52	11.02	2.45	
6	20	82.71	14.53	2.76		84.77	12.41	2.82	
6	30	81.6	14.65	3.76		84.73	12.1	3.18	
6	40	81.35	14.87	3.77		83.76	12.74	3.49	
6	60	81.94	14.54	3.52		83.69	12.98	3.33	
8	5	81.27	14.29	4.15	0.28	82.28	13.57	3.91	0.24
8	10	79.55	15.65	4.45	0.35	80.85	14.86	4.04	0.25
8	20	79.91	15.71	3.82	0.56	82.42	13.27	3.87	0.45
8	30	78.9	15.57	5	0.53	82.68	12.89	4	0.43
8	40	80.98	14.3	4.72		83.68	12.15	4.17	
8	60	81.01	14.81	4.18		82.85	12.82	4.33	
10	5	80.35	13.11	5.89	0.64	80.76	12.78	6.03	0.43
10	10	78.04	15.18	6.15	0.63	75.05	17.06	7.22	0.67
10	20	79.08	14.5	5.96	0.45	77.36	15.25	7	0.39
10	30	79.37	12.85	6.89	0.89	78.18	12.54	8.41	0.86
10	40	76.46	14.83	7.75	0.96	74.34	15.78	9.05	0.83
10	60	77.87	15.19	6.94		78.7	13.87	7.43	

Continued, next page

Table 19, continued
b. Deposition for 10 min at pH 8.

	15 deg.				75 deg.			
sample#	%C	%O	%N	%Cl	%C	%O	%N	%Cl
1	76.36	19.17	4.22	0.26	80.32	15.86	3.67	0.15
2	78.14	16.76	4.75	0.34	80.12	15.55	4.02	0.31
3	77.75	18.2	3.75	0.3	75.92	19.46	4.27	0.34

Table 20. XPS data for deposition of PAH onto PMP-COOH (1 M NaCl).

	time/	15 deg.				75 deg.			
pH	min	%C	%O	%N	%Cl	%C	%O	%N	%Cl
4	5	77.95	17.28	4.23	0.54	81.54	14.39	3.56	0.51
4	10	76.81	18	4.83	0.37	78.88	16.36	4.4	0.36
4	20	79.15	15.78	4.71	0.36	81.71	13.85	4.14	0.3
4	30	78.13	17.38	4.2	0.29	80.53	15.97	3.09	0.4
4	40	77.8	17.78	3.87	0.55	80.68	14.81	4.08	0.44
4	60	76.23	19.13	4.08	0.56	78.3	17.17	4.01	0.52
6	5	77.21	17.17	4.91	0.71	80.07	14.6	4.74	0.59
6	10	76.75	17.26	5.42	0.57	80.22	14.4	4.89	0.48
6	20	76.51	17.34	5.73	0.42	78.84	15.83	4.92	0.41
6	30	73.79	20.12	5.57	0.52	77.31	16.96	5.29	0.44
6	40	73.32	19.85	6.21	0.62	73.81	20.03	5.32	0.84
6	60	72.22	21.11	5.97	0.7	75.79	17.83	5.78	0.6
8	5	78.86	15.5	4.9	0.74	79.61	15.05	4.61	0.73
8	10	75.8	17.49	6.06	0.65	79.16	14.84	5.41	0.58
8	20	76.88	17.46	4.95	0.71	77.29	16.93	5.1	0.67
8	30	76.91	15.85	6.6	0.64	79.65	13.99	5.75	0.61
8	40	76.1	17.22	5.79	0.89	79.22	15.19	4.85	0.73
8	60	74.54	18.39	6.41	0.66	76.65	16.9	5.96	0.49
10	5	73.12	20.42	5.35	1.11	69.16	24.39	5.32	1.13
10	10	77.21	15.97	5.7	1.12	77.14	15.75	6.06	1.05
10	20	78.09	15.76	5.44	0.7	78.95	14.92	5.46	0.66
10	30	76.29	16.53	6.32	0.86	78.16	14.15	6.9	0.79
10	40	75.62	16.78	6.67	0.93	77.63	13.99	7.54	0.83
10	60	75.84	17.29	5.95	0.93	75.52	17.57	5.96	0.94

Table 21. XPS data for deposition of PSS onto PMP-COOH/PAH.
a. pH dependence and kinetics study.

	time/	15 deg.				75 deg.			
pH	min	%C	%O	%N	%S	%C	%O	%N	%S
4	10	70.65	23.07	3.48	2.79	72.05	22.55	3.11	2.3
4	20	72.87	21.36	3.22	2.55	74.33	20.33	3.29	2.05
4	30	69.9	23.56	3.67	2.87	71.1	23.06	3.42	2.43
4	60	69.24	24.17	3.7	2.89	69.73	23.92	3.64	2.72
6	10	75.62	19.44	3.21	1.73	76.92	18.14	3.62	1.32
6	20	71.84	22.36	4.03	1.76	73.58	21.34	3.69	1.39
6	30	73.36	21.02	3.98	1.65	76.51	18.58	3.64	1.26
6	60	72.87	21.21	4.21	1.71	75.66	19.03	3.86	1.45
8	10	73.98	20.69	3.84	1.5	76.41	18.61	3.8	1.19
8	20	71.06	24.07	3.56	1.32	73.42	21.87	3.58	1.14
8	30	76.86	18.07	3.58	1.49	80.14	15.72	3.07	1.07
8	60	73.74	20.8	4	1.47	70.24	24.73	3.76	1.26
10	10	76.53	18.8	3.38	1.29	78.32	17.11	3.59	0.99
10	20	72.5	22.25	4.23	1.02	76.97	18.06	4.2	0.77
10	30	73.11	21.58	3.86	1.45	74.21	21.02	3.36	1.41
10	60	74.92	19.77	3.7	1.6	72.78	22.54	3.62	1.06

Continued, next page

Table 21, continued
b. Deposition for 10 min at pH 4.

	15 deg.				75 deg.			
sample#	%C	%O	%N	%S	%C	%O	%N	%S
1	69.1	24.16	3.82	2.92	70.43	23.32	3.8	2.45
2	70.74	23.51	3.15	2.6	71.11	23.4	3.41	2.08
3	72.95	20.96	3.28	2.81	73.05	21.03	3.7	2.22
4	71.03	22.54	3.39	3.04	71.07	22.66	3.98	2.29

Table 22. XPS data for deposition of PAH onto PMP-COOH/PAH/PSS.

	time/	15 deg.					75 deg.				
pH	min	%C	%O	%N	%S	%Cl	%C	%O	%N	%S	%Cl
4	10	69.38	23.75	4	2.73	0.15	70.38	22.6	4.59	2.24	0.18
4	20	67.79	23.78	5.29	2.71	0.43	71.04	21.77	4.88	2.07	0.23
4	30	68.9	23.73	4.18	2.82	0.36	71.03	21.92	4.71	2.3	0.04
4	60	69.01	24	4.01	2.92	0.05	71.57	21.65	4.32	2.35	0.12
6	10	67.91	24.22	4.94	2.76	0.17	69.39	23.07	5.04	2.32	0.17
6	20	69.21	23.56	4.37	2.62	0.24	70.49	22.69	4.53	2.21	0.09
6	30	67.3	24.54	4.82	3.01	0.33	68.32	23.72	5.2	2.41	0.35
6	60	67.08	24.43	5	2.91	0.57	64.22	28.68	4.48	2.19	0.43
8	10	68.32	23.48	5.52	2.26	0.42	70.02	22.25	5.55	1.95	0.23
8	20	71.19	21.17	5.14	2.01	0.5	69.48	22.63	5.42	2.08	0.38
8	30	69.52	21.04	6.4	2.36	0.68	70.49	21.1	6.08	1.84	0.49
8	60	69.06	21.96	5.45	2.47	1.05	70.58	20.74	5.94	1.88	0.85
10	10	73.22	17.59	7.72	0.63	0.84	69.37	20.45	8.65	0.67	0.86
10	20	66.66	15.92	14.28	1.32	1.82	71.64	18.96	7.81	0.79	0.81
10	30	72.02	17	8.03	0.72	2.22	71.57	16.32	9.51	0.74	1.86
10	60	70.01	18.64	9.04	0.74	1.56	70.03	18.62	9.24	0.76	1.35

Table 23. XPS data for PMP-COOH/PAH/PSS multilayers.

	15 deg.					75 deg.				
layer#	%C	%O	%N	%S	%Cl	%C	%O	%N	%S	%Cl
3 (PAH)	76.45	15.69	5.07	2.42	0.36	73.73	17.02	6.04	2.76	0.45
3 (PAH)	76.2	15.19	5.23	2.72	0.66	75.58	16.2	5.78	2.06	0.38
3 (PAH)	75.21	15.7	5.79	2.75	0.55	75.87	16.13	5.6	2	0.4
4 (PSS)	72.73	17.73	4.71	4.53	0.3	70.24	19.65	5.36	4.48	0.27
4 (PSS)	72.57	18.34	4.34	4.43	0.33	72.1	18.99	5.05	3.73	0.13
4 (PSS)	73.37	17.69	4.55	4.15	0.23	72.4	19.29	4.49	3.66	0.16
5 (PAH)	76.28	15.72	4.9	3.02	0.08	74.26	16.53	5.96	2.98	0.27
5 (PAH)	76.29	15.18	5.18	3.34	0.01	72.4	17.79	6.12	3.41	0.29
5 (PAH)	75.85	16.11	4.56	3.07	0.41	71.92	18.45	5.93	3.35	0.35
6 (PSS)	73.5	16.81	5.03	4.35	0.31	70.65	18.61	6.06	4.37	0.31
6 (PSS)	73.2	17.59	4.55	4.44	0.21	69.58	20.27	5.39	4.5	0.26
6 (PSS)	73.2	17.18	4.81	4.51	0.3	70	19.73	5.46	4.62	0.18
7 (PAH)	76.16	15.06	5.2	3.21	0.38	71.61	17.21	6.91	3.87	0.4
7 (PAH)	76.74	14.86	4.86	3.08	0.46	72.4	17.12	6.58	3.53	0.37
7 (PAH)	73.9	16.85	5.58	3.17	0.5	71.64	17.99	6.24	3.77	0.35
8 (PSS)	74.52	16.93	4.27	4.11	0.18	70.79	18.56	5.84	4.6	0.2
8 (PSS)	76.17	14.96	4.44	4.02	0.42	70.32	19.17	5.62	4.65	0.24
8 (PSS)	73.92	16.3	5.16	4.3	0.33	69.73	19.49	5.95	4.56	0.26
9 (PAH)	76.95	13.84	5.3	3.53	0.39	71.28	17.38	6.82	4.12	0.4
21 (PAH)	76.5	14.54	5.71	3.19	0.06	70.47	17.66	7.39	4.23	0.24
22 (PSS)	77.57	13.66	4.83	3.94	0.01	70.18	18.71	6.15	4.77	0.19
31 (PAH)	76.32	15.23	5.21	3.09	0.15	70.39	17.97	7.25	4.1	0.3
32 (PSS)	72.56	18.54	4.59	3.99	0.33	69.55	19.05	6.22	4.8	0.38
41 (PAH)	78.61	13.28	4.99	2.78	0.34	71.39	17.73	6.65	3.98	0.24
42 (PSS)	76.58	14.97	4.39	3.69	0.37	69.85	19.02	6.07	4.78	0.29
51 (PAH)	77.08	13.29	6.14	3.21	0.29	72.62	16.47	6.94	3.79	0.18
52 (PSS)	75.5	15.99	4.41	3.91	0.19	69.01	19.18	6.69	4.94	0.18
61 (PAH)	79.22	13.9	4.2	2.54	0.15	71.77	16.72	7.1	4.05	0.36
62 (PSS)	79.19	15.78	3.83	3.62	0.58	69.91	19	6.16	4.67	0.27
71 (PAH)	77.2	14.74	4.99	2.82	0.26	70.59	17.98	7.1	4.11	0.22
72 (PSS)	76.82	15.24	4.15	3.61	0.17	70.03	19.08	5.93	4.82	0.14
81 (PAH)	78	14.59	4.38	2.83	0.21	71.56	17.5	6.88	4.04	0.01
82 (PSS)	75.02	16.02	4.77	4.09	0.09	70.24	18.57	6.37	4.82	0
91 (PAH)	77.81	15.14	4.28	2.53	0.24	71.28	17.27	7.45	3.87	0.13
92 (PSS)	74.59	17.95	3.76	3.53	0.16	70.86	18.29	6.26	4.6	0
101 (PAH)	77	14.32	5.48	3.14	0.06	72.13	16.65	7.02	4.13	0.08
102 (PSS)	76.78	15.58	3.85	3.79	0	71.32	18.02	5.88	4.76	0.01

Table 24. XPS data (15° take-off angle) for peel test of the PMP-COOH/PAH/PSS multilayers using 3M Scotch tape.

sample	% C	% O	% N	% S	% Cl
tape	85.4	14.6	-	-	-
7 layers (PAH surface)	75.6	15.6	5.2	3.2	0.4
8 layers (PSS surface)	74.9	16.1	4.6	4.1	0.3
tape (off PAH surface)	86.2	13.5	0.3	-	-
PAH surface (off tape)	78.8	16.0	3.0	2.2	-
tape (off PSS surface)	86.1	13.9	-	-	-
PSS surface (off tape)	78.2	16.0	2.7	3.1	-

Table 25. Multilayer thicknesses on aminofunctionalized Silicon wafers.

	total thickness / Å							corrected
			relative humidity					thickness/Å
#layers	**dry**	**10%**	**30%**	**50%**	**70%**	**90%**	**100%**	**dry**
0								
2								
4	26.6							21.6
6	42							37
8	61							56
10	70	74.3		79.2		87	89	65
20	176	187	190	194	197	201	203	171
30	282							277
30 (25C)	291	301	307	315	319	324	324	286
30 (40C)	291	309	317	323	327	339	349	286

Table 26. XPS data for Si-NH_2/PSS/PAH multilayers.

		15 deg.					75 deg.				
layer#	thickn./Å	%C	%N	%O	%Si	%S	%C	%N	%O	%Si	%S
0		40.36	4.42	34.14	21.08	0	18.89	1.41	33.97	45.73	0
2		60.05	3.39	21.55	11.46	3.55	29.69	2.9	26.89	33.12	7.41
4	26.6	69.24	4.03	18.19	5.79	2.74	45.98	4.97	23.19	20.48	5.38
6	42	71.37	4.58	18.61	3.01	2.43	53.58	6.22	21.5	13.85	4.86
8	61	69.18	4.89	20.1	2.69	3.15	62.42	6.55	19.59	7.2	4.25
10	70	71.57	4.51	16.59	4.51	2.82	66.31	6.08	17.77	5.75	4.09
20	176	69.36	3.53	18.98	5.32	2.81	69.88	6.64	17.78	0.94	4.77
30	282	74.18	4.46	15.63	2.97	2.76	70.48	7	17.39	0.69	4.44

Table 27. Gas permeability of PMP-COOH/PAH/PSS multilayer membranes.

sample	$P(N_2)^a$	$P(O_2)^a$	$P(H_2)^a$
PMP	1.3	5.4	22.0
PMP-COOH	1.3	4.1	17.5
PMP-COOH/PAH/PSS			
10 layers	0.95	4.2	16.8
20	0.35	2.1	16.4
50	0.13	1.0	13.3
100	0.13	0.97	13.3
200	0.080	1.2	9.7

[a] 10^{-9} cm^3(STP) cm/cm^2 s cmHg

Table 28. Gas selectivity of PMP-COOH/PAH/PSS membrane with 200 layers, and virgin PMP.

	selectivity		
sample	O_2/N_2	H_2/N_2	H_2/O_2
PMP	4.2	16.9	4.1
PMP-COOH/PAH/PSS 200 layers	15	121	8.1

Table 29. XPS data for deposition of PAn onto PMP-COOH.

	time/	15 deg.			75 deg.		
pH	min	%C	%O	%N	%C	%O	%N
2	5	86.07	13.01	0.93	88.98	10.35	0.67
2	10	85.44	13.36	1.2	88.53	11.09	0.38
2	20	85.4	13.37	1.23	88.78	10.76	0.46
2	60	85.22	13.38	1.4	88.75	10.65	0.6
4	5	84.05	12.08	3.87	85.79	10.1	4.11
4	10	82.79	12.58	4.63	85.28	9.98	4.75
4	20	82.67	12.41	4.92	85.47	10.27	4.26
4	60	83.72	10.84	5.44	85.16	10.54	4.3
6	5	84.41	14.46	1.13	87.9	11.36	0.74
6	10	85.5	13.69	0.81	87.61	11.58	0.81
6	20	86	12.84	1.16	88.22	11.18	0.6
6	60	82.51	16.39	1.1	86.86	11.78	1.36

Table 30. XPS data for deposition of PSS onto PMP-COOH/PAn.

	time/	15 deg.				75 deg.			
pH	min	%C	%O	%N	%S	%C	%O	%N	%S
0	5	78.1	15.6	4.11	2.19	80.27	14.22	3.69	1.81
0	10	79.2	15.27	3.6	1.93	80.33	14.26	3.53	1.88
0	20	79.87	14.61	3.5	2.03	80.38	14.11	3.76	1.75
0	60	79.66	15.45	2.88	2	81.19	14.58	2.43	1.8
2	5	79.83	14.89	4.09	1.19	82.41	12.58	4	1.02
2	10	80.71	14.24	3.86	1.19	82.01	12.94	4.03	1.02
2	20	78.03	16.31	4.12	1.54	81.95	13.45	3.58	1.02
2	60	79.9	14.81	3.92	1.37	83.09	12.61	3.31	0.98
4	5	80.33	14.99	3.91	0.76	84.46	11.91	3.15	0.48
4	10	81.21	13.99	3.83	0.97	84.04	12.01	3.23	0.71
4	20	81.32	14.27	3.62	0.79	84.22	12.14	3.05	0.6
4	60	82.59	12.74	3.95	0.72	84.21	12.03	3.16	0.6
6	20	80.97	15.14	3.29	0.6	83.07	13.17	3.29	0.46
6	60	81.62	14.1	3.75	0.52	83.93	12.22	3.38	0.47

Table 31. XPS data for PMP-COOH/PAn/PSS multilayers.

	15 deg.					75 deg.				
layer#	%C	%O	%N	%S	%Cl	%C	%O	%N	%S	%Cl
0										
1	82.96	10.77	5.51	0	0.75	85.32	10.29	3.85	0	0.53
2	79.2	15.15	3.34	1.89	0.41	79.65	14.69	3.55	1.81	0.3
3	78.82	15.22	3.71	1.33	0.92	79.83	13.79	4.33	1.23	0.81
4	78.63	15.22	3.11	2.22	0.82	80.42	14.01	3.51	1.68	0.38
5	79.43	13.36	4.71	1.45	1.06	80.66	13.06	4.4	1.12	0.75
6	77.19	16.21	3.56	2.39	0.65	77.73	15.11	4.26	2.37	0.53
7	76.74	14.55	5.73	2.05	0.93	77.58	14.64	5.1	1.92	0.76
8	75.21	17.74	3.84	2.55	0.66	78.1	15.02	4.21	2.2	0.47
9	76.99	13.88	5.77	1.89	1.47	77.72	13.74	5.49	2.01	1.04
10	75.58	16.46	4.57	2.67	0.72	77.73	14.89	4.54	2.34	0.49
20	76.58	16.12	4.01	2.62	0.67	76.44	15.94	4.52	2.52	0.58
21	76.45	14.94	5.28	2.39	0.94	76.58	14.9	5.24	2.4	0.87
24	78.46	13.89	4.19	2.91	0.56	77.09	15.32	4.54	2.61	0.44
25	76.96	14.39	5.45	2.52	0.67	76.19	15.32	5.33	2.49	0.67

Table 32. Gas permeability of multilayered membranes and virgin PMP.

sample	$P(N_2)^a$	$P(O_2)^a$	$P(H_2)^a$
PMP	1.3	5.4	22.0
PMP-COOH/PAn/PSS			
20 layers	1.2	4.7	19.9
50 layers	1.2	4.3	19.9
PMP-COOH/PAH/PSS			
50 layers	0.13	1.0	13.3

[a] 10^{-9} cm^3(STP) cm/cm^2 s cmHg

References

(1) Lvov, Y.; Decher, G.; Möhwald, H. *Langmuir* **1993**, *9*, 481.

(2) Fou, A. C.; Ellis, D.; Ferreira, M.; Rubner, M. F.
Polym. Prepr. (Am. Chem. Soc., Div. Polym. Chem.) **1994**, *35*, 221.

(3) Cheung, J. H.; Fou, A. F.; Rubner, M. F.
Polym. Prepr. (Am. Chem. Soc., Div. Polym. Chem.) **1993**, *34*, 757.

(4) Blaakmeer, J.; Böhmer, M. R.; Cohen Stuart, M. A.; Fleer, G. J.
Macromolecules **1990**, *23*, 2301.

(5) Cosgrove, T.; Obey, T. M.; Vincent, B. J.
J. Colloid Interface Sci. **1986**, *111*, 409.

(6) Van der Schee, H. A.; Lyklema, J. *J. Phys. Chem.* **1984**, *88*, 6661.

(7) Evers, O. A.; Fleer, G. J.; Scheutjens, H. M.; Lyklema, J.
J. Colloid Interface Sci. **1986**, *111*, 446.

(8) Decher, G.; Hong, J.-D. *Makromol. Chem., Macromol. Symp.* **1991**, *46*, 321.

(9) Lane, J. M.; Hourston, D. J. *J. Prog. Org. Coat.* **1993**, *21*, 269.

(10) Costello, C. A. Ph.D. Thesis, University of Massachusetts, 1987.

(11) Rasmussen, J. R.; Stedronsky, E. R.; Whitesides, G. M. *J. Am. Chem. Soc.* **1977**, *99*, 4736.

(12) Decher, G.; Hong, J. D.; Scmitt, J. *Thin Solid Films* **1992**, *210/211*, 831.

(13) Stockton, W. B.; Rubner, M. F. *Polym. Prepr. (Am. Chem. Soc., Div. Polym. Chem.)* **1994**, *35*, 319.

(14) Cheung, J. H.; Fou, A. F.; Rubner, M. F. *Thin Solid Films* **1994**, *244*, 985.

(15) Kleinfeld, E. R.; Ferguson, G. S. *Science* **1994**, *265*, 370.

(16) Lvov, Y.; Decher, G.; Sukhorukov, G. *Macromolecules* **1993**, *26*, 5399.

(17) Lvov, Y.; Haas, H.; Decher, G.; Möhwald, H. *Langmuir* **1994**, *10*, 4232.

(18) Cooper, T. M.; Campbell, A. L.; Crane, R. L. *Langmuir* **1995**, *11*, 2713.

(19) Malhotra, B. D. *J. Appl. Polym. Sci.* **1990**, *40*, 1049.

(20) Liao, Y.-H.; Levon, K. *Polym. Mater. Sci. Eng.* **1993**, *69*, 327.

(21) Keller, S. W.; Kim, H.-N.; Mallouk, T. E. *J. Am. Chem. Soc.* **1994**, *116*, 8817.

(22) Mao, G.; Tsao, Y.; Tirrell, M.; Davis, H. T. *Langmuir* **1993**, *9*, 3461.

(23) Lvov, Y.; Essier, F.; Decher, G. *J. Phys. Chem.* **1993**, *97*, 13773.

(24) Dahlgren, M. A. G.; Waltermo, Å.; Blomberg, E.; Claesson, P. M.; Sjöström, L.; Åkesson, T.; Jönsson, B. *J. Phys. Chem.* **1993**, *97*, 11769.

(25) Dahlgren, M. A. G. *Langmuir* **1994**, *10*, 1580.

(26) Lvov, Y.; Haas, H.; Decher, G.; Möhwald, H.; Kalachev, A. *J. Phys. Chem.* **1993**, *97*, 12835.

(27) Lee, H.; Kepley, L. J.; Hong, H.-G.; Akhter, S.; Mallouk, T. E. *J. Phys. Chem.* **1988**, *92*, 2597.

(28) Fou, A. C.; Rubner, M. F. *Macromolecules* **1995**, *28*, 7115.

(29) Decher, G. *private conversation*

(30) Decher, G.; Lvov, Y.; Schmitt, J. *Thin Solid Films* **1994**, *244*, 772.

(31) Schmitt, J.; Grünewald, T.; Decher, G.; Pershan, P. S.; Kjaer, K.; Lösche, M. *Macromolecules* **1993**, *26*, 7058.

(32) Mao, G.; Tsao, Y.-H.; Tirrell, M.; Davis, H. T. *Langmuir* **1995**, *11*, 942.

(33) Mao, G.; Tsao, Y.-H.; Tirrell, M.; Davis, H. T. *Langmuir* **1994**, *10*, 4174.

(34) Freeman, T. L.; Evans, S. D.; Ulman, A. *Langmuir* **1995**, *11*, 4411.

(35) Trivedi, D. C.; Dhawan, S. K. *Synth. Met.* **1993**, *58*, 309.

(36) Chiang, J.-C.; Macdiarmid, A. G. *Synth. Met.* **1986**, *13*, 193.

(37) Anderson, M. R.; Mattes, B. R.; Reiss, H.; Kaner, R. D. *Science* **1991**, *252*, 1412.

(38) Anderson, M. R.; Mattes, B. R.; Reiss, H.; Kaner, R. B. *Synth. Met.* **1991**, *41-43*, 1151.

APPENDIX A

DEPTH OF CHLORINATION

Thickness of the chlorinated PMP layer is calculated assuming a composite structure with two discrete layers: one with the density of PMP (unmodified PMP), and the other (chlorinated PMP) with a higher density that is related to the density of poly(vinyl chloride) (PVC) by the chlorine:carbon ratio (15° XPS data). Gravimetric and XPS data are used to calculate sample dimensions and chlorinated layer thicknesses as shown below.

Film area

$$A = \frac{m_i}{d_{PMP} \cdot l}$$

Weight after chlorination

$$m_a = m_{bulk} + m_{PMP-Cl}$$

$$m_a = d_{PMP} \cdot A \cdot (l - x) + \left[d_{PMP} + \frac{r}{0.5} \cdot (d_{PVC} - d_{PMP}) \right] \cdot A \cdot l_{Cl}$$

Total thickness of chlorinated layer

$$l_{Cl}(m_a, m_i, r) = \frac{\left(\frac{m_a}{m_i} - 1 \right) \cdot 0.5 \cdot d_{PMP} \cdot l}{\frac{r}{d_{PVC} - d_{PMP}}}$$

where

d_{PMP} = density of PMP

d_{PVC} = density of PVC

l = total film thickness

r = chlorine:carbon ratio

l_{Cl} = total thickness of chlorinated layers (both sides of the film)

m_i = initial mass

m_a = mass after chlorination

A = film area

V = volume

APPENDIX B

GAS PERMEABILITY EXPERIMENT

Gas permeabilities were determined with a home-built device (Figure 5). The sample compartment consists of two sample holders - one for a back-up membrane and the other one for the actual sample membrane. A clean PMP film was used as a back-up membrane. The purpose of this additional membrane was ensure that the pressure transducer (used to monitor the pressure change on the downstream side due to gas diffusion) would not break in case of a punctured sample membrane.

The upstream pressure was controlled with a regulator and typically adjusted to give a pressure gradient of 6 atm across the membranes. Heating tape was carefully wrapped around the membrane compartment and temperature was set for 40 ^{o}C with a variac. The temperature was measured with a resolution of 1 ^{o}C (Omega Engineering Inc. thermocouple thermometer model 660) in the sample holder that had a hole drilled for the probe close to the membrane. On the downstream side the membranes were supported by a metallic prefilter onto which they were pressed with an o-ring.

The downstream side of the membrane compartment was kept under 10^{-9} torr reduced pressure with a Pfeiffer pumping system (DUO 1,5A rotary vane pump and TPU 060 turbo molecular pump with TCP 121 electronic drive unit). Pressure change was monitored using a Celesco DP31 differencial pressure transducer with SE-2000 electronic gauge unit.

Downstream side was kept under vacuum with the valve No. 1 closed while setting up the membranes. The line to the membrane compartment was loosened slightly for purging the upstream side with the gas that is been used for the experiment. The valve was slowly opened after fastening the line connection to the sample compartment. The heating was adjusted for 40 ^{o}C and the gas was let diffuse through

the membranes. As the set temperature was reached, the first permeation data point was determined as follows; the pressure gauge was set to give a read-out of -0.01 mmHg and the valves No. 2 and 3 were closed (the total volume of the lines and the first gas container is 86 ml). Pressure change of 0.00 to 0.50 mmHg was timed and the valves were opened again for further unrecorded gas permeation. Timing was repeated until steady state of permeation rate was reached. This usually took a minimum of 3 days in order to ensure that no further changes were taking place.

Since it takes several days (in some cases two weeks) to reach the steady state of flow through the membrane, the existing set-up could be modified to accommodate several membranes simultaneously. This could be accomplished with a manifold in which a single membrane holder can be separately remain connected to the vacuum and the gas supply line while the rest of the samples are disconnected for the length of the actual measurement. The ability to handle several samples during the same experiment would increase the usefulness of the instrument.

Also, in the present sample holder the membrane is not supported on the upstream side. This easily leads to stretching of the membrane, when the pressure is carefully reduced in the head space on the upstream side. Remodeling the holder to have a membrane support also on the upstream side (in noncontact with the sample) would give the user an option of evacuating the sample quickly for time-lag experiments to determine the diffusion and solubility component of the permeability.

APPENDIX C

ABBREVIATIONS

ATR IR	attenuated total reflectance infrared
CDT	corona discharge treatment
CED	cohesive energy density
DMAc	dimethylacetamide
H&D	highly and deeply chlorinated sample
H&S	highly and shallowly chlorinated sample
L&D	lightly and deeply chlorinated sample
L&S	lightly and shallowly
LB	Langmuir-Blodgett
mm	mmHg
PAH	poly(allylamine hydrochloride)
PAn	polyaniline
PMIM	phase measurement interference microscopy
PMP	poly(4-methyl-1-pentene)
PMP-COOH	surface-oxidized poly(4-methyl-1-pentene)
PSS	poly(sodium styrene sulfonate)
$Si\text{-}NH_2$	silicon wafer surface coupled with 4-aminobutyldimethyl methoxysilane
XPS	X-ray photoelectron spectroscopy

BIBLIOGRAPHY

Anderson, M. R.; Mattes, B. R.; Reiss, H.; Kaner, R. B.
Synth. Met. **1991**, *41-43*, 1151.

Anderson, M. R.; Mattes, B. R.; Reiss, H.; Kaner, R. D.
Science **1991**, *252*, 1412.

Ashworth, A. J. *J. Membr. Sci.* **1992**, *71*, 169.

Blaakmeer, J.; Böhmer, M. R.; Cohen Stuart, M. A.; Fleer, G. J.
Macromolecules **1990**, *23*, 2301.

Charlet, G.; Delmas, G. *Polymer* **1984**, *25*, 1619.

Charlet, G.; Delmas, G. *J. Polym. Sci., Polym. Phys. Ed.* **1988**, *26*, 1111.

Cheung, J. H.; Fou, A. F.; Rubner, M. F.
Polym. Prepr. (Am. Chem. Soc., Div. Polym. Chem.) **1993**, *34*, 757.

Cheung, J. H.; Fou, A. F.; Rubner, M. F. *Thin Solid Films* **1994**, *244*, 985.

Chiang, J.-C.; Macdiarmid, A. G. *Synth. Met.* **1986**, *13*, 193.

Chiao, C. C. *U.S. Patent 4,828,585, 1989.*

Cooper, T. M.; Campbell, A. L.; Crane, R. L. *Langmuir* **1995**, *11*, 2713.

Cosgrove, T.; Obey, T. M.; Vincent, B. J.
J. Colloid Interface Sci. **1986**, *111*, 409.

Costello, C. A. Ph.D. Thesis, University of Massachusetts, 1987.

Cross, E.; McCarthy, T. J. *Macromolecules* **1992**, *25*, 2603.

Csernica, J.; Rein, D. H.; Baddour, R. F.; Cohen, R. E.
Macromolecules **1991**, *24*, 3612.

Dahlgren, M. A. G.; Waltermo, Å.; Blomberg, E.; Claesson, P. M.; Sjöström, L.;
Åkesson, T.; Jönsson, B. *J. Phys. Chem.* **1993**, *97*, 11769.

Dahlgren, M. A. G. *Langmuir* **1994**, *10*, 1580.

Decher, G.; Hong, J.-D. *Makromol. Chem., Macromol. Symp.* **1991**, *46*, 321.

Decher, G.; Hong, J. D.; Scmitt, J. *Thin Solid Films* **1992**, *210/211*, 831.

Decher, G.; Lvov, Y.; Schmitt, J. *Thin Solid Films* **1994**, *244*, 772.

Decher, G. *private conversation*

Elman, J. F.; Gerenser, L. J.; Goppert-Berarducci, K. E.; Pochan, J. M.
Macromolecules **1990**, *23*, 3922.

Evers, O. A.; Fleer, G. J.; Scheutjens, H. M.; Lyklema, J.
J. Colloid Interface Sci. **1986**, *111*, 446.

Fou, A. C.; Ellis, D.; Ferreira, M.; Rubner, M. F.
Polym. Prepr. (Am. Chem. Soc., Div. Polym. Chem.) **1994**, *35*, 221.

Fou, A. C.; Rubner, M. F. *Macromolecules* **1995**, *28*, 7115.

Freeman, T. L.; Evans, S. D.; Ulman, A. *Langmuir* **1995**, *11*, 4411.

He, T.; Porter, S. *Polymer* **1987**, *28*, 1321.

Keller, S. W.; Kim, H.-N.; Mallouk, T. E. *J. Am. Chem. Soc.* **1994**, *116*, 8817.

Kleinfeld, E. R.; Ferguson, G. S. *Science* **1994**, *265*, 370.

Koros, W. J.; Fleming, G. K. *J. Membr. Sci.* **1993**, *83*, 1.

Kusanagi, H.; Takase, M.; Chatani, Y.; Tadokoro, H. J.
J. Polym. Sci., Polym. Phys. Ed. **1978**, *1*, 131.

Lane, J. M.; Hourston, D. J. *J. Prog. Org. Coat.* **1993**, *21*, 269.

Lee, H.; Kepley, L. J.; Hong, H.-G.; Akhter, S.; Mallouk, T. E.
J. Phys. Chem. **1988**, *92*, 2597.

Liao, Y.-H.; Levon, K. *Polym. Mater. Sci. Eng.* **1993**, *69*, 327.

Lvov, Y.; Decher, G.; Möhwald, H. *Langmuir* **1993**, *9*, 481.

Lvov, Y.; Decher, G.; Sukhorukov, G. *Macromolecules* **1993**, *26*, 5399.

Lvov, Y.; Essier, F.; Decher, G. *J. Phys. Chem.* **1993**, *97*, 13773.

Lvov, Y.; Haas, H.; Decher, G.; Möhwald, H.; Kalachev, A.
J. Phys. Chem. **1993**, *97*, 12835.

Lvov, Y.; Haas, H.; Decher, G.; Möhwald, H. *Langmuir* **1994**, *10*, 4232.

Malhotra, B. D. *J. Appl. Polym. Sci.* **1990**, *40*, 1049.

Mao, G.; Tsao, Y.; Tirrell, M.; Davis, H. T. *Langmuir* **1993**, *9*, 3461.

Mao, G.; Tsao, Y.-H.; Tirrell, M.; Davis, H. T. *Langmuir* **1994**, *10*, 4174.

Mao, G.; Tsao, Y.-H.; Tirrell, M.; Davis, H. T. *Langmuir* **1995**, *11*, 942.

Mitsui Plastics, *commercial literature.*

Mohr, J. M.; Paul, D. R.; Mlsna, T. E.; Lagow, R. J.
J. Membr. Sci. **1991**, *55*, 131.

Mohr, J. M.; Paul, D. R.; Pinnau, I.; Koros, W. J. *J. Membr. Sci.* **1991**, *56*, 77.

Mohr, J. M.; Paul, D. R. *Polymer* **1992**, *33*, 57.

Petropoulos, J. H. *J. Membr. Sci.* **1990**, *53*, 229.

Puleo, A. C.; Paul, D. R. *Polymer* **1989**, *30*, 1357.

Rasmussen, J. R.; Stedronsky, E. R.; Whitesides, G. M.
J. Am. Chem. Soc. **1977**, *99*, 4736.

Rautenbach, R.; Janisch, I. *Ad. Polym. Technol.* **1987**, *7*, 221.

Schmitt, J.; Grünewald, T.; Decher, G.; Pershan, P. S.; Kjaer, K.; Lösche, M.
Macromolecules **1993**, *26*, 7058.

Spillman, R. W.; Sherwin, M. B. *CHEMTECH* **1990**, *June*, 378.

Stockton, W. B.; Rubner, M. F.
Polym. Prepr. (Am. Chem. Soc., Div. Polym. Chem.) **1994**, *35*, 319.

Sykes, P. *A Guidebook to Mechanism in Organic Chemistry;* 5 ed.;
Longman Group Limited: Essex, 1981, pp 397.

Takayanagi, M.; Kawasaki, M. J. *J. Macromol. Sci., Phys.* **1967**, *1*, 741.

Trivedi, D. C.; Dhawan, S. K. *Synth. Met.* **1993**, *58*, 309.

Van der Schee, H. A.; Lyklema, J. *J. Phys. Chem.* **1984**, *88*, 6661.

Zoller, P.; Starkweather, H. W.; Jones, G. A.
J. Polym. Sci., Polym. Phys. Ed. **1986**, *24*, 1451.